

The relationship between soil index properties and the cyclic shear strength from undrained cyclic tests

by

Jannetje Jacoba van der Klooster

In partial fulfilment of the requirements for the degree of
Master of Science in Civil Engineering
at the Delft University of Technology,
to be defended publicly on Friday August 27, 2021 at 10:00 AM.

Student number:	4494415	
Thesis committee:	Prof. dr. ir. C. Jommi,	TU Delft, chair
	Dr. Ir. M. Murali,	Fugro
	Dr. Ir. J. Marques Marçal Liça,	Fugro
	Dr. Ir. M. Korff,	TU Delft
	Dr. Ir. F. Pisanò,	TU Delft

An electronic version of this thesis is available at <http://repository.tudelft.nl/>.



Preface

Here I present my master thesis, written to obtain the degree of Masters of Science in Civil Engineering at Delft University of Technology.

This research is done in cooperation with Fugro Marine and I am grateful that they provided me the chance to obtain my master's degree within this company under supervision of Maddy Murali and José Marques Marçal Laça. Thanks for helping me and challenging me to learn more about cyclic behaviour of offshore structures. I also would like to express my gratitude to my committee chair, prof. Jommi to make time for me and to give feedback. It was not easy to work during these pandemic times. Lastly, I would like to thank my family and my good friend Billy to be a big support during tough moments in my study journey and personal life. They always remind me to believe in myself and to never give up.

*J.J van der Klooster
Wemeldinge, August 2021*

Abstract

Offshore wind power structures are subjected to cyclic loading. Several loads like wind and wave loading are acting on the structure and therefore its foundation. It is important to involve the impact of this cyclic loading into the design of the structure. A cyclic load influences the strength and deformation characteristics of the soil. Due to this the cyclic loading the cyclic shear strength will decrease. This cyclic shear strength depends on several factors which can be influenced by soil properties and shear mechanisms.

The aim of this Master thesis is to provide correlations between index parameters and the cyclic simple shear strength to observe how and which parameters influence the shear strength behaviour due to cyclic loading. This research focuses on the results from cyclic simple shear tests and only for cohesionless soil from North Sea sand. The project material was obtained from several offshore windfarm projects by Fugro, namely The Hollandse Kust West, The Hollandse Kust Noord and The Hollandse Kust Zuid.

Available data from these project locations is analysed and translated to cyclic resistance curves. In these curves the number of cycles to reach a nominal strain failure is plotted against a normalised cyclic shear strength, also called a cyclic stress ratio. The strain failure criterion was chosen at 3.75% and a commonly equivalent number of cycles of 10. The soil parameters that are elaborated for this research are based on characteristics compared to density of the soil, grain structure and in-situ characteristics. These parameters are the relative density, fines content, mean particle size and the normalised cone penetration resistance. The relative density is an unknown parameter in this research and is determined in two ways. First, by considering in-situ data where it was measured along depth and an assumption was made about the real value based on the known depth range of the borehole sample. The second method was based on the initial void ratio measured in the laboratory to obtain a relation between the in-situ measured relative density and the initial void ratio, which is called the theoretical value of the relative density.

From this thesis, it was concluded that due to the small range of data it was not possible to provide clear correlations and to observe trends of soil index parameters with the cyclic shear strength. By looking at the total range of the cyclic response of the data in the cyclic resistance curves and the elaborated soil parameters, the relative density and the fines content influence the shape of the power failure lines. A relatively high value of the relative density results in a larger range of different cyclic stress ratio values, i.e. a failure line with a higher gradient. An increment in fines content results in a relatively lower values for cyclic stress ratio and do not differ much by an increment of load cycles. This observation is based on the available results from this research with a relatively low amount of data and a small range of fines content.

Contents

List of Figures	ix
List of Tables	xi
1 Introduction	1
1.1 Research motivation	1
1.2 Research questions	1
1.3 Scope	2
1.4 Outline	3
2 Literature review and background information	5
2.1 Introduction to laboratory cyclic shear testing and failure modes	5
2.2 Soil behaviour in shear and the shear strength of cohesionless soils	6
2.3 Soil response under cyclic loading	8
2.4 Interpretation of cyclic test data	9
2.5 Principle of cyclic shear strain accumulation	11
2.6 Cyclic resistance curves	12
2.7 Soil parameters affecting soil response to undrained cyclic loading	12
2.7.1 Density of the soil	13
2.7.2 Particle size analyses	13
2.7.3 In situ characteristics	15
3 Elaboration and assessment of available dataset	17
3.1 Project locations	17
3.2 Performed tests and sample preparation	19
3.2.1 Soil samples for laboratory testing	19
3.2.2 Cyclic Direct Simple Shear test results	19
3.3 Cyclic resistance curves	24
3.3.1 Reference stresses	24
3.3.2 Strain failure criterion	24
3.3.3 Equivalent number of cycles	25
3.3.4 Results cyclic resistance curves	25
3.4 Soil index parameters	27
3.4.1 Relative density	28
3.4.2 Particle size distribution	29
3.4.3 In-situ parameters	31
3.5 Conclusion after elaboration and assessment of available dataset	32
4 Study on the correlations between index parameters and the cyclic shear strength	33
4.1 Details about test results	33
4.2 Presentation of the results	34
4.2.1 Further elaboration of cyclic resistance curves	34
4.2.2 Correlation with the Fines content	34
4.2.3 Correlation with the Relative density	35
4.2.4 Correlation with the mean particle size	36
4.2.5 Correlation with the Normalised cone penetration resistance	37
4.3 Conclusion after study on the correlations between index parameters and the cyclic shear strength	37
5 Conclusions and Recommendations	39
5.1 Conclusions	39
5.2 Recommendations for future work	41

A Appendix A	45
B Appendix B	57
C Appendix C	61

List of Figures

1.1	Offshore windfarm locations (windenergie magazine, 2020)	2
2.1	Soil elements along the failure surface under a shallow circular foundation (Das, 2019)	6
2.2	Shear strength characteristics of coarse-grained soils (Knappett & Craig, 2012)	6
2.3	Shearing of soil particles: (a) dense soil, showing dilatancy, (b) loose soil, showing contraction (Knappett & Craig, 2012)	7
2.4	Determination of peak strengths from direct shear test data (Knappett & Craig, 2012)	7
2.5	Amplitude and frequency of cyclic loading (Randolph M. F., 2012)	8
2.6	Effective stress paths for undrained tests with monotonic and cyclic loading (Andersen, 2015)	8
2.7	Pore pressure and shear strain as function of time under undrained cyclic loading (Andersen, 2015)	9
2.8	Stress-strain behaviour under cyclic loading (Andersen, 2015)	9
2.9	Classification of cyclic loading regimes (Randolph M. F., 2012)	10
2.10	Example results of a CSS test, saturated sand, $\sigma'_{vc} = 75$ kPa, $\sigma'_{hc} = 30$ kPa, $\tau_{cy} = 15$ kPa (Randolph & Gourvenec, 2011)	10
2.11	Example results of a CSS test, saturated sand at different CSR's, (a) $\tau_{cy}/\sigma'_{vc} = 0.23$ and (b) $\tau_{cy}/\sigma'_{vc} = 0.33$ (Randolph & Gourvenec, 2011)	11
2.12	Cyclic stress-strain curves with increasing cyclic shear stress (Andersen, 2015)	11
2.13	Principle of cyclic shear strain accumulation (Andersen, 2015)	12
2.14	Example of a strain contour diagram, 2-way cyclic loading, $\tau_a=0$ (Randolph & Gourvenec, 2011)	12
2.15	Increase of the liquefaction resistance with increasing density: tests of a) (Mori et al, 1978) and b) (Tatsuoka et al., 1986); (Wichtmann & T.Triantafyllidis, 2012)	13
2.16	Cyclic shear strength of 10 cycles with symmetrical cyclic loading in DSS tests on normally consolidated sand and silt as a function of relative density after consolidation (Andersen, 2015)	14
2.17	Influence of the mean grain size D50 on the liquefaction resistance: undrained cyclic tests of a) (Lee & J.A.Fitton, 1969) and b) (Dupla & J.Canou, 2003); (Wichtmann & T.Triantafyllidis, 2012)	14
2.18	: Influence of the coefficient of uniformity C_u for a constant relative density, undrained cyclic tests of (Vaid et al., 1990); (Wichtmann & T.Triantafyllidis, 2012)	15
2.19	: Influence of the coefficient of uniformity C_u for a constant relative density, undrained cyclic tests of (Vaid et al., 1990); (Wichtmann & T.Triantafyllidis, 2012)	15
2.20	Liquefied shear strength ratio and normalised CPT for clean sand (Robertson, 2010)	16
3.1	Project location HKW (Fugro Engineers B.V., 2020)	18
3.2	Project location HKN (Fugro Engineers B.V., 2019)	18
3.3	Project location HKZ I & II (Fugro Engineers B.V., 2017)	18
3.4	Project location HKZ III & IV (Fugro Engineers B.V., 2018)	18
3.5	First consolidation stage, vertical load increment and dissipating pore water pressures	21
3.6	Stress-strain diagram, example test result during pre-shearing	22
3.7	Number of cycles and shear stress, example test result during pre-shearing	22
3.8	Cyclic loading stage, number of cycles and shear stress, example test result	23
3.9	Cyclic loading stage, number of cycles and shear strain, example test result	23
3.10	Cyclic loading stage, stress-strain diagram, example test result	23
3.11	Cyclic resistance curve, project HKW, pre-shear	25
3.12	Cyclic resistance curve, project HKW, without pre-shear	26
3.13	Cyclic resistance curve, project HKN, pre-shear	26
3.14	Cyclic resistance curve, project HKZ, pre-shear	27
3.15	Theoretical Relative density D_r [%]	29
3.16	Grain size distribution curves (project HKW)	30
3.17	Grain size distribution curves (project HKN)	30

3.18 Grain size distribution curves (project HKZ)	30
4.1 Correlation of the FC [%] with the Cyclic Stress Ratio (CSR) at N =10 and N = 100, labels = Batch nr.	35
4.2 Correlation of the Dr [%] with the Cyclic Stress Ratio (CSR) at N = 10 and N = 100, labels = Batch nr.	35
4.3 Observed values for Dr [%] in combination with earlier observations found by (Andersen, 2015) , labels = FC [%]	36
4.4 Correlation of the D50 [mm] with the Cyclic Stress Ratio (CSR) at N = 10 and N = 100, labels = Batch nr.	36
4.5 Correlation of the Qtn [-] with the Cyclic Stress Ratio (CSR) at N = 10 and N = 100, labels = Batch nr.	37
A1 Cyclic resistance curve for $\gamma_{cy} = 15\%$, project HKW, pre-shear	48
A2 Cyclic resistance curve for $\gamma_{cy} = 7.5\%$, project HKW, pre-shear	49
A3 Cyclic resistance curve for $\gamma_{cy} = 5\%$, project HKW, pre-shear	49
A4 Cyclic resistance curve for $\gamma_{cy} = 3.75\%$, project HKW, pre-shear	49
A5 Cyclic resistance curve for $\gamma_{cy} = 2.5\%$, project HKW, pre-shear	50
A6 Cyclic resistance curve for $\gamma_{cy} = 1\%$, project HKW, pre-shear	50
A7 Cyclic resistance curve for $\gamma_{cy} = 15\%$, project HKW, without pre-shear	50
A8 Cyclic resistance curve for $\gamma_{cy} = 7.5\%$, project HKW, without pre-shear	51
A9 Cyclic resistance curve for $\gamma_{cy} = 5\%$, project HKW, without pre-shear	51
A10 Cyclic resistance curve for $\gamma_{cy} = 3.75\%$, project HKW, without pre-shear	51
A11 Cyclic resistance curve for $\gamma_{cy} = 2.5\%$, project HKW, without pre-shear	52
A12 Cyclic resistance curve for $\gamma_{cy} = 1\%$, project HKW, without pre-shear	52
A13 Cyclic resistance curve for $\gamma_{cy} = 15\%$, project HKN, pre-shear	52
A14 Cyclic resistance curve for $\gamma_{cy} = 7.5\%$, project HKN, pre-shear	53
A15 Cyclic resistance curve for $\gamma_{cy} = 5.0\%$, project HKN, pre-shear	53
A16 Cyclic resistance curve for $\gamma_{cy} = 3.75\%$, project HKN, pre-shear	53
A17 Cyclic resistance curve for $\gamma_{cy} = 2.5\%$, project HKN, pre-shear	54
A18 Cyclic resistance curve for $\gamma_{cy} = 1\%$, project HKN, pre-shear	54
A19 Cyclic resistance curve for $\gamma_{cy} = 15\%$, project HKZ, pre-shear	54
A20 Cyclic resistance curve for $\gamma_{cy} = 7.5\%$, project HKZ, pre-shear	55
A21 Cyclic resistance curve for $\gamma_{cy} = 5\%$, project HKZ, pre-shear	55
A22 Cyclic resistance curve for $\gamma_{cy} = 3.75\%$, project HKZ, pre-shear	55
A23 Cyclic resistance curve for $\gamma_{cy} = 2.5\%$, project HKZ, pre-shear	56
A24 Cyclic resistance curve for $\gamma_{cy} = 1\%$, project HKZ, pre-shear	56
C1 Cyclic resistance curve for HKW	62
C2 Cyclic resistance curve for HKN	63
C3 Alternative resistance curve for HKN	63
C4 Alternative resistance curve for HKZ	64
C5 Cyclic resistance curve HKW, no pre-shear	64
C6 Relationship between Dr [%] and the slope of the cyclic resistance curves	65

List of Tables

3.1	Sample depths and locations for HKW	19
3.2	Sample depths and locations for HKN	19
3.3	Sample depths and locations for HKZ	20
3.4	Details performed cyclic tests	21
3.5	Values of Cyclic Stress Ratio's observed from diagram, project HKW, pre-shear	25
3.6	Values of Cyclic Stress Ratio's observed from diagram, project HKW, without pre-shear	26
3.7	Values of Cyclic Stress Ratio's observed from diagram, project HKN, pre-shear	27
3.8	Values of Cyclic Stress Ratio's observed from diagram, project HKZ, pre-shear	27
3.9	Values of Relative density $D_r\%$ for different sand batches	29
3.10	Values of Relative density $D_r\%$ for different sand batches	31
3.11	Measured Normalised cone resistance (Q_{tn}) for different depth intervals	32
4.1	Collected details for correlation graphs	34
A1	Shear strain data, project HKW, test type: constant volume, stress controlled, 2 way loaded with pre-shear	45
A2	Shear strain data, project HKW, test type: constant volume, stress controlled, 2 way loaded no pre-shear	46
A3	Shear strain data, project HKN, test type: constant volume, stress controlled, 2 way loaded with pre-shear	47
A4	Shear strain data, project HKN, test type: constant volume, stress controlled, 2 way loaded no pre-shear	47
A5	Shear strain data, project HKZ, test type: constant volume, stress controlled, 2 way loaded with pre-shear	48
B1	Details about data to construct the cyclic resistance curve, project: HKW, pre-shear	57
B2	Details about data to construct the cyclic resistance curve, project: HKW, no pre-shear	58
B3	Details about data to construct the cyclic resistance curve, project: HKN, pre-shear	59
B4	Details about data to construct the cyclic resistance curve, project: HKZ, pre-shear	60
C1	Collected test results	61
C2	Collected test results	62
C3	Collected test results for each batch for $N = 10$ and $N = 100$ cycles, after assessment of the observed cyclic resistance curves	62

1

Introduction

1.1. Research motivation

Wind power structures are nowadays more frequently placed offshore. These structures are subjected to significant cyclic loading from the wind in addition to the wave loading that is acting on the structure and specifically its foundation. In the places where the structures are sensitive to cyclic loading, these effects should be considered in connection with foundation design. Different types of offshore foundation structures can be distinguished. The offshore structures could be fixed by piles, monopiles, skirted foundations or with gravity platforms. In the latter, the structure is fixed with the use of their own weight (Andersen, 2015).

Cyclic loading will influence the strength and deformation characteristics of the soil and the effects of cyclic loading should be incorporated in foundation design. Therefore, offshore foundation design needs an estimation of the cyclic response of soil and this response can be obtained from cyclic laboratory tests of soil samples. Correlations that can be observed between the cyclic soil parameters and index properties of the soil will also become more important in practical design and in predicting the cyclic response (Andersen, 2015).

To get a better understanding of the cyclic response, a large amount of laboratory test results is recommended. In this thesis research, offshore projects are considered to justify and to analyse sufficient test results to get a comparable outcome for cyclic response of offshore sand in the North Sea. Various investigations have been carried out by Fugro through in-situ and laboratory testing to identify the characteristics of soil in the North Sea.

Cyclic laboratory tests, such as the Cyclic Direct Simple Shear (CSS) test provides an indication of the overall cyclic soil response. The results are used most often for evaluating the ability of a soil to resist shear stresses, such as those induced during cyclic loading, e.g. offshore storm loading or earthquake loading. The undrained CSS test shows a cyclic response that is comparable with the conditions observed in-situ during cyclic undrained shearing caused by wave or wind loading.

In a shear test, the soil sample is first consolidated and then sheared under a specific applied normal stress and shear rate. The measured shear strength parameters depend on several factors which can be influenced by the soil properties and shear mechanisms. The cyclic strength is a function of several factors like density, frequency and characteristics of the cyclic loading applied (ASTM International, 2019).

The aim of this thesis is to provide correlations between index parameters and the cyclic simple shear strength. These are based on CSS test results of sands performed for offshore wind monopile foundation design. The background motivation for this research is that when correlations are observed, an estimation could be made of soil parameters even before data is available from the project site. These correlations could guide the specification and interpretation of site-specific laboratory programs (Andersen, 2015).

1.2. Research questions

The main research question of this thesis is: "What is the relationship between soil index parameters and the cyclic simple shear strength based on test results of undrained Cyclic Direct Simple Shear (CSS) tests in sands?" To answer this question available projects in the North Sea will be analysed for which CSS tests are performed. The following sub-questions are formulated:

1. Are the sample conditions of the CSS tests comparable, and are the tests performed in a comparable way?
2. Which soil parameters, that are known to influence the cyclic response of the soil, best correlate with the cyclic shear strength?
3. How could the observed trends between these parameters be explained and what is missing in order to improve such correlations?

1.3. Scope

The scope, boundaries and limitations concerning this research are listed and summarised as follows:

- The soil type is chosen as sand and therefore only soil samples made of cohesionless material/offshore sand will be analysed, clay samples are beyond this research.
- The thesis research will focus on the cyclic response of sands in undrained, stress controlled Cyclic Direct Simple Shear (CSS) tests, results from other soil element tests will be not analysed.
- The research will focus on cyclic loading coming from offshore wind and wave action, cyclic response from earthquake loading will be not analysed.
- The available test results come from different offshore windfarm projects obtained by Fugro, namely The Hollandse Kust West (HKW), The Hollandse Kust Noord (HKN) and The Hollandse Kust Zuid (HKZ), (Figure 1.1).
- This thesis will not look at uncertainties arising due to system compliance and limitations of the apparatus or human factors that may affect the results of the performed test.

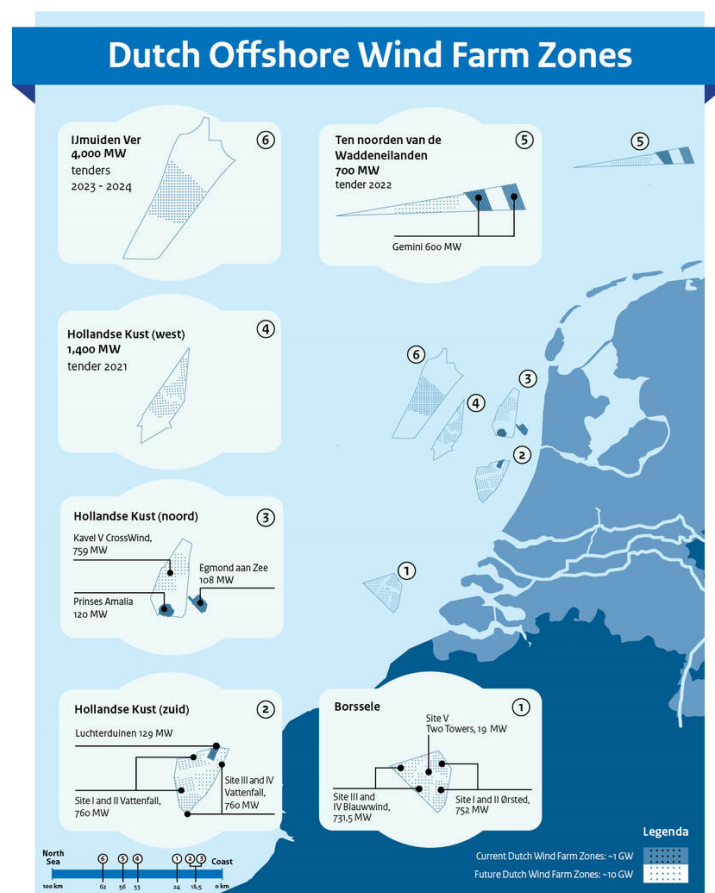


Figure 1.1: Offshore windfarm locations (windenergie magazine, 2020)

1.4. Outline

This thesis report consists of five chapters outlined as below.

Chapter 1 (this chapter) includes an introduction, the research motivation, problem statement, objectives, research questions and scope, boundaries and limitations concerned in this research. Chapter 2 is a literature review which reports the main background information about cyclic loading with regard to offshore structures. In this review, the cyclic response of soil and the soil behaviour subjected to (cyclic) shear were considered. Additionally, an explanation about the performed tests and analyses of the soil parameters which may influence the cyclic strength, is included. Chapter 3 is assessment of the dataset on which this research is based. From this information the soil parameters are to be determined in a consistent way. Chapter 4 presents the resulting correlations between the cyclic shear strength measured in the laboratory and various soil classification state parameters. Finally, the conclusions of this research and recommendations for future study to improve the correlations, are reported in Chapter 5.

2

Literature review and background information

This chapter contains the background information of reference for cyclic loading in offshore foundation design. Among the considered aspects are the cyclic response of the soil and the soil behaviour subjected to (cyclic) shear. Additionally, an analysis is made of (cyclic) soil parameters which could influence foundation design especially for offshore structures. This, in accordance with observations from previous research regarding to correlations of soil parameters with the cyclic strength. Considering the scope of the project, the focus is on cohesionless soil in undrained conditions under the influence of (cyclic) simple shearing. The behaviour in triaxial compression and extension is not included.

2.1. Introduction to laboratory cyclic shear testing and failure modes

For soil mechanics and civil engineering practice, soil samples are tested in the laboratory to investigate the soil behaviour. The characteristics of the soil are estimated based on tests which are mostly carried out on small samples.

The cyclic loading needs to be considered in offshore design because offshore structures are subjected to wind and wave loading. To examine the effects of cyclic loading, the main focus is on quantifying the reduction in (cyclic) shear strength (Andersen, 2015). Mostly this cyclic, environmental, loading has a higher impact compared to the monotonic, permanent, loading (Randolph & Gourvenec, 2011). A typical frequency of wave loading is of 0.05-0.1 Hz and tests should be carried out at this frequency (Randolph & Gourvenec, 2011).

Laboratory element tests are used to evaluate the damage due to cyclic loading and to obtain soil strengths for engineering design calculations. Figure 2.1 shows different failure modes under a foundation. These failure mechanisms follow different stress paths.

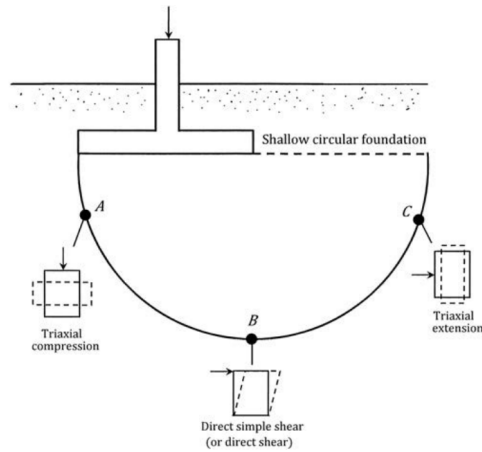


Figure 2.1: Soil elements along the failure surface under a shallow circular foundation (Das, 2019)

The simple shear test method could be seen as a test that obtains the most representative response of the soil comparable to in-situ conditions (Andersen, 2015). A benefit about cyclic testing on simple shear tests is that it requires much less material than other element tests, like triaxial tests (Andersen, 2015). The tests can be performed over a smaller depth range of a borehole, and therefore with more uniform material. The elements belonging to the failure plane will experience different combinations of the cyclic shear stress, τ_{cy} and the average shear stress, τ_{av} , as will be explained later.

In the laboratory, the samples should be first consolidated to an in-situ effective stress before shear stresses will be applied (Randolph & Gourvenec, 2011). This is done to simulate the stress conditions of the different elements from in-situ conditions during cyclic loading. The soil parameters needed in foundation design are determined after this consolidation is performed.

2.2. Soil behaviour in shear and the shear strength of cohesionless soils

This section describes soil behaviour in shear and the shear strength of cohesionless soils. When the shear stress becomes equal to the shear strength within a soil mass, failure occurs (Knappett & Craig, 2012). The shear strength of soils is an important aspect for foundation engineering problems such as the bearing capacity of shallow foundations and piles (Das, 2019). Following the Mohr-Coulomb model, the shear strength of a granular, cohesionless soil could be defined as:

$$s = c + \sigma' \tan(\phi), \quad (2.1)$$

where σ' is the effective stress on the plane and ϕ the friction angle.

Figure 2.2 illustrates typical curves relating to shear stress and shear strain for a dense and a loose sand.

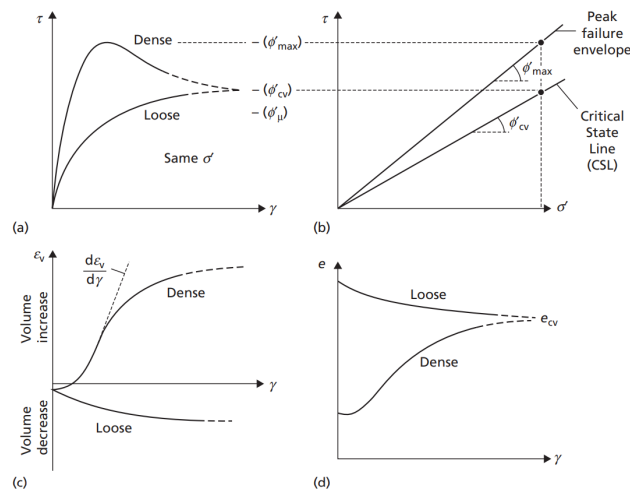


Figure 2.2: Shear strength characteristics of coarse-grained soils (Knappett & Craig, 2012)

In the stress-strain curve for a dense sand, a peak stress could be observed at a relatively low strain. Before a dense sand could fail because of shear failure the interlocking between the particles should be overcome and this interlocking gives a high resistance in dense sands. After overcoming this interlocking resistance, the stress will decrease with increasing strain. Also, an increase in volume, dilatancy, takes place due to this reduction in the degree of interlocking. This volume change could also be presented in terms of void ratio, e . In the end the shear stress reduces to an asymptotic value after the soil becomes loose enough and particles could move (Knappett & Craig, 2012).

For a loose sand, no peak value could be observed. No interlocking should be overcome and the shear stress will increase to a maximum value with a slightly decrease in volume, which is called contraction (Knappett & Craig, 2012).

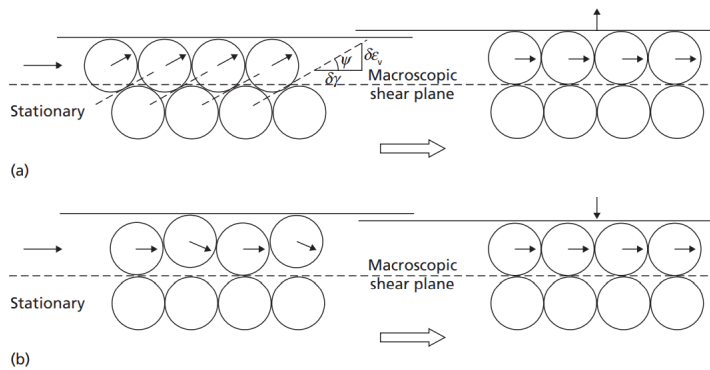


Figure 2.3: Shearing of soil particles: (a) dense soil, showing dilatancy, (b) loose soil, showing contraction (Knappett & Craig, 2012)

Figure 2.3 illustrates shearing of soil particles where dilation (a) and contraction (b) occurs. The terms used are the angle of dilation Ψ and the gradient $d\epsilon_v/d\gamma$. The latter is the maximum rate that corresponds with the peak stress shown in Figure 2.2 (Knappett & Craig, 2012).

A critical state occurs when there is no further change in volume or in shear stress. At this point the ultimate values of shear stress and void ratio are equal for both a dense and a loose sand. The corresponding angle of shearing resistance at critical state is usually denoted as ϕ'_{cv} (Knappett & Craig, 2012).

Figure 2.4 shows also results from a direct shear test but here the results are plotted as a stress ratio against the shear strain. Three different sands, labelled as A, B and C, are shown for different effective stresses and the same void ratio for each test (Knappett & Craig, 2012).

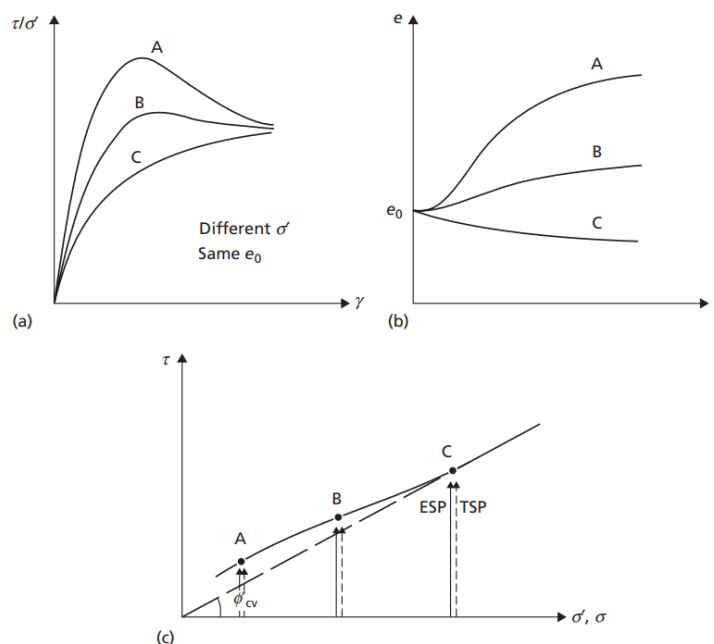


Figure 2.4: Determination of peak strengths from direct shear test data (Knappett & Craig, 2012)

With an increase in effective stress, both the maximum stress ratio and the void ratio will decrease. This explains that dilation is suppressed by increasing mean stress. Also, the peak of ultimate stress decreases with increasing effective normal stress.

In plot (c), the plotted points lie on a curved envelope. Here, the maximum shear stress is plotted against the effective normal stress (Knappett & Craig, 2012). Two different stress paths are plotted, the TSP (Total stress path) and the ESP (Effective stress path). In an ESP the variation of σ' and τ is plotted. The horizontal distance between the TSP and ESP, at a given value of τ , represents the pore water pressure. Because the pore water pressures in direct shear tests are approximately zero, the stress paths lie on the same line. When the ESP reaches the failure envelope, failure will occur (Knappett & Craig, 2012).

2.3. Soil response under cyclic loading

This section describes the soil response due to undrained cyclic loading. This response is considerably different from that during monotonic loading as described in the previous section. A cyclic load generates excess of pore water pressure, reduces effective stress and causes cyclic shear strains that develop during continued cycling. At the end, cyclic loading leads to a loss of shear strength or stiffness in the soil.

The response of the soil depends on the mode, amplitude and frequency of the cyclic loading (Randolph & Gourvenec, 2011). Figure 2.5 shows that the amplitude and frequency of cyclic loads caused by wave and wind are irregular. However, in the laboratory tests the cyclic behaviour is frequently investigated with a constant stress amplitude and frequency.

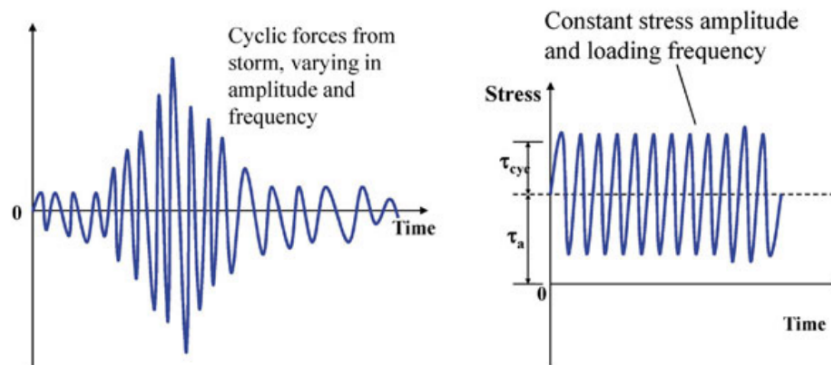


Figure 2.5: Amplitude and frequency of cyclic loading (Randolph M. E, 2012)

Figure 2.6 shows the effective stress path for a soil subjected to both monotonic and cyclic loading. Under the influence of the cyclic loading the fabric of the soil is modified, which can generate volumetric compression. In a situation where the soil is saturated and undrained cyclic shearing is applied. Volumetric changes are prevented because of the lower compressibility of water in comparison with the soil skeleton. Some of the normal stresses are transferred to the pore water and the effective stresses decrease.

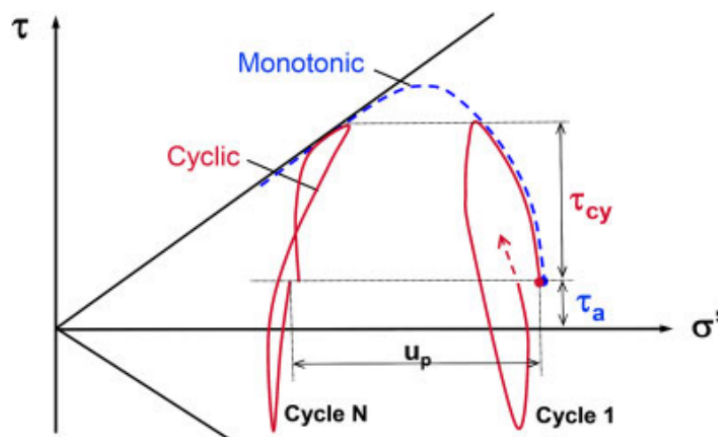


Figure 2.6: Effective stress paths for undrained tests with monotonic and cyclic loading (Andersen, 2015)

Figure 2.6 is an example of the typical behaviour for undrained tests with monotonic and cyclic loading. The blue line represents the behaviour due to monotonic loading. The test reaches a peak shear stress and after softening the shear stress follows the failure envelope. The red lines represent the cyclic loading for an increasing number of cycles (N). The soil is loaded with a smaller shear stress than the peak shear stress observed from monotonic tests. The load cycles around a constant shear stress τ_a , with a single amplitude shear stress, τ_{cy} . During the first cycle the stress path forms a loop that ends up to the left of the initial effective stress, corresponding to a permanent pore pressure, u_p . Each cycle gives an additional incremental pore pressure, and after some cycles the stress path reaches the failure envelope (Andersen, 2015).

Figure 2.7 and Figure 2.8 show the behaviour of the development in pore pressure, the shear strain with time and the stress-strain behaviour of soil elements under undrained cyclic loading with a constant cyclic shear stress. The effective stresses in the soil are reduced by increasing the pore pressure. This results in an increase in the shear strains with time (Andersen, 2015).

The graphs consist of different components for pore pressure and shear strain:

- For the permanent values of pore pressure (u_p) and shear strain (γ_p) applies that this are the values at the end of a cycle when shear stresses return to the shear stress at the start of the cycle.
- The cyclic values are single amplitudes values of half of the peak shear stress (τ_{cy} and γ_{cy}).
- The average values represent the average of the high and low peak values of a cycle (τ_a and γ_a).

2.4. Interpretation of cyclic test data

Cyclic loading could be applied in four different ways (Figure 2.9). The most common type applied to cyclic laboratory testing programs is the two-way, symmetric, cyclic loading (Randolph & Gourvenec, 2011). Other types are asymmetric two-way loading, pure one-way asymmetric cyclic loading, and biased one-way asymmetric cyclic loading. In the latter the shear stresses do not cross the origin and therefore does not reverse in sign. Figure 2.10 provides an example of the processes that take place during cyclic loading tests and to explain the response mechanisms to cyclic loading of a soil. The cyclic simple shear test in this example, was carried out on a saturated sand consolidated under vertical and horizontal consolidation stresses of $\sigma'_{vc} = 75$ kPa and $\sigma'_{hc} = 30$ kPa respectively. A two-way symmetric cyclic loading was applied with a cyclic shear stress of $\tau_{cy} = 15$ kPa.

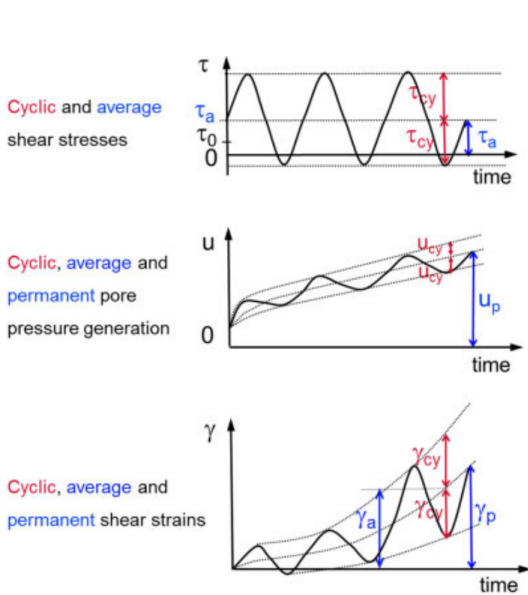


Figure 2.7: Pore pressure and shear strain as function of time under undrained cyclic loading (Andersen, 2015)

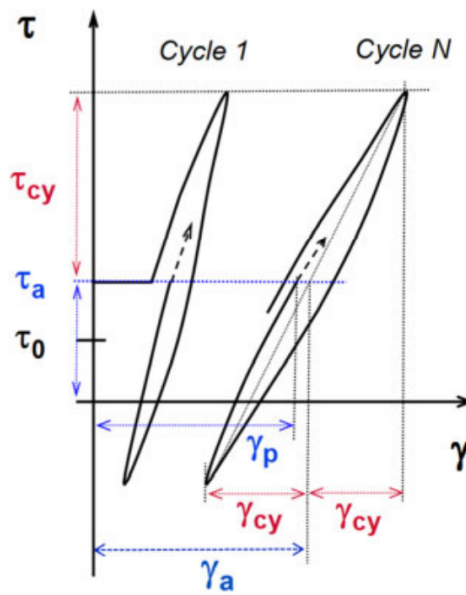


Figure 2.8: Stress-strain behaviour under cyclic loading (Andersen, 2015)

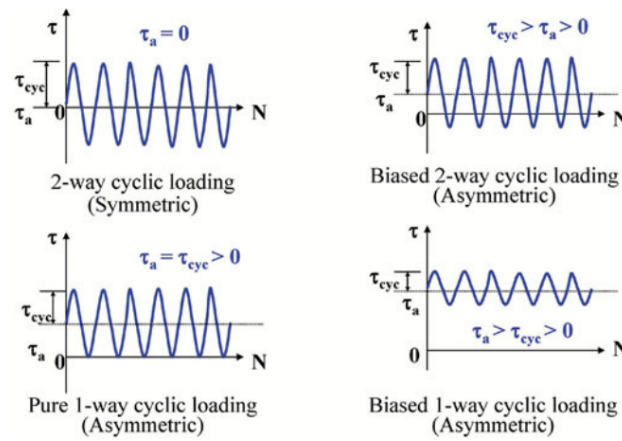
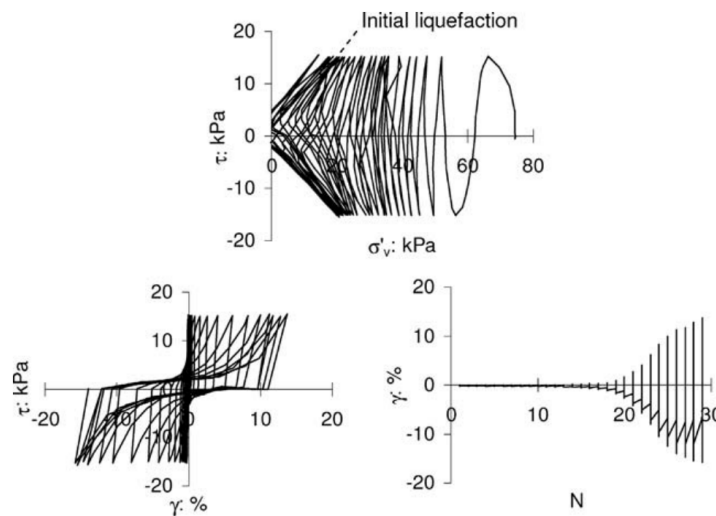


Figure 2.9: Classification of cyclic loading regimes (Randolph M. F., 2012)

Figure 2.10: Example results of a CSS test, saturated sand, $\sigma'_{vc} = 75$ kPa, $\sigma'_{hc} = 30$ kPa, $\tau_{cy} = 15$ kPa (Randolph & Gourvenec, 2011)

The changes in pore pressure and effective vertical stress that are observed are caused by the applied cyclic loading by a constant vertical stress. During the first stage of the first graph, excess pore pressures are generated because of the contraction of the sample which leads to a reduction in vertical effective stress. The shearing will continue until a shear stress of 15 kPa is reached. The excess pore pressure builds up with each cycle. At some point, the excess pore pressure at the middle of each cycle will reach the total vertical stress that is applied and the effective vertical stress will become zero. This point is called initial liquefaction. After this stage, the sample tends to dilate as it is sheared and provides a butterfly shaped stress path and S-shaped cycles in the (γ, τ) space. After initial liquefaction, shear strain increases and the stiffness reduces rapidly (Randolph & Gourvenec, 2011).

The cyclic shear strength at failure introduced by (Andersen, 2015) is defined as:

$$\tau_{f,cy} = (\tau_a + \tau_{cy})f \quad (2.2)$$

Where, the sum at the right-hand side is the sum of the average and cyclic shear stresses at failure. The term f is a failure mode which represent a percentage of cyclic strain as it will be explained later. The cyclic stress and average stress are defined, respectively, as the amplitude of cyclic stress and the average of the applied stress around which cyclic loading is applied (Andersen, 2015).

In cyclic tests, failure occurs as large strains develop. Cyclic tests should be performed with cyclic stress ratios and frequency that reflect the conditions appropriate for the design situation. Failure is not necessarily the strain level at which failure occurs but usually a failure criterion of a predetermined level of shear strain is defined (Randolph & Gourvenec, 2011).

A cyclic stress ratio (CSR) is the cyclic shear stress, τ_{cy} normalised with the effective stress, σ'_{vc} . Figure 2.11 shows an example of results of a CSS test on saturated sand where two different CSR's are applied of $\tau_{cy}/\sigma'_{vc} = 0.23$ and 0.33 respectively. First the excess pore pressure is generated rapidly. Subsequently, it increases at a slower rate. The point of initial liquefaction or failure is visible in these graphs. The shear strain increases at a slow rate until this point and subsequently the shear strain increases rapidly and the soil loses shear strength. The overall response of these two examples is the same but at the number of cycles to reach failure is different. Nf 100 for $\tau_{cy}/\sigma'_{vc} = 0.23$ and Nf 7 for $\tau_{cy}/\sigma'_{vc} = 0.33$ (Randolph & Gourvenec, 2011).

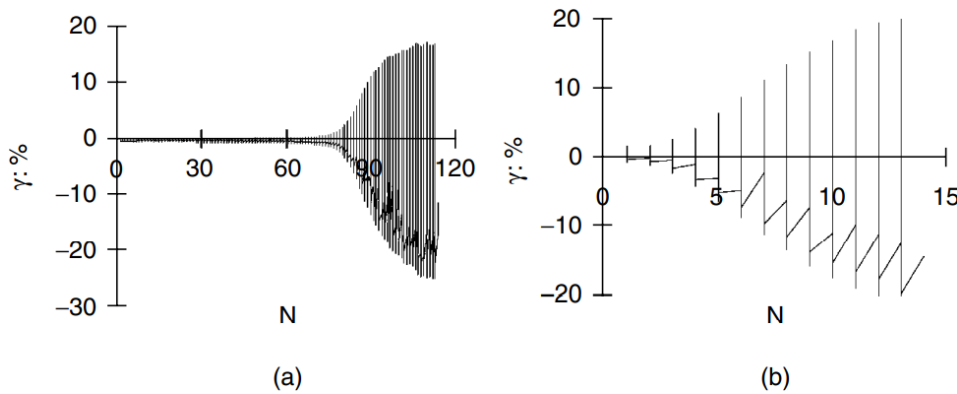


Figure 2.11: Example results of a CSS test, saturated sand at different CSR's, (a) $\tau_{cy}/\sigma'_{vc} = 0.23$ and (b) $\tau_{cy}/\sigma'_{vc} = 0.33$ (Randolph & Gourvenec, 2011)

2.5. Principle of cyclic shear strain accumulation

This section explains the principle of cyclic shear strain accumulation. This procedure gives a reasonable reflection of the behaviour of cyclic laboratory tests where the cyclic shear stresses are variable and increasing (Andersen, 2015). Figure 2.12 shows that there is an increase in the cyclic shear strain if the cyclic shear stress increases.

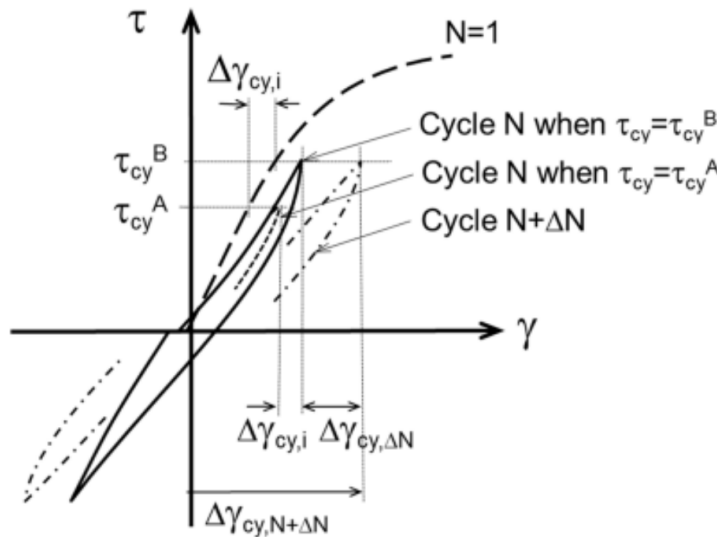


Figure 2.12: Cyclic stress-strain curves with increasing cyclic shear stress (Andersen, 2015)

To illustrate the increase of shear strain, Figure 2.13 shows an example of a cyclic shear strain contour diagram. In this example, 100 cycles are applied with a cyclic shear stress of $\tau_{cy} = 36$ kPa (Point B). The cyclic shear strain here is $\gamma_y = 0.75\%$. After this, the cyclic shear stress is increased from 36 kPa to 41 kPa following the cyclic shear strain of $\gamma_{cy} = 0.75\%$ (Point C). As explained, the cyclic shear strain increases with increasing cyclic shear stress and becomes $\gamma_{cy} = 0.85\%$. This is point D in the graph with $N = 35$ cycles. Based on this procedure, a prediction of the development of cyclic shear strain could be given for an increasing number of cycles and an increment of the shear stresses.

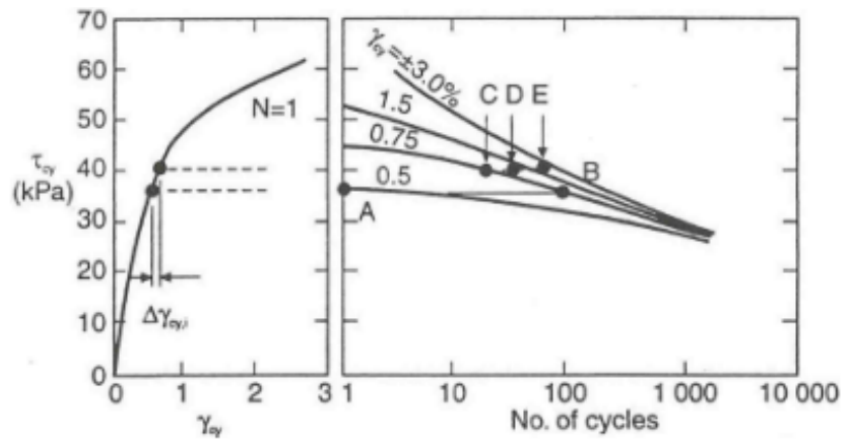


Figure 2.13: Principle of cyclic shear strain accumulation (Andersen, 2015)

2.6. Cyclic resistance curves

Based on the principle of cyclic shear strain accumulation, a cyclic resistance curve is used to define the cyclic shear stress τ_{cy} , needed to reach a given value of shear strain, γ , after a certain number of cycles N . The shear stress is typically normalised by the consolidation stress, τ_{cy}/σ'_{vc} . This ratio is called the cyclic stress ratio (CSR) as explained before. Results of cyclic loading tests can be used to construct cyclic resistance curves in terms of strain and can be then used in design. Based on the cyclic strain accumulation an example is given of a strain contour diagram (Figure 2.14). This example shows results from one monotonic and four cyclic direct simple shear tests. These tests were performed undrained and with two-way cyclic loading. The number of cycles (N) are determined to reach, consecutively, shear strains of 0.2%, 0.5%, 1%, 2%, 5% and 15%. The values are plotted towards this CSR (τ_{cy}/σ'_{vc}). Based on this, the number of cycles needed to reach a certain strain level could be identified for any value of the normalised cyclic shear stress (Randolph & Gourvenec, 2011).

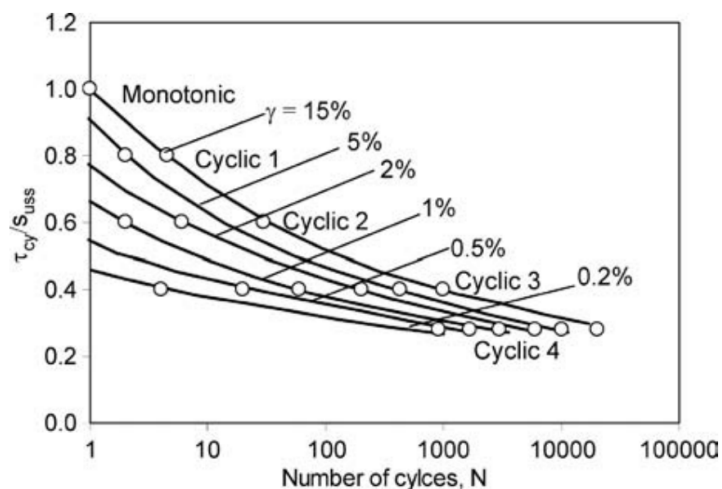


Figure 2.14: Example of a strain contour diagram, 2-way cyclic loading, $\tau_a=0$ (Randolph & Gourvenec, 2011)

In offshore design, usually an equivalent number of cycles is chosen to present the amount of cumulative damage instead of modelling the complete loading series. Typically, the equivalent number of cycles will be in the range of 10 to 20 cycles (Randolph M. F., 2012).

2.7. Soil parameters affecting soil response to undrained cyclic loading

This research is about the influence of different soil parameters towards the cyclic shear strength. In this section an analysis is made based on soil mechanics theory and previous research regarding soil parameters that could affect the cyclic shear strength of a cohesionless soil. As explained in the previous sections, the cyclic strength is a peak shear stress that can be mobilised during cyclic loading and can be defined as the

sum of the average and cyclic shear stresses at failure. In general, this cyclic strength depends on the average cyclic shear stress, the cyclic load history or number of cycles and the type of test that is applied and therefore the followed stress path. This shear stress is usually normalised by the consolidation stress, τ_{cy}/σ'_{vc} . This ratio is called the cyclic stress ratio (CSR).

2.7.1. Density of the soil

From soil behaviour under undrained cyclic loading it is observed that an increase in the stress amplitude causes a decrease in the number of cycles necessary to reach a certain failure criterion. Also, that pore water pressure accumulates faster with increasing shear strain amplitudes.

The density of the soil is an important parameter that influences the accumulation of pore water pressure during undrained cyclic simple shearing (Wichtmann & T.Triantafyllidis, 2012). In a dense sand, the number of cycles needed to reach failure or initial liquefaction is much larger compared to a loose sand (Wichtmann & T.Triantafyllidis, 2012). Therefore, an increase in soil density means a higher CSR and the point on a stain contour plot will shift upwards and to the left. This is shown in Figure 2.15, based on a research done by (Mori, Seed, & Chan, 1978) which shows increase of the liquefaction resistance with increasing density. Another research done by (Tatsuoka et al., 1986) found a linear relationship between the liquefaction resistance and the relative density up to $D_r = 75\%$. For larger relative densities the cyclic stress ratio increases to cause initial liquefaction.

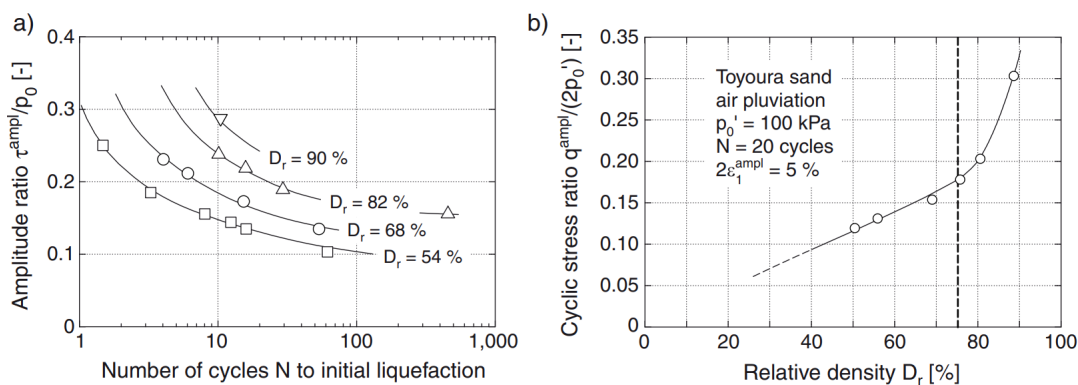


Figure 2.15: Increase of the liquefaction resistance with increasing density: tests of a) (Mori et al, 1978) and b) (Tatsuoka et al., 1986); (Wichtmann & T.Triantafyllidis, 2012)

This same kind of correlation is found by (Andersen, 2015) (Figure 2.16). Here the CSR is plotted against the relative density. The shear stress here is normalized to a reference stress, as will further explained in Chapter 3. This reference stress could give a better approximation for cyclic tests. The values are after 10 cycles and the shear strength was in these cases defined as the shear stress at a shear strain of 5% or 7.5%. Labels given to the data points are the fines content and the clay content to illustrates the influence of the fines content. A lower percentage of fines show a stronger increase in the resistance against shear.

From this research, it can be inferred that the resistance against shear will increase with increasing relative density. This tendency is influenced by the fines content, where a lower fines content $< 5\%$ fines shows a stronger increase.

2.7.2. Particle size analyses

Based on particle size analyses, correlations are considered towards the main grain size D_{50} , the coefficient of uniformity C_u and the Fines Content FC .

Figure 2.17 shows results of the influence of the D_{50} on the liquefaction resistance. (Lee & J.A.Fitton, 1969) reported about a significant decrease in the liquefaction resistance with decreasing D_{50} . In the right graph the results found by (Dupla & J.Canou, 2003) are presented. They found an acceleration of the accumulation of pore water pressure with decreasing D_{50} and state that, for in-situ conditions, a decrease in the grain size is accompanied by a decrease in the permeability of a soil.

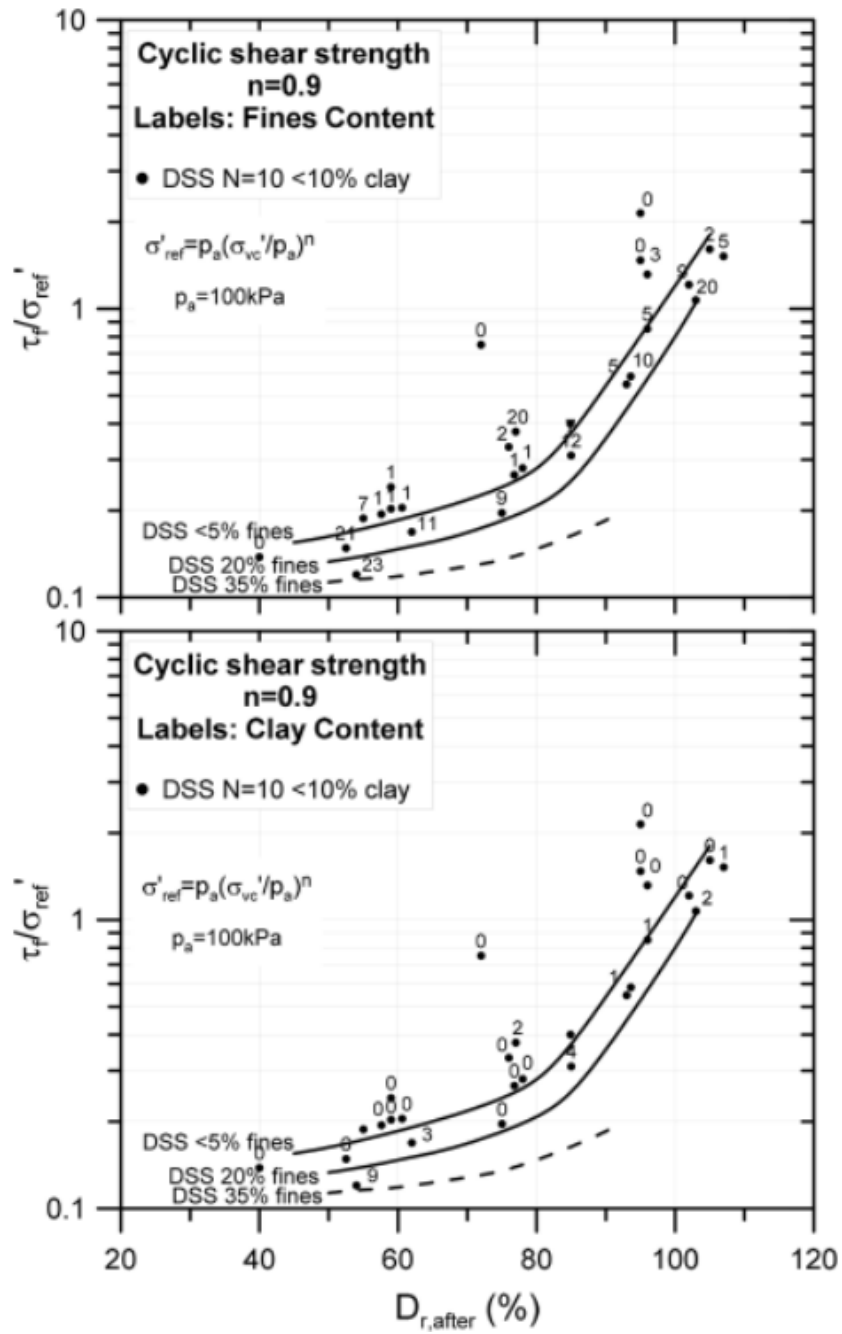


Figure 2.16: Cyclic shear strength of 10 cycles with symmetrical cyclic loading in DSS tests on normally consolidated sand and silt as a function of relative density after consolidation (Andersen, 2015)

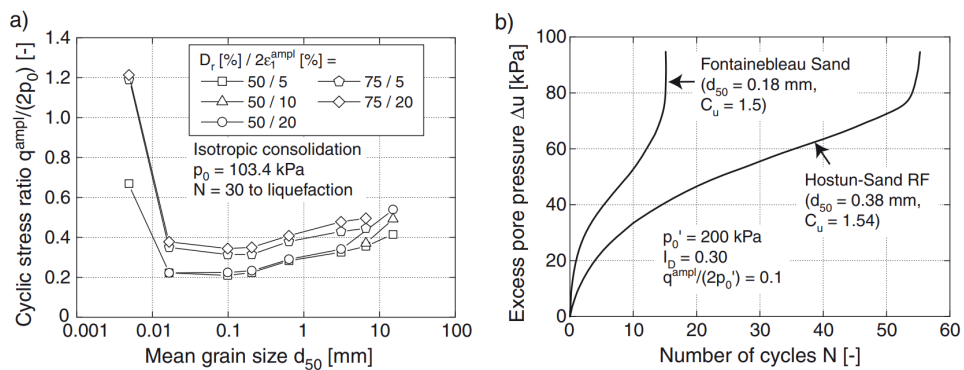


Figure 2.17: Influence of the mean grain size D50 on the liquefaction resistance: undrained cyclic tests of a) (Lee & J.A.Fitton, 1969) and b) (Dupla & J.Canou, 2003); (Wichtmann & T.Triantafyllidis, 2012)

Figure 2.18 shows a study of (Vaid et al., 1990) who studied the influence of the coefficient of uniformity, $C_u = D_{60}/D_{10}$ on the liquefaction resistance. The D_{50} was the same for all sands but the C_u values were different. The CSR as a function of the relative density is plotted. From these graphs it could be concluded that, for a constant D_r , the liquefaction resistance is similar for the three different sands. This means that there is not a clear dependence observed on the C_u .

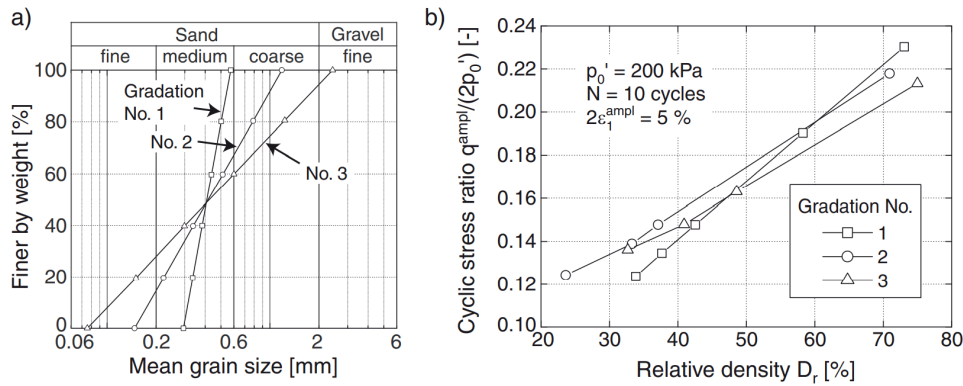


Figure 2.18: : Influence of the coefficient of uniformity C_u for a constant relative density, undrained cyclic tests of (Vaid et al., 1990); (Wichtmann & T.Triantafyllidis, 2012)

Figure 2.19 presents the results obtained by (Chien, Oh, & C.H.Chang, 2002). They tested a fine sand mixed with different amounts of non-plastic fines. They state that the liquefaction resistance will increase by a plastic (cohesive) fines content. The graphs show that for a constant relative density, the resistance towards liquefaction decreases with an increment of fines content. This effect of different fines content was even more clear for constant void ratios (e).

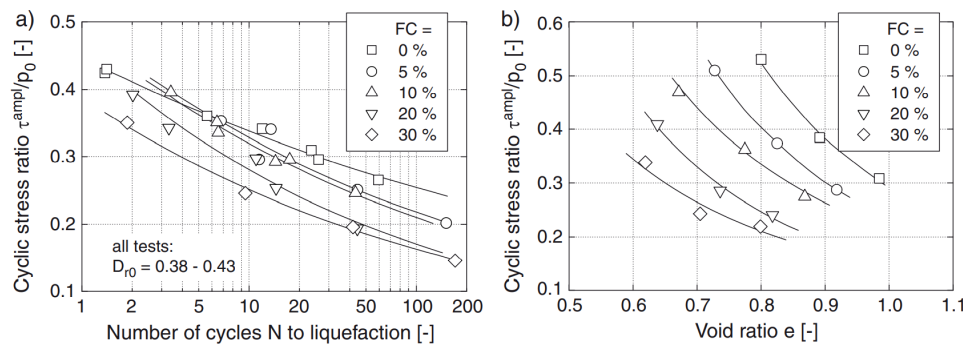


Figure 2.19: : Influence of the coefficient of uniformity C_u for a constant relative density, undrained cyclic tests of (Vaid et al., 1990); (Wichtmann & T.Triantafyllidis, 2012)

2.7.3. In situ characteristics

Figure 2.20 shows a curve found by (Robertson, 2010) through the evaluation of flow liquefaction and liquefied strength using the cone penetration test (CPT). The CPT-based relationship is presented to evaluate the susceptibility to strength loss and the CSR. The latter is called as the liquefied strength ratio for a wide range of soils.

The normalised cone penetration resistance is given by:

$$Q_{tn} = \left(\frac{q_t - \sigma_{v0}}{P_{a2}} \right) \left(\frac{P_a}{\sigma_{v0}} \right)^n, \tag{2.3}$$

$$Q_t = \left(\frac{q_t - \sigma_{v0}}{\sigma'_{v0}} \right), \tag{2.4}$$

where the first term in the right hand side of equation 2.3 is the dimensionless net cone resistance and the second term is the stress normalization factor. The exponent n varies with soil type. P_a is the atmospheric pressure in the same units as q_t and σ_v . Note that when $n=1$, $Q_{tn} = Q_t$

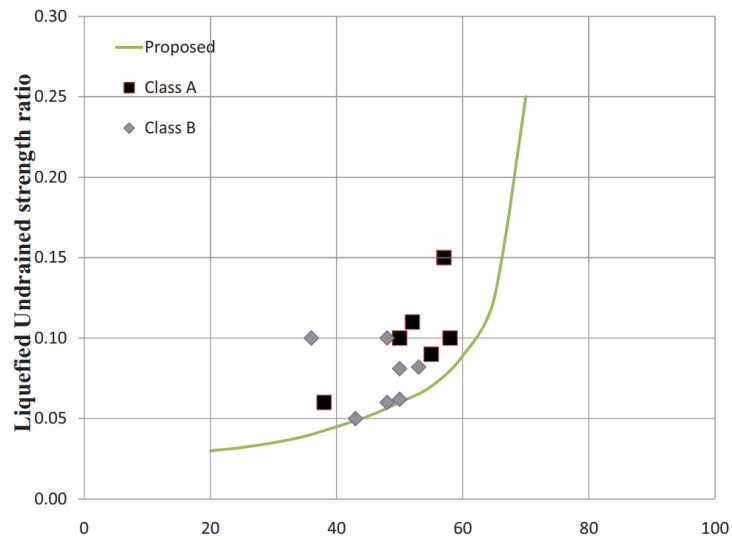


Figure 2.20: Liquefied shear strength ratio and normalised CPT for clean sand (Robertson, 2010)

Figure 2.20 shows the best estimate values of the CSR plotted against the normalised cone penetration data of clean sand equivalent penetration resistance values. The results are presented for two classes, A and B, which represent the results from several case studies used in that research. From the results could be observed that a higher normalised cone resistance causes a higher resistance towards liquefaction (Robertson, 2010).

3

Elaboration and assessment of available dataset

This chapter includes an analysis of the available geotechnical data. A collection of data is available from test results that are performed by Fugro. This intensive test program consists of results from site investigation and laboratory tests intended as input for offshore foundation design.

As the correlations between index parameters with the cyclic strength of the soil are sought, it is important to know if the considered soil samples and performed index tests are reliable, consistent and if they are comparable with each other.

In this chapter, the range of different data will be analysed by considering the specimen preparation of the soil samples for laboratory testing and through the determination of the soil index parameters. The particle size distribution (PSD), Fines Content (FC) and Relative Density (Dr), among others, are important to compare in this analysis. The considered soil is classified as a cohesionless specimen and within the scope of the research only the available CSS tests will be studied.

3.1. Project locations

Three locations are selected for this research. The areas are all located in the North Sea and are marked as new locations for a windfarm program in the North Sea. The geotechnical investigation is performed for the specific purpose of providing input for the design of offshore wind structures like monopiles and jacket piles. The locations are labelled as Hollandse Kust West (HKW), Hollandse Kust Noord (HKN) and Hollandse Kust Zuid (HKZ). The geotechnical site investigation included seafloor in-situ testing and sampling, geotechnical borehole drilling with downhole sampling, in-situ testing and sampling, geotechnical borehole drilling with downhole sampling, in-situ testing, borehole geophysical logging and geotechnical laboratory testing.

The locations are shown in the Figure 3.1 to Figure 3.4. The boreholes are located within these areas. Cone penetration tests (CPT) were performed close to the borehole locations. The soil samples for laboratory testing are retrieved from these boreholes and reconstituted in batch samples. This process is described in the next sections. The project areas consist of different geological formations, the geology of the areas can be summarised as follows:

- The geology of the HKW area is characterised by continue sea level changes and repeating cycles of glaciation and deglaciation. The upper 100 meters of the sediments were depositions consisting of fluvatile, deltaic, estuarine and shallow marine sediments deposited in the Middle Pleistocene. The sediments are sands and silty sands with clay intercalation. Channels or glacial valleys could be infilled and show thicker cohesive sediment layers (Netherlands Enterprise Agency, 2018).
- The HKN location is characterised by deposits from the Yarmouth Roads Formation and the Wintterton Shoal Formation. These formations were deposited in a fluvial and tidal deltaic environment comprise fine to coarse sands with clay and silt intercalation and with locally gravel and boulders on the seabed (Fugro Engineers B.V., 2017).

- The geological development of the southern North Sea is dominated by periods of fluvial deposition and erosion during the Pleistocene. The Urk Formation and the Kreftenheye Formation occur at different stratigraphic levels having been deposited in different spatial positions across time (Fugro Engineers B.V., 2016).

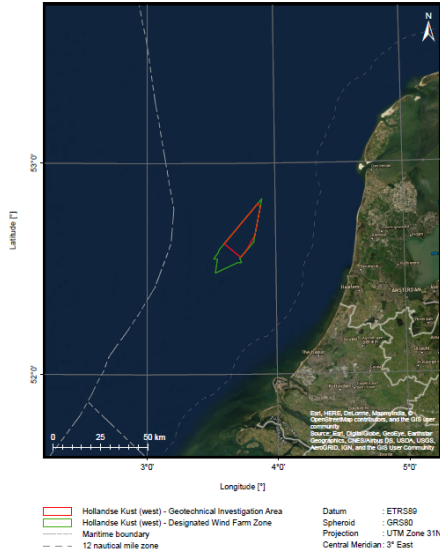


Figure 3.1: Project location HKW (Fugro Engineers B.V., 2020)



Figure 3.2: Project location HKN (Fugro Engineers B.V., 2019)

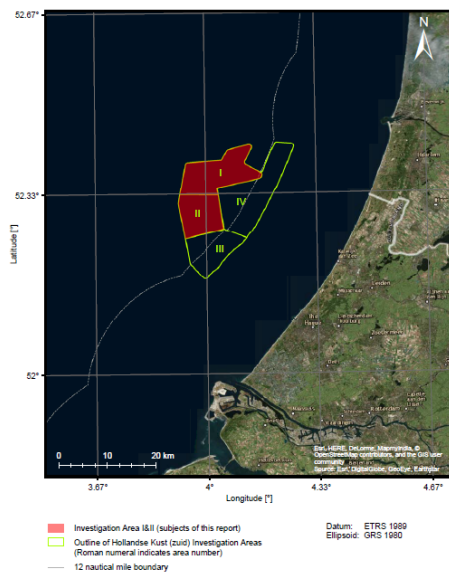


Figure 3.3: Project location HKZ I & II (Fugro Engineers B.V., 2017)

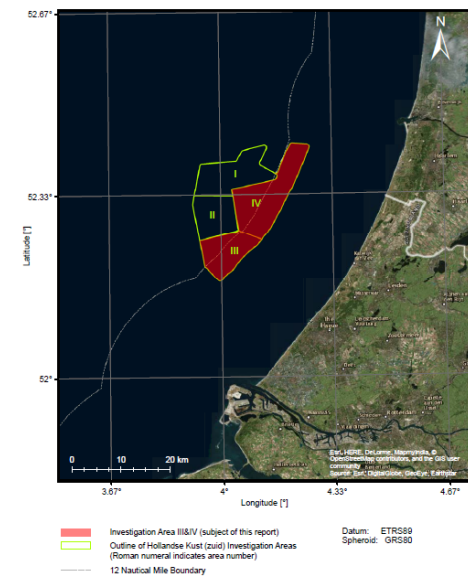


Figure 3.4: Project location HKZ III & IV (Fugro Engineers B.V., 2018)

3.2. Performed tests and sample preparation

This section describes the soil samples used for research and provides a closer look at the laboratory tests performed.

3.2.1. Soil samples for laboratory testing

For tests on coarse grained, cohesionless soil it is common to batch the material for laboratory testing. The reconstituted batch samples are performed from one or multiple borehole locations with a recommended small depth interval. In some cases, the batches are constructed from multiple boreholes due to limited availability from only one borehole. Then, the batched samples provide uniform soil material for each test series and sufficient material for laboratory testing for all tests. The selection of the material considered for batching has been performed based on the similarity in soil characteristics and on minimisation of the use of material from not too many different locations in one batch. Table 3.1 to Table 3.3 provide information of each project and for each batch, the information about the different locations and depths.

Table 3.1: Sample depths and locations for HKW

Batch number	Sample depth [m]	Location(s)
Batch 1	0.00 to 4.15	HKW053-BH
Batch 2	1.70 to 7.60	HKW053-BH
Batch 3	13.35 to 17.30	HKW107-BH
Batch 4	11.60 to 17.85	HKW065-BH
Batch 5	4.00 to 11.50	HKW016-BH
Batch 6	15.00 to 22.20	HKW016-BH
Batch 7	19.50 to 28.80	HKW112-BH
Batch 8	6.85 to 20.05	HKW062-BH
Batch 9	24.50 to 34.30	HKW062-BH
Batch 10	14.25 to 26.65	HKW038-BH

Table 3.2: Sample depths and locations for HKN

Batch number	Sample depth [m]	Location(s)
Batch 1	0.00 to 3.65	HKN25-BH
Batch 2	6.50 to 10.10	HKN25-BH
Batch 3	1.50 to 3.40	HKN27-BH
Batch 4	8.10 to 10.40	HKN39-BH
Batch 5	7.00 to 10.40	HKN19-BH
Batch 6	19.00 to 21.30	HKN21-BH
Batch 7	26.50 to 29.10	HKN26-BH
Batch 8	18.00 to 20.30	HKN37-BH
Batch 9	17.00 to 18.50	HKN47-BH

3.2.2. Cyclic Direct Simple Shear test results

Tests performed and analysed for this research are CSS tests. The CSS tests are performed according to the standard test method for consolidated undrained cyclic direct simple shear tests ASTM D8296-19, (ASTM International, 2019). This test method describes the specific equipment and testing procedures for the measurement of cyclic strength, the number of cycles to (initial) liquefaction and the cyclic properties of the soil after one dimensional consolidation.

The CSS test consists of different stages; a consolidation stage, a cyclic stage also called pre-shearing, a second consolidation stage and finally, the main cyclic loading is applied. The first cyclic stage is only applied for tests with pre-shear. These stages will be described below with the use of example test results. Examples are illustrated with the use of test results from Batch 8, test ID CSS49. Further details about tests results are included in the next section.

Table 3.4 shows details regarding the performed cyclic tests. Next, an explanation is given about the different stages and test conditions, like the difference of stress and strain-controlled testing but also about the application of pre-shear.

Table 3.3: Sample depths and locations for HKZ

Batch number	Sample depth [m]	Location(s)
Batch 7	5.00	HKZ2-BH21-SA
	33.30	
	37.00	
	53.30	
Batch 102	5.5	HKZ3-BH01-SA
	10.1	HKZ3-BH01-SA
	11.5	HKZ3-BH07-SA
	4.5	HKZ3-BH14-SA
	6.5	HKZ3-BH22-SA
	5.5	HKZ3-BH24-SA
	8.5	HKZ4-BH01-SA
	9.5	HKZ4-BH03-SA
	14	HKZ4-BH03-SA
	4	HKZ4-BH04-SA
	9	HKZ4-BH04-SA
	6.5	HKZ4-BH05A-SA
	9	HKZ4-BH05A-SA
	14	HKZ4-BH05A-SA
	5.5	HKZ4-BH06-SA
	10.2	HKZ4-BH07-SA
	4.5	HKZ4-BH09-SA
	13	HKZ4-BH09-SA
	4.5	HKZ4-BH10-SA
14.5	HKZ4-BH21-SA	
Batch 103	10.4	HKZ3-BH06-SA
	15	HKZ3-BH06-SA
	9	HKZ3-BH08-SA
	25.5	HKZ3-BH08-SA
	32.5	HKZ3-BH08-SA
	16.1	HKZ3-BH14-SA
	31	HKZ3-BH14-SA
	21	HKZ3-BH22A-SA
	25	HKZ3-BH22A-SA
	30	HKZ3-BH22A-SA
	21.3	HKZ3-BH24-SA
	24	HKZ4-BH03-SA
	28	HKZ4-BH04-SA
	34	HKZ4-BH04-SA
	30.5	HKZ4-BH05A-SA
	32.2	HKZ4-BH06-SA
	32	HKZ4-BH08-SA
	36	HKZ4-BH08-SA
	24.5	HKZ4-BH09-SA
	31.5	HKZ4-BH09-SA
39.8	HKZ4-BH09-SA	
32	HKZ4-BH10-SA	
42.8	HKZ4-BH21-SA	

- First consolidation stage. In this first stage of the test the sample is loaded in vertical direction to allow the sample to consolidate one-dimensionally. Every vertical load increment is maintained until excess pore water pressures are dissipated. As an example, Figure 3.5 shows a test result where the vertical load is increased until $\Delta\sigma_v$ becomes zero, this corresponds to dissipated excess porewater pressure.

Table 3.4: Details performed cyclic tests

Test Method	Accordance with test method ASTM D8296-19
Test Specimen	Coarse-grained cohesionless, reconstituted (batch sample)
Test conditions	No project-specific requirements
Specimen Saturation	Not applied
Consolidation	Vertical consolidation to estimated effective in- situ vertical stress conditions
Cyclic Pre-shear applied to a selection of specimens	<ul style="list-style-type: none"> - Constant vertical stress conditions - Reference stress: effective vertical consolidation stress - Loading frequency of 0.1 Hz (T = 10 s) - Two-way symmetrical cyclic loading with target average shear stress $\tau_{av} = 0$ - 400 cycles
Consolidation	<ul style="list-style-type: none"> - Re-consolidation of specimen after pre-shear stage (drainage of any excess pore pressure)
Cyclic Loading	<ul style="list-style-type: none"> - Constant volume conditions - Reference stress: effective vertical consolidation stress - Loading frequency of 0.1 Hz (T = 10 s) - two-way cyclic loading with target average shear stress $\tau_{av} = 0$

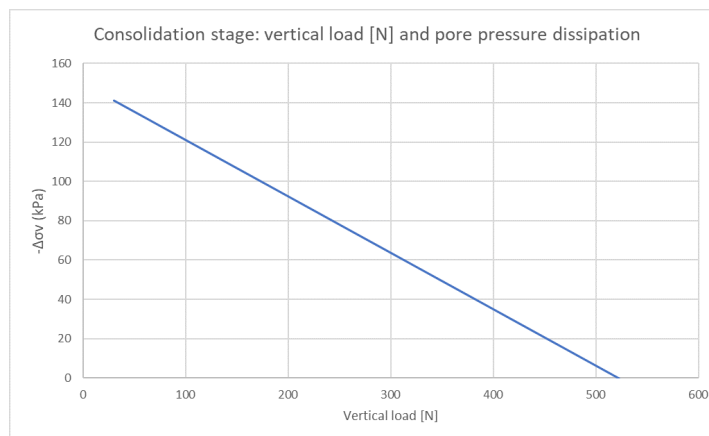


Figure 3.5: First consolidation stage, vertical load increment and dissipating pore water pressures

- Pre-shearing.

During pre-shearing of a soil sample, cyclic loading occurs with drainage during or after cyclic loading. For soil samples like cohesionless specimens, it is common and recommended to apply pre-shear because these are usually disturbed samples and commonly subjected to cyclic loading accompanied by drainage before and/or during the cyclic loading events. For undisturbed samples pre-shear may not be required because the effects of pre-shearing are still embedded in their fabric.

Usually, the pre-shear phase is applied after the consolidation stage where the sample is consolidated to a specified vertical stress. For offshore structures on (dense) sand the pre-shearing has typically been estimated to 400 cycles at a cyclic stress of $\tau_{cy}/\sigma'_{vc} = 0.04$. This is a load level that is estimated to occur during the accumulation period of a design storm or during storms before. Figure 3.6 shows the stress-strain graph for an example during pre-shearing. Figure 3.7 shows an example of the cyclic shear stress during pre-shearing.

- Second consolidation stage.

This second consolidation stage is applied to allow a full drainage of the sample.

- Cyclic loading stage.

This is the main cyclic loading stage of the test. The cyclic shearing can be performed as a stress-controlled or a strain-controlled test. The tests analysed for this research are based on stress-controlled tests.

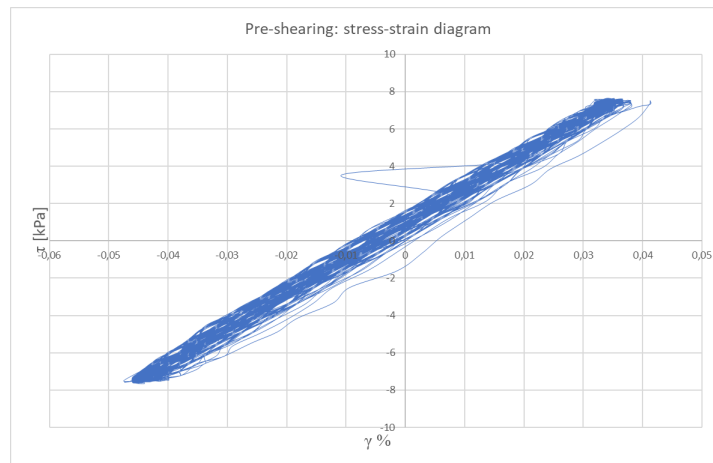


Figure 3.6: Stress-strain diagram, example test result during pre-shearing

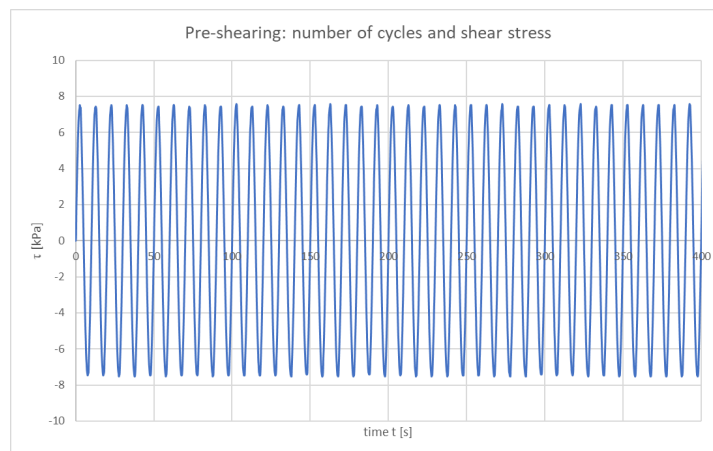


Figure 3.7: Number of cycles and shear stress, example test result during pre-shearing

In a stress-controlled test, the conditions are equivalent to the undrained condition of a saturated specimen and could therefore be seen as a good representation for cyclic events caused by offshore wind and wave loading. After completion of the consolidation stage and, if required, pre-shearing, a combination of average shear stress (τ_{av}) and cyclic shear stress (τ_{cy}) is applied to the sample. The constant volume condition is kept by varying the normal load that is applied to the sample or by blocking the displacement in the vertical direction. The change in vertical stress during a shearing stage can be related to the change in pore water pressure that usually occurs in tests under undrained conditions. A stress-controlled test does not mean that the stress is limited but that the strain is limited and that a specific stress level is applied. The sample will deform but keeps the same volume because no drainage of the sample is allowed.

In strain-controlled testing, the tests are performed with a specified constant cyclic shear strain by applying an average shear strain (γ_{av}) and cyclic shear strain (γ_{cy}). For these tests, the cyclic shear stress required to maintain the specified cyclic shear strain is measured.

An overview about which test is performed with or without pre-shearing is included in the next sections. A reason to perform tests with and without the pre-shearing is to observe possible differences in the outcomes. Additionally, two-way cyclic loading was applied to every test.

Figure 3.8 shows an example of the cyclic shear stress during the cyclic loading stage.

Figure 3.9 shows an example of the cyclic shear strain during the cyclic loading stage.

Figure 3.10 gives an example of the stress-strain diagram for an example during the cyclic loading stage.

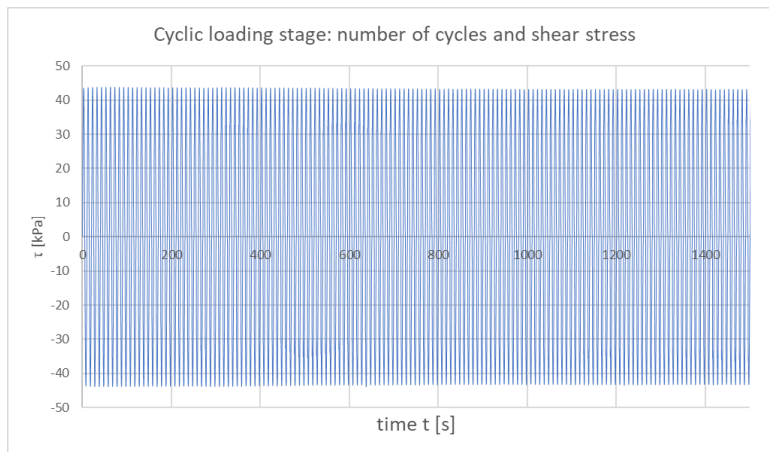


Figure 3.8: Cyclic loading stage, number of cycles and shear stress, example test result

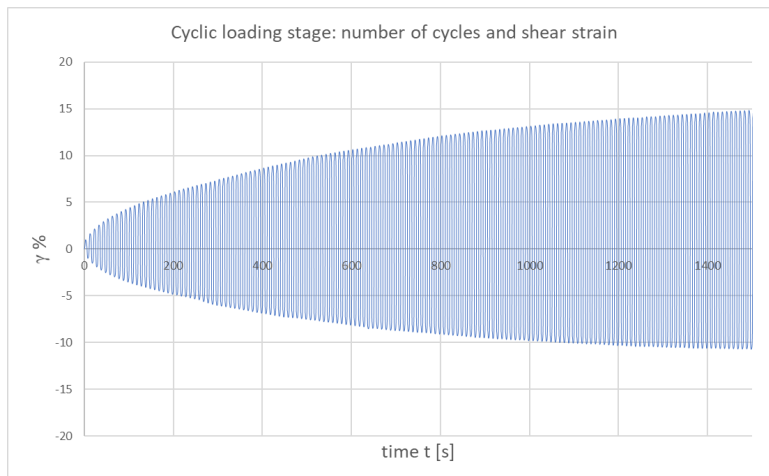


Figure 3.9: Cyclic loading stage, number of cycles and shear strain, example test result

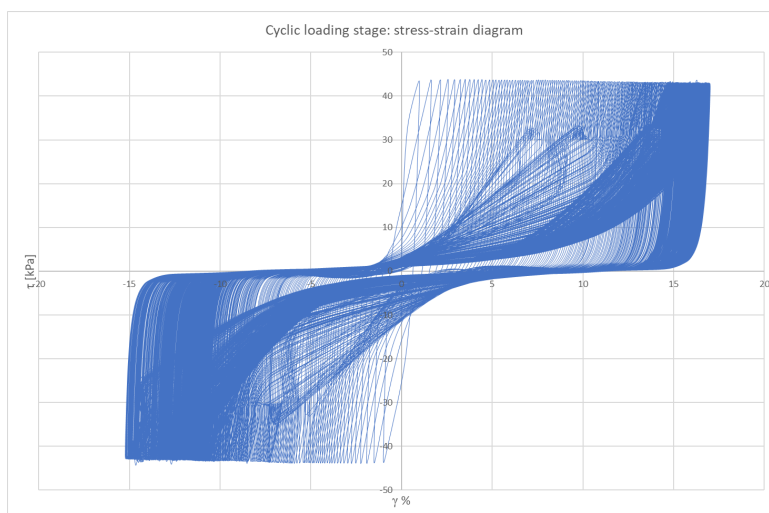


Figure 3.10: Cyclic loading stage, stress-strain diagram, example test result

3.3. Cyclic resistance curves

To present the results of the CSS tests cyclic resistance curves are developed. As described in Chapter 2, the principle of resistance curves is based on shear strain contour diagrams from cyclic tests. In these diagrams the cyclic shear strength will be presented as a cyclic stress ratio (CSR), where the cyclic shear stress is normalised with a vertical stress. The curves here are also presented in terms of a determined CSR against the number of cycles (N) required to reach a certain nominal shear strain level. To present the test results of the CSS tests this principle is used to construct failure lines for the different batch samples. As described in the previous section, the tests are performed in a stress-controlled manner, where a specific stress is applied to the sample. Different tests were carried out on samples from the same batch samples. If a sample did not reach the point of initial liquefaction, or did not fail within 1500 cycles, then the stress level was increased in the subsequent CSS test.

The following steps outline the data processing methodology that was followed to develop the cyclic resistance curves:

1. Make a collection of the different test results that are derived from the same sample batches, these results include the cyclic shear strength, τ_{cy} , and the vertical effective consolidation stress, σ'_{vc} .
2. To determine the CSR, a reference stress is determined following the approach of (Andersen, 2015).
3. Determination of the failure criterion for the nominal shear strain level.
4. Determination of the amount of cycles N to reach this nominal failure criterion.
5. The datapoints could give a failure line for the investigated sample batch.

3.3.1. Reference stresses

To determine the CSR, the vertical effective consolidation stress, σ'_{vc} , needs to be considered. (Andersen, 2015) found another interpretation of this CSR and stated that for sands and silts, the normalisation could be better performed with respect to a reference stress σ'_{ref} instead of a vertical effective stress.

The equation used to calculate a reference stress is given in Equation (3.1). It can be observed that by using a reference stress, a difference could be applied for static and cyclic strengths.

$$\sigma'_{ref} = P_a * \left(\frac{\sigma'_{vc}}{P_a} \right)^n, \quad (3.1)$$

where P_a is the atmospheric pressure (-100 kPa), σ'_{vc} is the vertical effective consolidation stress, n is an empirical exponent:

- n = 0.5 for undrained static strength of sand and silt.
- n = 0.9 for undrained static strength of clay.
- n = 0.9 for cyclic shear strength of sand and silt

3.3.2. Strain failure criterion

In Appendix A, tables are given with the number of cycles needed to reach strain levels from 0.10% to 15%. Based on these data the strain failure criterion is defined. For each tested batch sample a cyclic resistance curve is illustrated and there, it can be observed that the majority of the tests do not show failure within the applied 1500 cycles with 15% cyclic shear strain as a failure criterion. There could be state that the sample probably failed before the 15% cyclic shear strain and to obtain more accurate cyclic resistance curves, an alternative nominal (lower) failure criterion of cyclic shear strain is chosen. Different researches before chose for 7.5%, 5% or 3.75% as a common alternative strain failure level (Andersen, 2015), (Fugro Engineers B.V., 2020), (Wijewickreme & Sanin, 2004). This approach is described in ISO 199901-8, which does not specify an exact failure criteria for cyclic laboratory tests, but requires a selection of one.

Based on the data illustrated and analysed in Appendix A, a nominal failure criterion of 3.75% cyclic shear strain is chosen for future elaboration in this research. This specific value was, as described before, also chosen in previous research regarding these project locations and as can be observed from Appendix A also shows reasonable cyclic resistance curves.

3.3.3. Equivalent number of cycles

In the next diagrams the CSR is given for $(\tau_{cy,3,75\%}/\sigma'_{ref})_{N=10}$ with $\tau_a=0$. This means a cyclic shear stress ratio after 10 cycles. (Andersen, 2015) stated that a value of 10 load cycles would be representative as an equivalent number of cycles to minimise the effect of the number of cycles to failure in design approaches.

3.3.4. Results cyclic resistance curves

For selected test series, cyclic resistance curves are presented in the following graphs. These curves are generated using a best-fit power regression based on selected data points and expected trends. For each graph, the value of the determined CSR is given. This value is representative for 10 load cycles valid for a strain level of $\gamma_{cy} = 3.75\%$. For each trend, the power function is presented in the tables after each graph. With increasing stress levels and with an increasing CSR, cyclic resistance curves are constructed for each batch. If a series of test results did not show a clear trend, these results are not included in the graphs as a failure line. Details about the data to construct the cyclic resistance curves for each project are collected in Appendix B, Table B.1 to Table B.4.

Figure 3.11 presents the cyclic resistance curve for the tests for project location HKW, for the tests with pre-shear applied. For the batches 4 and 6 the resistance curve could be drawn. Batch 6 is observed to show higher CSR for a number of cycles lower than 10 cycles compared to the results of the other batch.

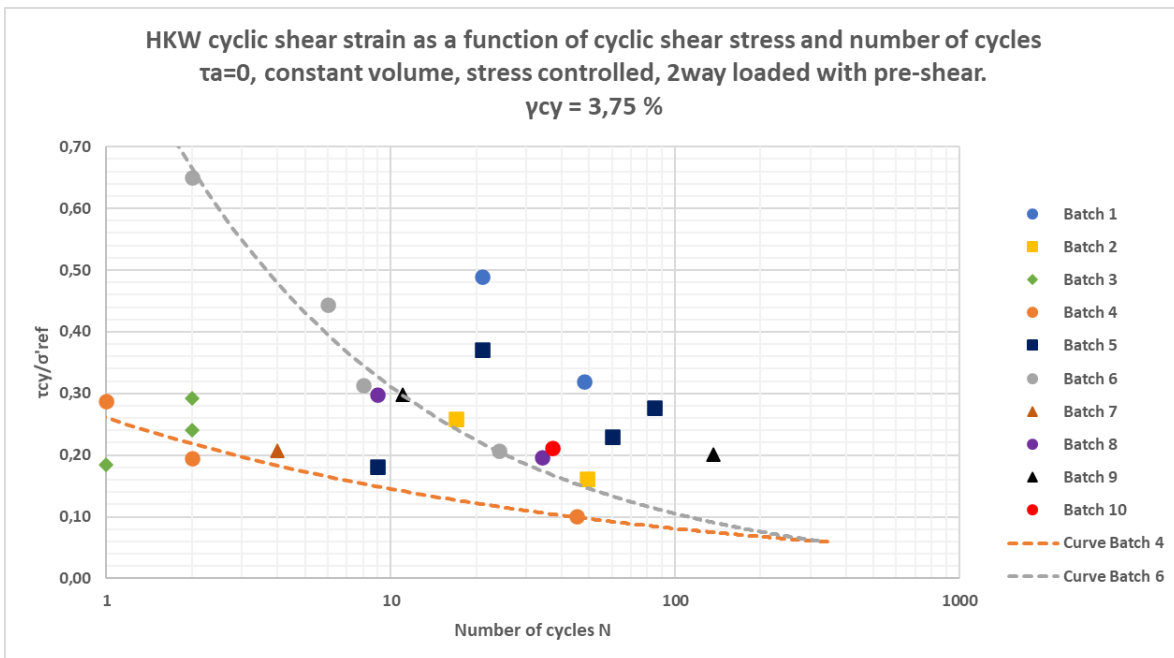


Figure 3.11: Cyclic resistance curve, project HKW, pre-shear

Table 3.5: Values of Cyclic Stress Ratio's observed from diagram, project HKW, pre-shear

Batch	Number of tests	Power function	$(\tau_{cy}/\sigma'_{ref})_{N=10}$
4	4	$y = 0,26x^{-0,25}$	0.15
6	4	$y = 0,92x^{-0,47}$	0.31

Figure 3.12 shows the cyclic resistance curve for the tests for project location HKW when no pre-shear was applied. For the batches 3 and 5 the resistance curve could be drawn. Batch 5 shows a higher value of CSR compared to batch 3 but in general the two tests do not show higher resistance compared to the tests results where pre-shear was applied.

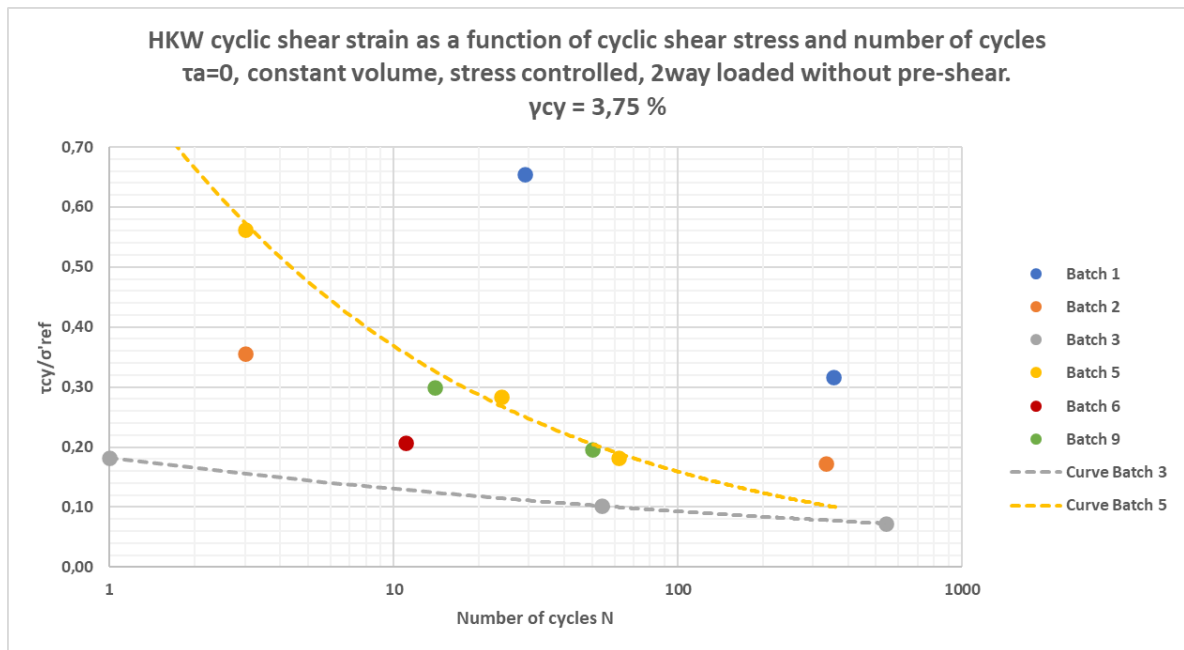


Figure 3.12: Cyclic resistance curve, project HKW, without pre-shear

Table 3.6: Values of Cyclic Stress Ratio's observed from diagram, project HKW, without pre-shear

Batch	Number of tests	Power function	$(\tau_{cy}/\sigma'_{ref})_{N=10}$
3	5	$y = 0,18x^{-0.15}$	0.13
5	5	$y = 0,86x^{-0.37}$	0.37

Figure 3.13 presents the cyclic resistance curve for the tests for project location HKN for tests where pre-shear was applied. For the batches 5, 6, 7, 8 and 9 the resistance curves could be drawn.

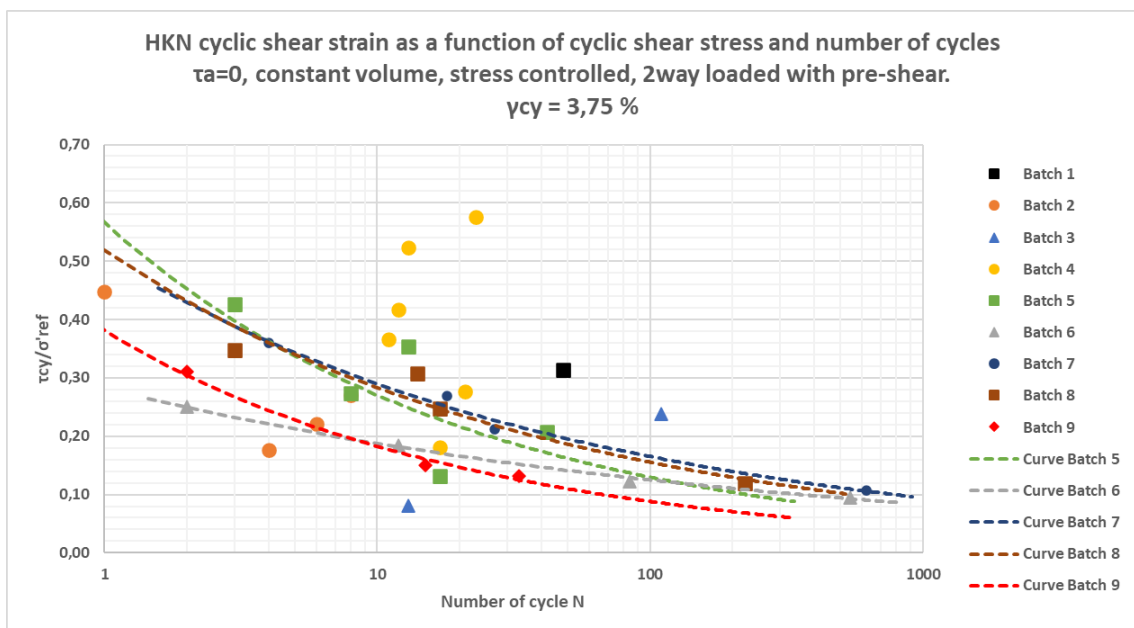


Figure 3.13: Cyclic resistance curve, project HKN, pre-shear

Table 3.7: Values of Cyclic Stress Ratio's observed from diagram, project HKN, pre-shear

Batch	Number of tests	Power function	$(\tau_{cy}/\sigma'_{ref})_{N=10}$
5	5	$y = 0,56x^{-0.32}$	0.27
6	4	$y = 0,28x^{-0.18}$	0.18
7	4	$y = 0,51x^{-0.24}$	0.29
8	4	$y = 0,52x^{-0.26}$	0.29
9	2	$y = 0,38x^{-0.32}$	0.18

Figure 3.14 presents the cyclic resistance curve for the tests for project location HKZ for tests where pre-shear was applied. For the batches 7, 102 and 103 the resistance curve could be plotted.

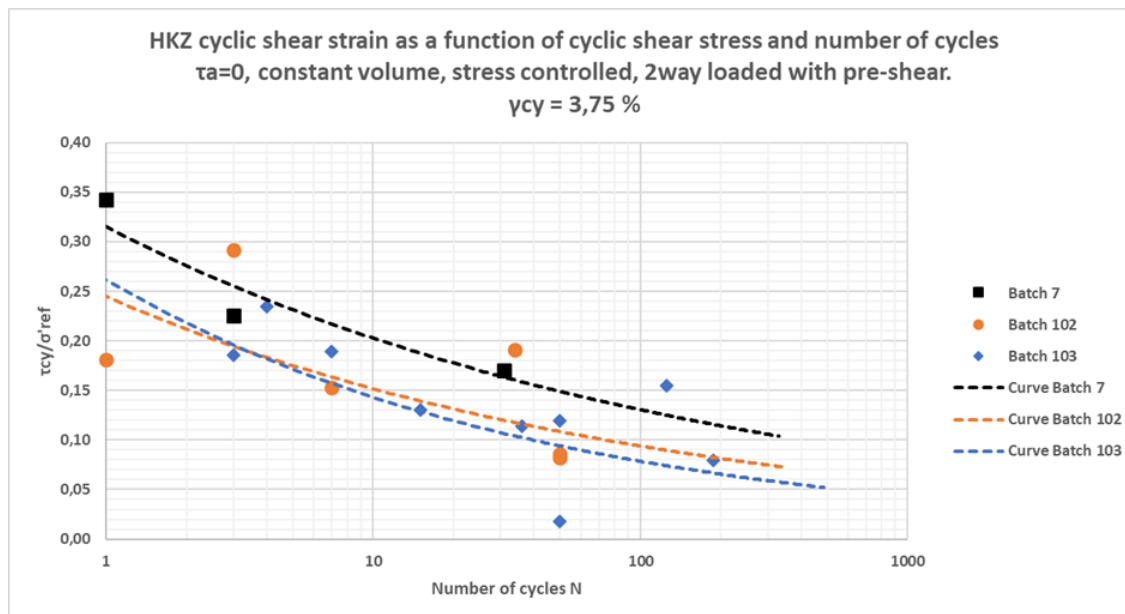


Figure 3.14: Cyclic resistance curve, project HKZ, pre-shear

Table 3.8: Values of Cyclic Stress Ratio's observed from diagram, project HKZ, pre-shear

Batch	Number of tests	Power function	$(\tau_{cy}/\sigma'_{ref})_{N=10}$
7	3	$y = 0.32x^{-0.19}$	0.21
102	6	$y = 0.24x^{-0.20}$	0.15
103	9	$y = 0.26x^{-0.26}$	0.14

3.4. Soil index parameters

The soil index parameters for all tests are sourced from different projects. Not every project features the same data or the tests were performed differently. The index parameters were collected for the samples for which the CSR was investigated in the previous section. The parameters that are elaborated for this research are based on characteristics compared to density of the soil, grain structure and in-situ characteristics. Based on this and previous research the following particular parameters are selected for further research:

- Relative density.
- Fines Content.
- Mean particle size.
- Normalised cone penetration resistance.

3.4.1. Relative density

The Relative density (D_r) is expressed as a relationship between the void ratio (e) of the sample (either in the laboratory or in-situ) and the limiting values e_{max} and e_{min} , representing the loosest and densest possible soil packing states, respectively. In these terms, the D_r of a soil in its densest possible state, when e is equal to e_{min} , is 1 or 100%. In its loosest possible state, when e is equal to e_{max} is 0:

$$D_r = \frac{e_{max} - e}{e_{max} - e_{min}} \quad (3.2)$$

Usually, the values of the densest possible state and the loosest possible state are directly measured in the laboratory. In this study, none of the tests in the database included a test to determine the minimum and maximum void ratios. Therefore, the D_r for the soil samples had to be calculated in an alternative way.

As an alternative, the initial void ratios (e_0), which are actually measured, are determined from the CSS tests to observe or explain some correlations later with the cyclic strength. In this case the maximum and minimum void ratios are considered to be the same for all North Sea sands analysed in this research.

The initial void ratio (e_0) is based on the following equation:

$$e_0 = \frac{AH_0 - V_S}{V_S}, \quad (3.3)$$

where A is the cross-sectional area, H_0 is the initial sample height and V_S is the volume of the soil particles.

This parameter is calculated in a consistent way for all tests and should be considered as comparable. For the third project, HKZ, it could already be observed that the batches used in the CSS tests, consisted of reconstituted samples from several different locations. Therefore, for this thesis, the D_r is not calculated. Observed values for the initial void ratio are given in the Table 3.9.

An alternative approximation to determine the D_r is to use information measured directly from the field out of in-situ tests from cone penetration test (CPT) data. The D_r is measured along depth and is directly correlated with the normalised cone resistance (Q_{tn}). This provides information about in-situ values of the density of the soil. Note that this approach actually only works for undisturbed samples but is applied as an alternative to give an approximation of the original D_r .

The theory behind this CPT correlated determination is described in the Robertson guide for cone penetration tests and based on the simplified version of Kulhaway and Mayne (1990).

Kulhaway and Mayne (1990) suggested a simpler relationship for estimating the relative density:

$$D_r^2 = \frac{Q_{tn}}{305Q_cQ_{OCR}Q_A}, \quad (3.4)$$

where Q_{tn} is the normalised CPT resistance, Q_c the compressibility factor and ranges from 0.90 (low compression) to 1.10 (high compression), Q_{OCR} Over consolidation factor = $OCR^{0.18}$, Q_A Aging factor = $1.2 + 0.05 \log(t/100)$.

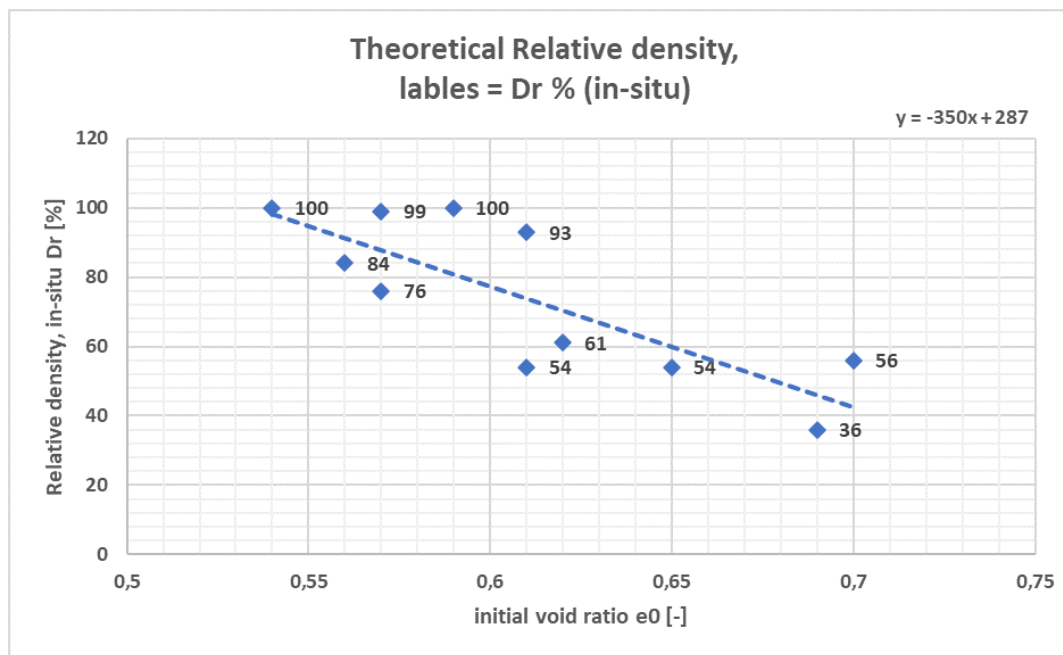
Assuming the connection factors are approximately 1, the relationship can be written as a first approximation as:

$$D_r^2 = \frac{Q_{tn}}{350}. \quad (3.5)$$

This D_r is directly measured along depth and was used as reference for the batches taken over the corresponding depth interval. Observed values for the D_r based on this in-situ approximation are also presented in the Table 3.9.

The uncertainty of the values is high. This, because in the laboratory the soil samples that were investigated were batches of sand that were reconstituted. This means that they are distributed and that the real characteristics from in-situ conditions cannot be observed anymore. Based on the in-situ measured values of the D_r and the initial void ratio measured in the laboratory, a theoretical relative density is determined. This gives a theoretical correlation that gives the void ratio range as a function of the D_r range. The theoretical correlation can be used to infer the D_r of a batch sample. i.e. the theoretical correlation can be used to assign through the void ratio in the lab the corresponding theoretical relative density. Values that can be observed from the equation of the theoretical relative density will be used for further elaboration in this research in the next chapter.

Figure 3.15 shows the relation between the in-situ based approximation of D_r and the initial void ratio measured in the laboratory. Observed values for theoretical relative density are also presented in Table 3.9.

Figure 3.15: Theoretical Relative density D_r [%]Table 3.9: Values of Relative density D_r % for different sand batches

Project	Batch	Depth range	e_0 [-]	D_r , in-situ [%]	D_r , theoretical [%]
HKW	3	13.35-17.30	0.70	56	42
HKW	4	11.60-17.85	0.62	61	70
HKW	5	4.00-11.50	0.61	94	74
HKW	6	15.00-22.20	0.57	99	88
HKN	5	7.00-10.50	0.59	100	81
HKN	6	19.00-21.30	0.69	36	46
HKN	7	26.50-29.10	0.56	84	91
HKN	8	18.00-20.30	0.65	55	60
HKN	9	17.00-18.50	0.54	100	98
HKZ	7	Several depths	0.64	-	63
HKZ	102	Several depths	0.57	-	88
HKZ	103	Several depths	0.62	-	70

3.4.2. Particle size distribution

The particle size distribution (PDS) curves are presented for the different soil batches selected in the previous section. A PSD curve is derived before testing and can be used for comparing and classifying different granular soils. Additionally, basic soil parameters can be determined from these curves.

A coarse-grained material is characterised primarily by its particle size distribution, which contributes in following different aspects of the soil behaviour, including e.g. hydraulic conductivity and shear strength. The PSD can be described in a symmetric way by means of few scalar parameters, given the uniformity of the samples grading, here the D50 and the fine content were chosen as representative.

3.4.2.1 Fines content

To know the effect of the fines content (FC) towards the cyclic strength of the soil, the FC is determined for the selected sand batches from the previous chapter. The FC is determined based on information from PSD data and corresponds to the percentage of clay and silt in the soil sample. From the analyses it can be concluded that the FC for the soil samples is particularly low (mostly around 5% or lower). There are some higher values obtained around the 20% FC and a higher value of 56.5%. The effect of these higher values towards the cyclic strength is observed later. The Fines content FC% for different sand batches are presented in Table 3.10.

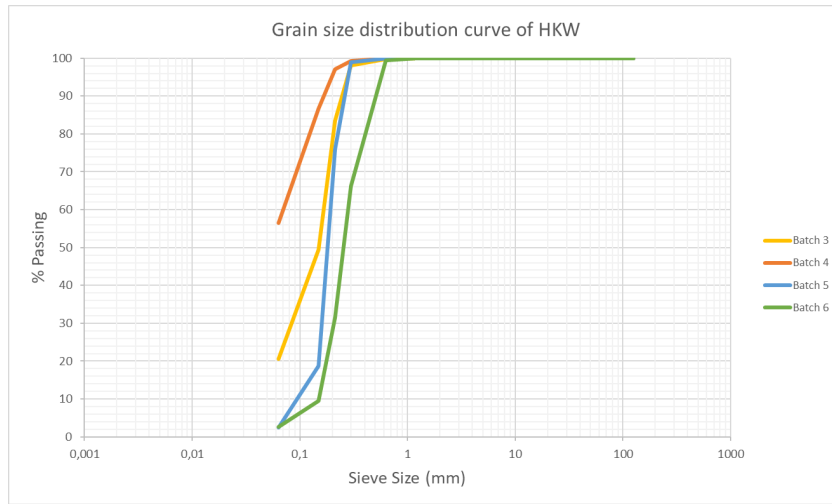


Figure 3.16: Grain size distribution curves (project HKW)

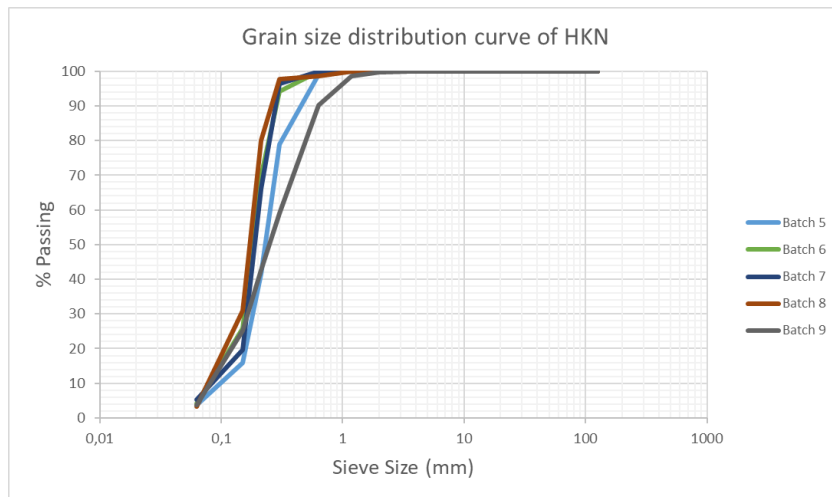


Figure 3.17: Grain size distribution curves (project HKN)

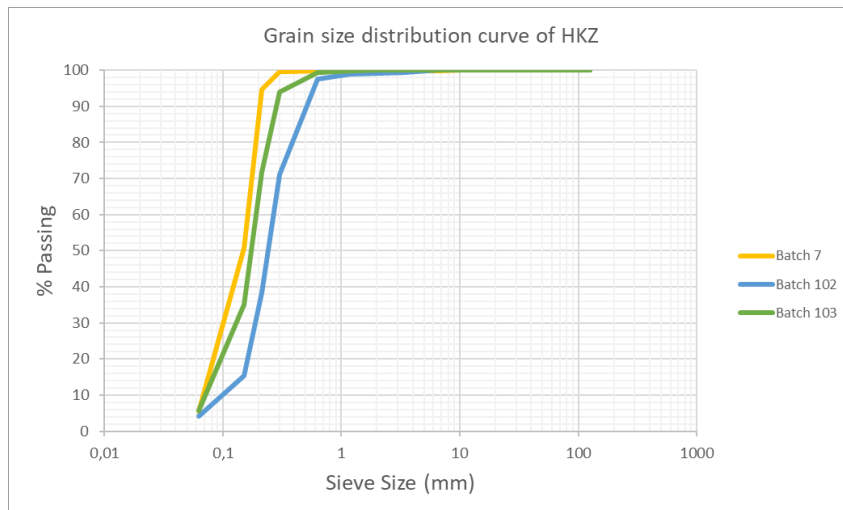


Figure 3.18: Grain size distribution curves (project HKZ)

3.4.2.2 The mean particle size and uniformity

The particle size corresponding to any specified percentage value can be read from the particle size distribution (PSD) curves. The particle size analysis is done based on the PSD diagrams given in this section. From these diagrams the particle sizes below 60%, 50% and 10% of the soil weight known as the values D60, D50 and D10, respectively, could be analysed. D50 represents the mean particle size and the D60 and D10 are used to obtain the coefficient of uniformity (Cu).

D50 means a cumulative of 50% passing particle size. D10 and D60 can be defined in a similar way. The size D10 is defined as the effective size. The equation to derive the coefficient of uniformity (Cu):

$$C_u = \frac{D_{60}}{D_{10}}. \quad (3.6)$$

The general slope and shape of the distribution curve can be described by means of the coefficient of uniformity (Cu). The higher the value of the coefficient of uniformity, the larger the range of particle sizes in the soil.

Table 3.10 gives a summary of the values for D50, D60, D10, and the coefficient of uniformity (Cu). Some values could not be defined from the graphs. Similar values were shown for the different batches in this research. Also, the Cu values are low and comparable between the samples. The values or the Particle size analysis for different sand batches is presented in Table 3.10.

Table 3.10: Values of Relative density Dr% for different sand batches

Project	Batch	D50 [mm]	D60 [mm]	D10 [mm]	Cu [-]	FC [%]
HKW	3	0.15	0,17	-	-	20.5
HKW	4	-	-	-	-	56.5
HKW	5	0.18	0,19	0,09	2.05	2.5
HKW	6	0.26	0,28	0,15	1.86	2.6
HKN	5	0.23	0,25	0,10	2.54	3.0
HKN	6	0.18	0,20	0,08	2.47	4.0
HKN	7	0.19	0,20	0,08	2.42	4.0
HKN	8	0.17	0,18	0,08	2.37	5.0
HKN	9	0.25	0,31	0,08	3.79	3.0
HKZ	7	0.15	0,16	0,07	2.35	3.0
HKZ	102	0.24	0,27	0,10	2.70	5.0
HKZ	103	0.17	0,19	0,07	2.65	4.0

3.4.3. In-situ parameters

The normalised cone resistance (Qtn), also called the corrected cone resistance, is included in the study because it allows establishing a link with the in-situ situation and to obtain possible correlations with the cyclic strength. The Qtn is, as described before, directly correlated with the Dr and is therefore calculated in the same way. The Qtn, is the cone resistance expressed in a non-dimensional form considering the in-situ vertical stresses and where the stress exponent (n) varies with soil type and stress level. When n is equal to 1, Qtn = Qt.

$$Q_{tn} = \left(\frac{q_t - \sigma_{v0}}{P_{a2}} \right) \left(\frac{P_a}{\sigma_{v0}} \right)^n, \quad (3.7)$$

$$Q_t = \left(\frac{q_t - \sigma_{v0}}{\sigma'_{v0}} \right), \quad (3.8)$$

where n = 0.5.

The values of the Qtn are given below, see Table 3.11. These values are directly measured along depth as well and based on the depth interval of the batches. The determined Qtn is an average along this depth interval.

Table 3.11: Measured Normalised cone resistance (Q_{tn}) for different depth intervals

Project	Batch	Depth range	Q_{tn}	Dr, in-situ [%]
HKW	3	13.35-17.30	105	56
HKW	4	11.60-17.85	102	61
HKW	5	4.00-11.50	293	94
HKW	6	15.00-22.20	350	99
HKN	5	7.00-10.50	418	100
HKN	6	19.00-21.30	36	36
HKN	7	26.50-29.10	229	84
HKN	8	18.00-20.30	91	55
HKN	9	17.00-18.50	436	100
HKZ	7	Several depths	139	-
HKZ	102	Several depths	271	-
HKZ	103	Several depths	172	-

3.5. Conclusion after elaboration and assessment of available dataset

The database analyses performed on the different sites provide important data on the soil engineering parameters. Based on this information cyclic strength correlations with soil index parameters will be presented and discussed in the next chapter. As a result of elaboration of the available data the following observations are assumed:

- From the project HKZ, it can be observed that the batches consist of several different locations and at different depths. Therefore, obtaining data from in-situ tests at these depths comes with high uncertainty. From the PSD diagrams it can be concluded that the samples are comparable. Then, sample based parameters could be determined based on this information.
- The laboratory tests performed for this research are executed in the same way and are therefore assumed to be comparable with each other.
- A difference between tests is if pre-shear was applied. If this will have an influence of the cyclic strength can be observed in the next chapter where the correlations are given.
- Uncertainty arises in determining the Dr of each sand batch. The Dr of a soil is a term generally used to describe the degree of compaction of coarse-grained soils. The maximum and minimum possible void ratios of the sample are measured in the laboratory. However, among the available tests none of the results included measured maximum and minimum possible void ratios. To infer the Dr, a procedure based on CPT data is suggested.
- An assumption is made that North Sea sands would have comparable void ratios in minimum and maximum compaction. These were determined for each soil sample, assuming that the range of void ratios investigated in the laboratory was representing the Dr range in the field.
- Based on the in-situ measured values of the Dr and the initial void ratio measured in the laboratory, a theoretical relative density is determined. The theoretical correlation can be used to assign through the void ratio in the lab the corresponding theoretical relative density. Values that can be observed from the equation of the theoretical relative density will be used for further elaboration in this research in the next chapter.

4

Study on the correlations between index parameters and the cyclic shear strength

In this fourth chapter, the results of the correlations between various soil classification and state parameters and the cyclic shear strength, τ_{cy} , of the analysed data from the previous chapters, are presented. The cyclic shear strength is presented for the test material, North Sea sands at 10 load cycles as a function of relative density and grain structure. To correlate with the in-situ conditions, a comparison with the normalised cone resistance (Qtn) is made.

The cyclic resistance curves obtained in the previous chapter are relatively based on a small amount of datapoints and therefore the uncertainty of the actual obtained curves is increased. Because of this, in this chapter the correlations of the soil parameters towards the cyclic shear strength will be analysed by using the difference in soil characteristics. Possibly, also other factors might influence the shape of the resistance curves. Based on observations and expectations, a suggestion of a probably more accurate approximation of the failure lines is given. The difference could be explained in comparison with density of the soil, grain structure and in-situ characteristics.

First an overview of the obtained details about the test results is given. These results include the CSR at 10 load cycles as well as the observed soil parameters. Then the correlations between the CSR and the different soil parameters are given. These correlation graphs are a direct observation from the observed values including an analysis of the resistance curves itself. The values of the resistance curves are further elaborated to see if this could give a better interpretation of the observed correlations. Other influences are explored if needed, e.g. looking at $N = 100$ load cycles instead of only looking at $N = 10$, as it was chosen as an equivalent number of cycles.

4.1. Details about test results

The correlation results are based on the following assumptions and observations:

- The cyclic shear strength, τ_{cy} , is calculated at 10 load cycles.
- The cyclic shear strength, τ_{cy} , is normalised with a reference stress, σ'_{ref} , and termed as cyclic stress ratio (CSR) calculated according to equation (3.1).
- The tests are evaluated based on a nominal failure strain criterion of $\gamma_{cy} = 3.75\%$.
- All sample-based soil parameters are determined after consolidation.

The results are collected in Table 4.1. For each batch the CSR at 10 load cycles is obtained from the cyclic resistance curves. This is done based on a failure at a nominal strain failure criterion for each batch. The soil classification and state parameters were derived in the previous chapter. The values for the $D_{r,th}$ and the Qtn for the third project location, HKZ are determined based on a theoretical curve and are approximations of the real values which are unknown in this research. The batches are given a simplified label number instead of the official batch name and project location. Batch results 1 and 5 are derived without pre-shear.

Table 4.1: Collected details for correlation graphs

Batch	Project + Batch ID	$(\tau_{cy}/\sigma'_{ref})_{N=10}$	Dr %	Dr, th %	$e_0[-]$	FC %	D50 [mm]	Cu[-]	Qtn [-]
1.	HKW 3	0.13	56	42	0.70	20.5	0.15	-	105
2.	HKW 4	0.15	61	70	0.62	56.5	-	-	102
3.	HKW 5	0.37	94	74	0.61	2.5	0.18	2.05	293
4.	HKW 6	0.31	99	88	0.57	2.6	0.26	1.86	350
5.	HKN 5	0.27	100	81	0.59	3.0	0.23	2.54	418
6.	HKN 6	0.18	36	46	0.69	4.0	0.18	2.47	36
7.	HKN 7	0.29	84	91	0.56	4.0	0.19	2.42	229
8.	HKN 8	0.29	55	60	0.65	5.0	0.17	2.37	91
9.	HKN 9	0.18	100	98	0.54	3.0	0.25	3.79	436
10.	HKZ 7	0.21	-	63	0.64	3.0	0.15	2.35	139
11.	HKZ 102	0.15	-	88	0.57	5.0	0.24	2.70	271
12.	HKZ 103	0.14	-	70	0.62	4.0	0.17	2.65	172

4.2. Presentation of the results

In this section the correlation graphs are given for each soil parameter. In previous research a collection of datapoints to observe trends in scatterplots was usually based on the range in FC or Dr. This approach is also followed in this section to make an approximation of the cyclic correlations between soil parameters and the CSR. The graphs in this section give the correlation of the individual soil parameter with the observed CSR and give an analysis about applicability of the data. Besides this, the same correlation is made visible after a further elaboration of the cyclic resistance curves. In this elaboration is analysed what could influence the cyclic resistance curves and if possible a better approximation of this curves is given what might show a better interpretation for the observed correlations.

4.2.1. Further elaboration of cyclic resistance curves

Appendix C provides an analysis of the previously derived resistance curves. As mentioned before, the cyclic resistance curves are relatively based on a small amount of datapoints and therefore make the actual value at $N = 10$ more uncertain. The shape of the curves is explained and when possible a better interpretation of the failure line is given based on the observed soil parameters or other factors that could be explained based on the available information about the performed tests. Conclusions about this analysis are included in the conclusions of this chapter. The elaboration show the influence of the FC and the Dr on the slope and position of the cyclic resistance curves. These observations are used in the analysis for the correlations with the different soil index parameters in the following sections.

4.2.2. Correlation with the Fines content

Figure 4.1 shows a correlation graph of the FC towards the CSR at both $N = 10$ and $N = 100$ cycles. Another value of N besides the commonly chosen value of 10 is applied to investigate the shape of the failure lines to observe a possible better approximation of the possible spreading of the values in the plot. Only the correlations are shown with the values obtained after the analyses of the resistance curves done in Appendix C.

The influence of the different values of N does not lead directly to another observation within this small range of FC. The clustering of the data points suggest that the observed values for the CSR are higher in general for a lower N . This also applies for the power function trendlines that are drawn as failure lines. The range of the FC within this research is smaller than expected to give a reasonable observation about possible trends or correlations with the CSR. Most of the observed FC values are 5% or lower with some higher values of 20.5% and 56.5%. The higher values differ considerably from the other observed FC. Therefore, the higher values are not included in the graphs.

A correlation could be not observed within this small range of FC. It is remarkable that for same values of FC different values for CSR are observed. This observation is visible at FC values of 3%, 4% and 5%. Consequently, a reason for this small difference in observed CSR could not be explained within this small range.

A decrease in shear strength would have been expected by an increment of FC. An increment of fines means that the fine particles will occupy the space between the coarse particles (Alshameri, B. et al., 2017). This decreases the friction surface between coarse particles and therefore would decrease the shear strength

(Alshameri, B. et al., 2017). The data shows a small range of fines content around 5% or lower so a decrease in shear strength could not be observed.

From the elaboration in Appendix C is observed that the FC influences the cyclic resistance curves in a way that it effects the position of the failure line. An increment of fines would lead in this sense to lower values of CSR.

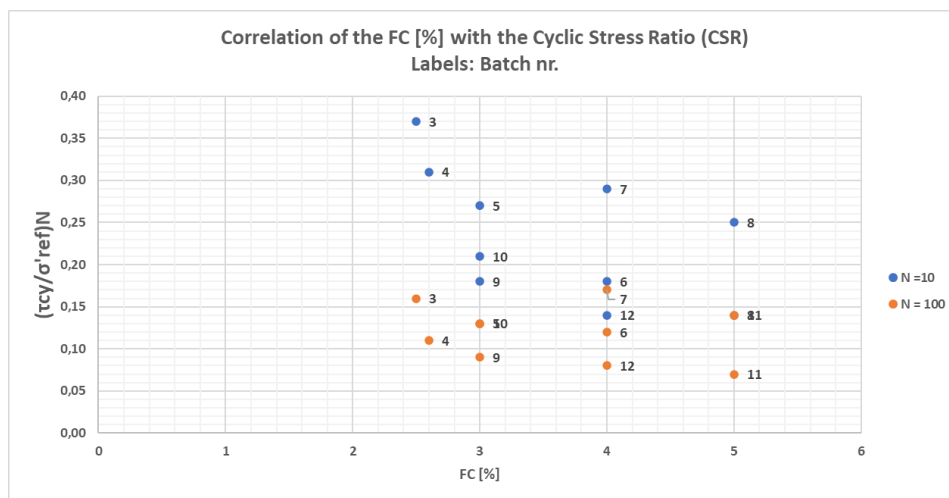


Figure 4.1: Correlation of the FC [%] with the Cyclic Stress Ratio (CSR) at N = 10 and N = 100, labels = Batch nr.

4.2.3. Correlation with the Relative density

As described in Chapter 3, a theoretical D_r is calculated based on the values of the initial void ratio, e_0 , measured in the laboratory and the D_r measured in-situ. Following this approach, the expected values for the D_r for the tested batches of project location HKZ are also approximated.

Figure 4.2 gives the correlation of the D_r with the CSR. The graph do not show a clear correlation. The strong increase of the resistance against shear, as expected form previous research is not visible in this graph.

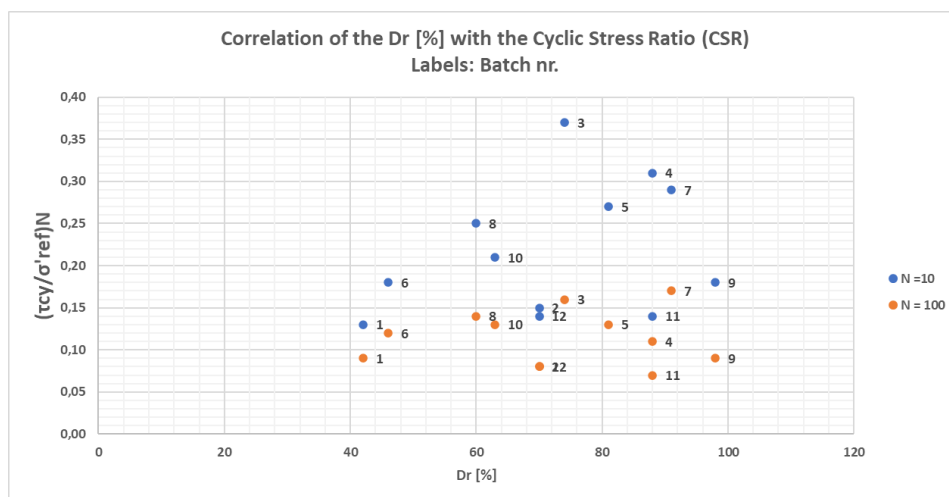


Figure 4.2: Correlation of the D_r [%] with the Cyclic Stress Ratio (CSR) at N = 10 and N = 100, labels = Batch nr.

From the elaboration in Appendix C is observed that higher values of D_r show a steeper slope of the cyclic resistance curves. An increment of D_r would lead in this sense to higher CSR values.

Figure 4.3 illustrates the observed values for D_r in combination with observations from previous research done by (Andersen, 2015). In combination with these curves can be observed that the values corresponding with N = 10 follow the observed trends. The vertical axis is a logarithmic scale.

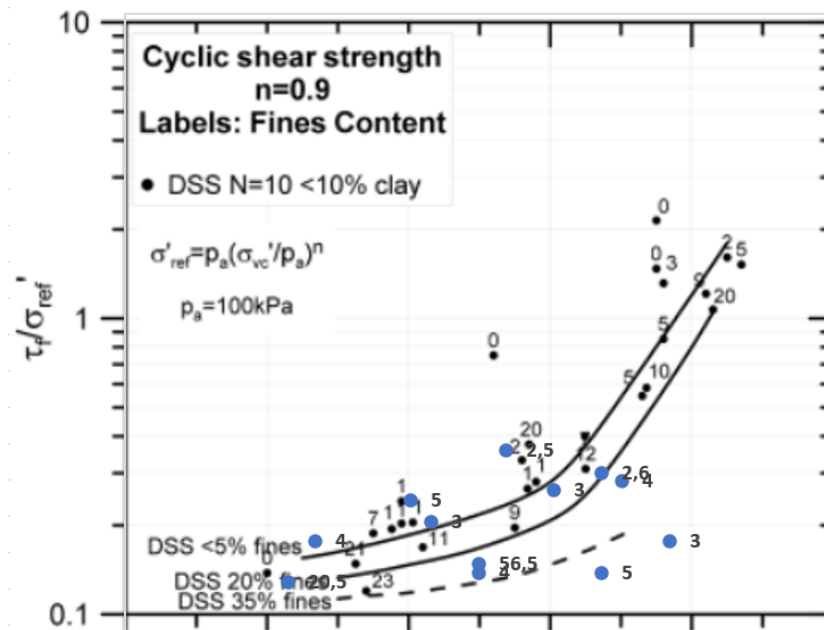


Figure 4.3: Observed values for Dr [%] in combination with earlier observations found by (Andersen, 2015) , labels = FC [%]

4.2.4. Correlation with the mean particle size

Figure 4.4 show the correlation of the D50, mean particle size, with the CSR. Within this data range a high scattering could be observed. The D50 is, as mentioned before, the diameter for which 50% of the particles in a soil sample are finer, i.e., related to the particle size in a sample that one half of all particles is larger and the other half is smaller than the D50 value. Therefore, for small values of D50, the soil skeleton is mostly constituted of small particles. This means that the voids are occupied by a large number of small particles with similar orientation (Harehdasht, S.A. et al., 2018).

For larger values of D50, the soil skeleton is not dominated by small particles, but the voids are confined by a limited number of larger particle pairs (Harehdasht, S.A. et al., 2018). Because an increment in FC is expected to lead to a decrease in shear strength, an increase in shear strength could be expected for increasing values of D50.

For the analysed test material, the range of the FC is low and therefore a correlation could not be checked.

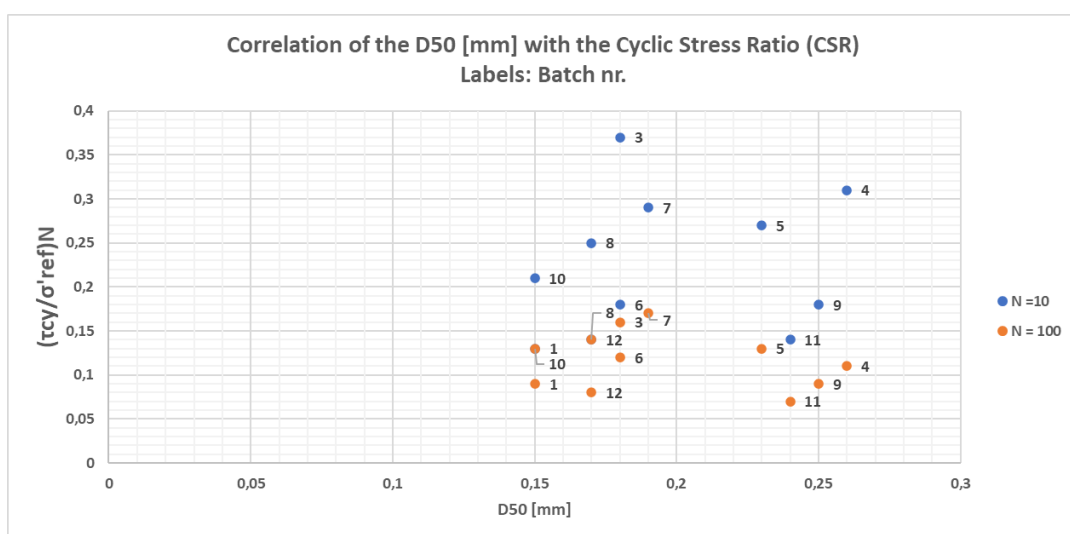


Figure 4.4: Correlation of the D50 [mm] with the Cyclic Stress Ratio (CSR) at N = 10 and N = 100, labels = Batch nr.

4.2.5. Correlation with the Normalised cone penetration resistance

Figure 4.5 shows the correlation of the Q_{tn} , normalised cone penetration resistance, with the CSR. This graph shows high scattering. A higher cone resistance in-situ would be expected to correspond to a higher resistance in soil behaviour in shear. Additionally, a higher relative density could be correlated with an increasing cone resistance. In the results found by (Robertson, 2010), an increasing CSR is shown for increasing Q_{tn} . However, these values for Q_{tn} are below 100. The data in this research consist of larger values of Q_{tn} . The proposed trend of rapidly increasing resistance against shear is not observed. As mentioned in the previous chapter, the Q_{tn} and the D_r are related to each other. However, in this thesis the batch samples are disturbed and there is no direct relationship observable anymore between the batch and the original in-situ characteristics.

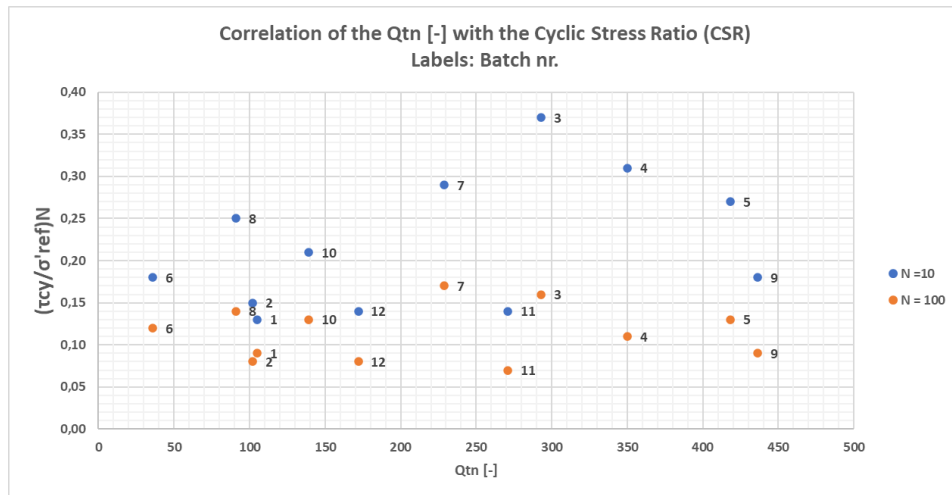


Figure 4.5: Correlation of the Q_{tn} [-] with the Cyclic Stress Ratio (CSR) at $N = 10$ and $N = 100$, labels = Batch nr.

4.3. Conclusion after study on the correlations between index parameters and the cyclic shear strength

This section includes the conclusions regarding the study on the correlations between index parameters and the cyclic shear strength. The following can be assumed:

- The correlation graphs are based on the values obtained from cyclic resistance curves. The cyclic resistance curves are based on a relatively small amount of datapoints and therefore make the actual value at $N = 10$ cycles more uncertain.
- In an elaboration about the obtained resistance curves, the shape of these curves is explained based on the determined soil parameters and if possible a better interpretation of the failure lines is given.
- From the further elaboration of the resistance curves it could be assumed that:
 - From the index parameters observed in this research, the FC and D_r have an influence on the shape of the resistance curve.
 - A higher value of the D_r shows a higher slope and therefore a steeper failure line in comparison with lower D_r values.
 - The FC influences the vertical position of the resistance curve. As different values lead to higher or lower values for CSR, this means that batch samples with the same D_r value can show the same shape of the failure line. However, the influence of the FC leads to different positions of the failure lines. The C_u also show a small influence of the position of the line in one of the projects. An increase of this value would lead to lower CSR values, although this was not visible in all project data.
- Clear correlations between index parameters and the cyclic shear strength could be not observed. The following observations are made for each soil parameter:

- The range of the FC is lower than expected. Only values of 5% or lower are observed. Within this small range it is not possible to give a conclusion about the influence of the FC towards the shear strength at both $N = 10$ or $N = 100$ cycles. From previous research, a decrease in shear strength was expected by an increment in FC. This trend could be not observed because of the small range in FC. However, this observation was visible in the resistance curves where higher values of FC show lower values of CSR in comparison with results from other batches.
 - The graph with observed D_r and the cyclic shear strength does not show a correlation. From previous research the expected trend was a high increase of the CSR by increasing D_r . However, in combination with curves from previous research can be observed that the values corresponding with $N = 10$ follow the observed trends.
 - The mean particle size, D_{50} , does not show a correlation with the CSR. An increase in shear strength was expected for increasing values of D_{50} . For the analysed test material, the range of the FC is low and therefore a correlation could not be checked.
 - To correlate with the in-situ conditions, a comparison with the normalised cone resistance (Q_{tn}) was made. The correlation graph with this parameter shows high scattering. A higher cone resistance in-situ would be expected to correspond to a higher resistance in soil behaviour in shear, but an increase of CSR by an increment of the Q_{tn} was not observed.
- The correlations and observations about the test results are based on a small amount of data. To improve the outcome, a larger range of test results is needed but also data that consist of a larger range of FC and D_r values. This will lead to a more accurate observation about correlations with the cyclic shear strength.

5

Conclusions and Recommendations

This final chapter addresses the conclusions and discussion of the research for different aspects of the project regarding the formulated research questions. Firstly, general conclusions and discussions are given about the observed correlations and influences of the index soil parameters with the cyclic shear strength. At the end of this chapter, recommendations to improve the research outcome and suggestions for further research are discussed. The main objective of this Master thesis is to provide correlations between the index parameters and the cyclic simple shear strength. These are based on the CSS test results of sands performed for offshore wind monopile foundation design.

5.1. Conclusions

This section includes a conclusion and discussion regarding the formulated research questions. The main research question of this thesis was:

"What is the relationship between soil index parameters and the cyclic simple shear strength based on test results of undrained Cyclic Direct Simple Shear (CSS) tests in sands?"

The scope of this research was focused on sandy material from the North Sea and the tests results of undrained CSS tests performed on the test material from offshore windfarm locations.

1. *Are the sample conditions of the CSS tests comparable, and are the tests performed in a comparable way?*

In this research, only test results from the CSS tests are analysed. An elaboration and assessment about the available dataset were performed.

The test material, and therefore the test results are from three different locations in the North Sea, labelled as Hollandse Kust West (HKW), Hollandse Kust Noord (HKN) and Hollandse Kust Zuid (HKZ). The test material was reconstituted in batch samples performed from one or multiple borehole locations. Concerning these borehole locations, the test material from project location HKZ comes from several locations at different depths. This makes the sample conditions less comparable with the batch of samples provided from the other two project locations. The latter come also from different depths but from a single borehole location.

The tests analysed in this research are CSS tests performed following ASTM D8296-19, (ASTM International, 2019). This is a standard test method for consolidated undrained cyclic direct simple shear tests. Therefore, the tests are assumed to be comparable with each other. As a difference, some tests were performed without pre-shearing. Pre-shearing is an extra phase applied after the first consolidation stage that occurs with drainage during or after cyclic loading. As explained previously in this research, only two test results could be used without pre-shear and therefore the influence on the cyclic shear strength could be not analysed.

2. *Which soil parameters, that are known to influence the cyclic response of the soil, best correlate with the cyclic shear strength?*

The cyclic (simple) shear strength, τ_{cy} , is normalised with a reference stress to obtain a Cyclic Stress Ratio (CSR). This CSR is also the value that is used to present the correlations with the determined soil parameters.

Cyclic resistance curves are translated from the test results. These are failure lines for the different soil sample batches at a nominal failure criterion shown as number of cycles to reach this strain failure against the CSR. A nominal failure criterion of 3.75% cyclic shear strain was applied in this research. From these curves, the CSR value at $N=10$ cycles could be observed, as it was chosen as an equivalent number of cycles.

The parameters that are elaborated for this research are based on characteristics compared to density of the soil, grain structure and in-situ characteristics. These parameters are the Relative density D_r [%], Fines content FC [%], Mean particle size D_{50} [mm] and the Normalised cone penetration resistance Q_{tn} [-].

The obtained cyclic resistance curves are based on a relatively small amount of datapoints and therefore the uncertainty of the actual obtained curves is increased. Because of this, the correlations of the soil parameters towards the cyclic shear strength are analysed by using the difference in soil characteristics. The shape of the curves is explained and when possible, a better interpretation of the failure line is given based on the observed soil parameters or other factors that could be explained based on the available information about the performed tests.

The following can be assumed:

- As a result of elaboration of the available dataset could be assumed that:
 - Uncertainty arises in determining the D_r of each sand batch. The maximum and minimum possible void ratios of the samples are measured in the laboratory. However, among the available tests none of the results included measured maximum and minimum possible void ratios. To infer the D_r , a procedure based on CPT data is suggested.
 - Based on the in-situ measured values of the D_r and the initial void ratio measured in the laboratory, a theoretical relative density is determined.
- From the further elaboration of the resistance curves, it could be assumed that:
 - From the index parameters observed in this research, the FC and D_r have an influence on the shape of the resistance curve.
 - A higher value of the D_r shows a higher gradient and therefore a steeper failure line in comparison with lower D_r values.
 - The FC influences the vertical position of the resistance curve. As different values lead to higher or lower values for CSR, this means that batch samples with the same D_r value can show the same shape of the failure line. However, the influence of the FC leads to different positions of the failure lines. The C_u also shows a small influence to the position of the line in one of the projects. An increase of this value would lead to lower CSR values, although this was not visible in all project data.
- Clear correlations between index parameters and the cyclic shear strength could be not observed. The following observations are made for each soil parameter:
 - The range of the FC is lower than expected. Only values of 5% or lower are observed. Within this small range it is not possible to give a conclusion about the influence of the FC towards the shear strength at both $N = 10$ or $N = 100$ cycles. From previous research, a decrease in shear strength was expected by an increment in FC . This trend could be not observed because of the small range in FC . However, this observation was visible in the resistance curves where higher values of FC show lower values of CSR in comparison with results from other batches.
 - The graph with observed D_r and the cyclic shear strength does not show a correlation. From previous research the expected trend was a high increase of the CSR by increasing D_r . However, in combination with curves from previous research can be observed that the values corresponding with $N = 10$ follow the observed trends.
 - The mean particle size, D_{50} , does not show a correlation with the CSR. An increase in shear strength was expected for increasing values of D_{50} . For the analysed test material, the range of the FC is low and therefore a correlation could not be checked.
 - To correlate with the in-situ conditions, a comparison with the normalised cone resistance (Q_{tn}) was made. The correlation graph with this parameter shows high scattering. A higher cone resistance in-situ would be expected to correspond to a higher resistance in soil behaviour in shear, but an increase of CSR by an increment of the Q_{tn} was not observed.

3. *How could the observed trends between these parameters be explained and what is missing in order to improve such correlations?*

As mentioned before, clear trends could be not observed. The correlations and observations about the test results are based on a small amount of data. To improve the outcome, a larger amount of test results is needed but also data that consist of a larger range of FC values. This will lead to a more accurate observation about correlations with the cyclic shear strength. Besides this, it is also important that the soil characteristics are obtained in a consistent way. For this research the D_r could not be obtained from the test results and the values had to be obtained in an alternative way. More suggestions and recommendations for future work are included in the following section.

5.2. Recommendations for future work

The following recommendations for future research are listed below:

- One of the possible reasons for the absence of correlations, is the relatively low amount of test results and the small range of fines content. In order to improve the correlations, and to observe possible correlations, more test results are needed with a larger range of FC. To increase the amount of test results but without changing the research approach more test results from other locations could be analysed and possibly also other soil types, instead of only sand, could be included. This increases the range of data but also makes the comparability more questionable.
- If more data would be available, and therefore more test results are available, then besides only one nominal failure criterion, also the influence of different strain failure levels could be analysed to obtain the influence and therefore the sensitivity of this chosen level.
- If correlations could be found, a comparison with design would be recommended. In a design research the observed correlations and therefore the influence of a soil parameter can be analysed in an actual design calculation or case study.
- To observe correlations of a soil parameter against the cyclic shear strength, the research approach could have been also performed in another way. As a suggestion could be to choose for a test approach where the soil parameters can be controlled. The full range of a selected soil parameter is then applied and more tests are needed.

References

- Andersen, K. (2015). *Cyclic soil parameters for offshore foundation design*. London: Taylor & Francis Group.
- ASTM International. (2019). *Standard Test Method for Consolidated Undrained Cyclic Direct Simple Shear Test under Constant Volume with Load Control or Displacement Control Designation: D8296 - 19*. West Conshohocken: ASTM International.
- Alshameri, B., Madun, A., & Bakar, I., (2017). Comparison of the Effect of Fine Content and Density towards the Shear Strength Parameters. *Geotechnical Engineering Journal of the SEAGS & AGSSEA Vol. 48 No. 2*.
- Boulanger, R., & Idriss, I. (2014). *CPT and SPT based liquefaction triggering procedures*. Davis, California: Department of Civil & environmental engineering college of engineering University of California at Davis.
- Chien, L., Oh, Y., & C.H.Chang. (2002). Effects of fines content on liquefaction strength and dynamic settlement of reclaimed soil. *Canadian Geotechnical Journal*, 254-265.
- Das, B. M. (2019). *Advanced Soil Mechanics*. Boca Raton: CRC Press Taylor & Francis Group.
- Dupla, J., & J.Canou. (2003). Cyclic pressuremeter loading and liquefaction properties of sands. *Soils and Foundations*, 17-31.
- Fugro Engineers B.V. . (2020). *Geotechnical Report Laboratory Test Data Hollandse Kust (west) Wind Farm Zone Dutch Sector, North Sea*. Nootdorp: Fugro Engineers B.V.
- Fugro Engineers B.V. (2016). *Hollandse Kust (Zuid) WFZ, WFS I-Dutch Sector, North Sea*. Rijksdienst voor Ondernemend Nederland (RVO).
- Fugro Engineers B.V. (2017). *Geophysical Site Investigation Survey, Hollandse Kust (noord) Wind Farm Zone Survey 2017*. Nootdorp: Rijksdienst voor Ondernemend Nederland.
- Fugro Engineers B.V. (2017). *Geotechnical Report Laboratory Test Data Wind Farm Sites WFS I&II Hollandse Kust (zuid) Wind Farm Zone Dutch Sector, North Sea*. Nootdorp: Fugro Engineers B.V.
- Fugro Engineers B.V. (2018). *Geotechnical Report Laboratory Test Data Wind Farm Sites WFS III&IV Hollandse Kust (zuid) Wind Farm Zone Dutch Sector, North Sea*. Nootdorp: Fugro Engineers B.V.
- Fugro Engineers B.V. (2019). *Geotechnical Report Laboratory Test Data Hollandse Kust (noord) Wind Farm Zone Dutch Sector, North Sea*. Nootdorp: Fugro Engineers B.V.
- Knappett, J., & Craig, R. (2012). *Craig's soil mechanics*. Abingdon: Spon Press.
- Lee, K., & J.A.Fitton. (1969). Factors affecting the cyclic loading strength of soil. *In Vibration Effects of Earthquakes on Sils and Foundations, ASTM Special Technical Publication*, 71-95.
- Mori, K., Seed, H., & Chan, C. (1978). Influence of sample disturbance on sand response to cyclic loading. *Journal of the Geotechnical Engineering Division*, 323-339.
- Netherlands Enterprise Agency. (2018). *Geological Desk Study, Hollandse Kust (west) Wind Farm Zone*. Rijksdienst voor Ondernemend Nederland (RVO).
- Randolph, M. F. (2012). *Offshore Design Approaches and Model Tests for Sub-Failure Cyclic Loading of Foundations*. Udine: C. di Prisco et al. (eds.), Mechanical Behaviour of Soils under Environmentally Induced Cyclic Loads, SpringerWienNewYork.
- Randolph, M., & Gourvenec, S. (2011). *Offshore Geotechnical Engineering*. New York: Spon Press.
- Robertson, P. (2010). Evaluation of Flow Liquefaction and Liquefied Strength. *JOURNAL OF GEOTECHNICAL AND GEOENVIRONMENTAL ENGINEERING*, 842-853.
- Harehdasht, S. A., Hussien, M. N., Roubtsova, V., & Chekired, M. (2018). Influence of particle size and gradation on shear strength-dilation relation of granular materials. *Canadian Geotechnical Journal*, 1-20.
- Tatsuoka, F., Ochi, K., Fujii, S., & Okamoto, M. (1986). Cyclic undrained triaxial and torsional shear strength of sands for different sample preparation methods. *Soils and Foundations*, 23-41.
- Vaid, Y. Fisher, M., Kuerbis, R. H., & Negissey, D. (1990). Particle gradation and liquefaction. *Journal of Geotechnical Engineering*, 698-703.
- Wichtmann, T., & T.Triantafyllidis. (2012). *Behaviour of Granular Soils Under Environmentally Induced Cyclic Loads*. Udine: C. di Prisco et al. (eds.), Mechanical Behaviour of Soils under Environmentally Induced Cyclic Loads, SpringerWienNewYork.
- Wijewickreme, D., & Sanin, M. (2004). Cyclic shear loading response of Fraser River Delta Silt. *13th World Conference on Earthquake Engineering*, 499.

windenergie magazine. (2020, June 18). News. Retrieved from windenergie-magazine: <https://windenergie-magazine.nl/blix-to-supervise-soil-investigation-for-ijmuiden-ver/>

A

Appendix A

Test location: Hollandse kust West

Table A1: Shear strain data, project HKW, test type: constant volume, stress controlled, 2 way loaded with pre-shear

Batch	ID	CSR	0,10%	0,25%	0,50%	1,00%	2,50%	3,75%	5,00%	7,50%	15,00%
1	CSS12	0,16	104	148	227	332	1500	1500	1500	1500	1500
1	CSS13	0,24	48	95	147	328	1087	1500	1500	1500	1500
1	CSS93	0,32	-	-	2	6	29	48	70	208	1500
1	CSS106	0,49	-	-	-	2	11	21	32	57	1500
2	CSS21	0,16	-	1	4	9	28	49	68	111	1500
2	CSS22R	0,26	-	-	1	3	12	17	23	40	1500
3	CSS01	0,18	-	-	1	1	1	1	1	2	2
3	CSS02	0,29	-	-	-	-	1	2	4	7	23
3	CSS94	0,24	-	-	-	1	2	2	3	3	4
3	CSS108	0,06	1500	1500	1500	1500	1500	1500	1500	1500	1500
4	CSS30	0,19	-	-	1	1	2	2	2	3	6
4	CSS31	0,29	-	-	-	-	-	1	1	1	2
4	CSS95	0,10	15	39	42	44	45	45	45	46	47
4	CSS109	0,05	1500	1500	1500	1500	1500	1500	1500	1500	1500
5	CSS32	0,18	-	1	2	3	6	9	11	18	193
5	CSS33	0,28	-	-	1	3	35	85	134	285	1500
5	CSS96	0,23	-	5	9	16	38	60	93	462	1500
5	CSS110	0,37	-	-	-	1	10	21	31	51	259
6	CSS41	0,21	-	-	2	4	11	24	40	89	1500
6	CSS42	0,31	-	-	-	1	4	8	14	29	741
6	CSS97	0,44	-	-	-	-	3	6	9	16	628
6	CSS111	0,65	-	-	-	-	-	2	5	9	30
7	CSS113	0,21	-	-	1	2	3	4	4	4	5
8	CSS48R	0,20	-	4	9	15	26	34	40	53	443
8	CSS49	0,30	-	-	-	1	4	9	16	37	1024
8	CSS98	0,34	-	-	-	-	-	-	-	-	1
8	CSS114	0,10	1500	1500	1500	1500	1500	1500	1500	1500	1500
9	CSS57	0,20	-	-	69	96	126	137	148	165	215
9	CSS58	0,30	-	-	-	1	6	11	17	28	88
9	CSS99R	0,10	1500	1500	1500	1500	1500	1500	1500	1500	1500
10	CSS112	0,21	-	-	3	8	20	37	54	98	-

Table A2: Shear strain data, project HKW, test type: constant volume, stress controlled, 2 way loaded no pre-shear

Batch	ID	CSR	0,10%	0,25%	0,50%	1,00%	2,50%	3,75%	5,00%	7,50%	15,00%
1	CSS20	3,81	3	14	20	159	805	1500	1500	1500	1500
1	CSS87	7,47	-	-	1	11	139	354	574	1500	1500
1	CSS101	15,06	-	-	-	2	16	29	42	78	1500
2	CSS29R	8,33	1	13	34	126	229	334	1500	1500	1500
2	CSS103	17,32	-	-	-	-	1	3	7	35	1500
3	CSS03	25,69	-	-	-	1	1	1	1	1	2
3	CSS88	14,31	15	46	50	52	53	54	54	55	56
3	CSS104	10,17	488	533	536	537	540	542	543	545	552
5	CSSS40	14,90	-	4	6	12	33	62	101	570	1500
5	CSS92	22,65	-	-	1	4	14	24	37	118	1500
5	CSS130	46,01	-	-	-	-	1	3	6	13	43
6	CSS47	36,87	-	-	1	3	6	11	18	42	1500
9	CSS65	28,17	-	-	8	13	33	50	64	92	622
9	CSS90	43,18	-	-	-	1	8	14	21	32	83

Test location: Hollandse kust Noord

Table A3: Shear strain data, project HKN, test type: constant volume, stress controlled, 2 way loaded with pre-shear

Batch	ID	CSR	0,10%	0,25%	0,50%	1,00%	2,50%	3,75%	5,00%	7,50%	15,00%
1	CSS01	6,33	-	-	-	-	4	48	411	1500	1500
1	CSS02	3,12	2	4	6	11	1500	1500	1500	1500	1500
1	CSS26	9,44	-	-	-	-	-	1190	1500	1500	1500
1	CSS38	1,73	1500	1500	1500	1500	1500	1500	1500	1500	1500
2	CSS03	32,47	-	-	-	-	-	1	2	5	13
2	CSS04	19,59	-	-	-	1	4	8	13	23	62
2	CSS30	16,08	-	-	-	1	4	6	8	12	29
2	CSS39R	12,75	-	-	2	2	4	4	5	5	6
3	CSS05	13,86	-	-	-	-	-	-	3	48	1500
3	CSS06R2	6,80	-	-	-	1	17	110	272	1500	1500
3	CSS37	2,30	-	-	-	-	2	13	30	102	1500
3	CSS40	9,13	412	442	482	1500	1500	1500	1500	1500	1500
4	CSS07	31,53	-	-	-	-	6	11	16	27	323
4	CSS08	15,69	-	-	1	3	10	17	25	48	463
4	CSS31	36,09	-	-	-	-	7	12	17	26	137
4	CSS41	45,20	-	-	-	-	6	13	20	32	133
4	CSS63	49,83	-	-	-	-	3	23	61	398	1500
4	CSS73	23,87	-	-	1	4	14	21	27	46	874
5	CSS09R	24,87	-	-	-	1	4	8	14	29	98
5	CSS10	12,03	-	5	8	10	13	17	23	53	1500
5	CSS33	18,73	-	1	3	6	21	42	64	115	1500
5	CSS42	32,11	-	-	-	1	6	13	21	44	235
5	CSS74	38,83	-	-	-	-	-	3	9	27	187
6	CSS11	43,67	-	-	-	-	2	2	3	5	13
6	CSS12	21,38	-	64	69	72	78	84	90	103	152
6	CSS32	16,60	263	528	534	538	541	543	544	546	554
6	CSS43	32,07	-	3	6	8	11	12	13	15	20
7	CSS13	51,84	-	-	2	9	19	27	34	46	200
7	CSS14R	26,02	-	510	534	553	594	620	646	723	1500
7	CSS34	65,86	-	-	-	3	10	18	28	48	235
7	CSS44	87,89	-	-	-	-	2	4	8	16	46
8	CSS15	40,92	-	-	1	2	9	17	27	51	196
8	CSS16	19,63	-	163	173	182	204	223	250	320	1500
8	CSS35	50,80	-	-	-	1	8	14	19	29	90
8	CSS45	57,57	-	-	-	-	2	3	5	7	17
9	CSS17	55,37	-	-	-	-	1	2	4	7	22
9	CSS18	26,77	-	4	6	7	11	15	19	28	88
9	CSS36	18,96	-	1500	1500	1500	1500	1500	1500	1500	1500
9	CSS60	23,43	3	22	24	26	30	33	35	40	126

Table A4: Shear strain data, project HKN, test type: constant volume, stress controlled, 2 way loaded no pre-shear

Batch	ID	CSR	0,10%	0,25%	0,50%	1,00%	2,50%	3,75%	5,00%	7,50%	15,00%
9	CSS70	4,83	-	-	605	605	605	605	605	605	605
9	CSS71R	9,53	1500	1500	1500	1500	1500	1500	1500	1500	1500
9	CSS72	18,80	1500	1500	1500	1500	1500	1500	1500	1500	1500
5	CSS48	12,92	-	840	840	840	840	840	840	840	840
6	CSS49	21,01	-	6	9	13	61	147	236	453	1500
6	CSS47	16,36	-	18	22	25	30	33	37	46	78
8	CSS50	19,66	31	60	63	64	67	68	69	70	76

Test location: Hollandse kust South

Table A5: Shear strain data, project HKZ, test type: constant volume, stress controlled, 2 way loaded with pre-shear

Batch	ID	CSR	0,10%	0,25%	0,50%	1,00%	2,50%	3,75%	5,00%	7,50%	15,00%
7	CSS20	61,78	-	-	18	24	29	31	33	36	52
7	CSS21	82,13	-	-	-	-	2	3	3	5	12
7	CSS22	124,53	-	-	-	-	-	1	1	3	7
102	CSS05	14,80	-	-	-	-	-	1	1	1	23
102	CSS07	11,92	-	-	-	1	4	7	10	20	1357
102	CSS27	6,70	-	-	50	50	50	50	50	50	50
102	CSS29	6,98	-	-	-	-	-	50	50	50	50
102	CSS46	10,26	-	5	9	14	26	34	44	120	1500
102	CSS49	13,90	-	-	-	-	1	3	6	18	1478
103	CSS21	25,40	-	26	29	31	34	36	37	40	48
103	CSS22	44,40	-	-	1	2	2	3	3	4	5
103	CSS23	17,98	111	178	182	184	186	188	189	191	200
103	CSS35	28,15	-	-	50	50	50	50	50	50	50
103	CSS37	4,22	-	-	-	-	-	50	50	50	50
103	CSS42	38,22	-	92	110	116	123	125	127	131	143
103	CSS43	55,49	-	-	-	1	3	4	6	9	23
103	CSS44	44,81	-	-	-	1	4	7	9	12	23
103	CSS45	27,18	-	7	9	11	13	15	17	20	41

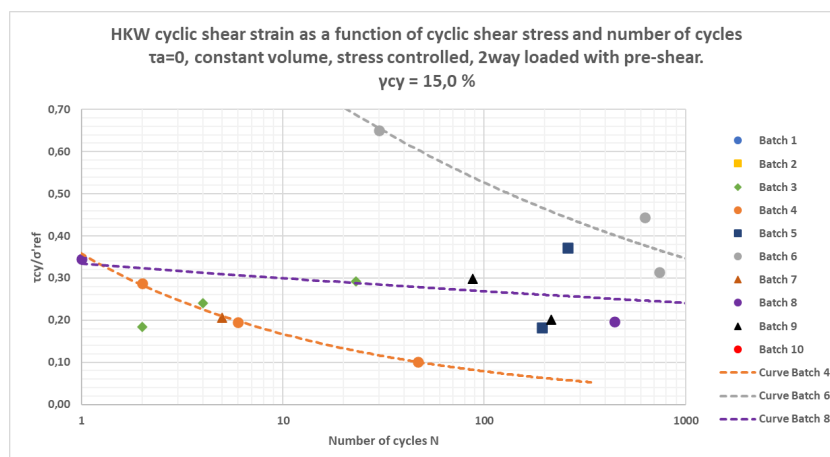
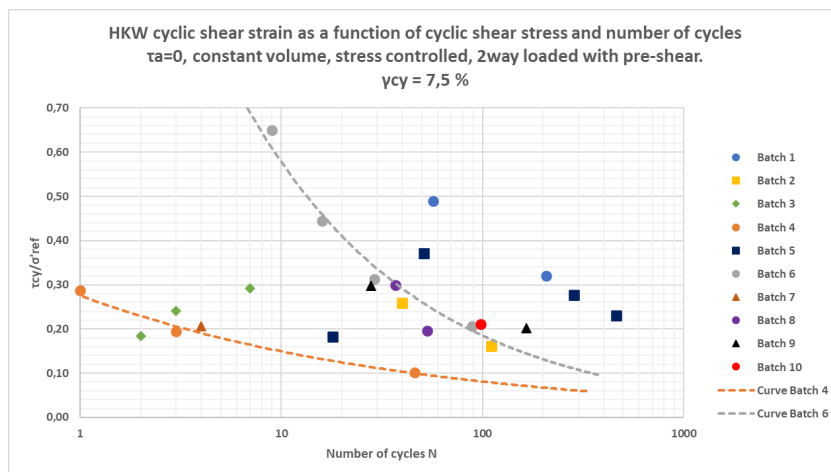
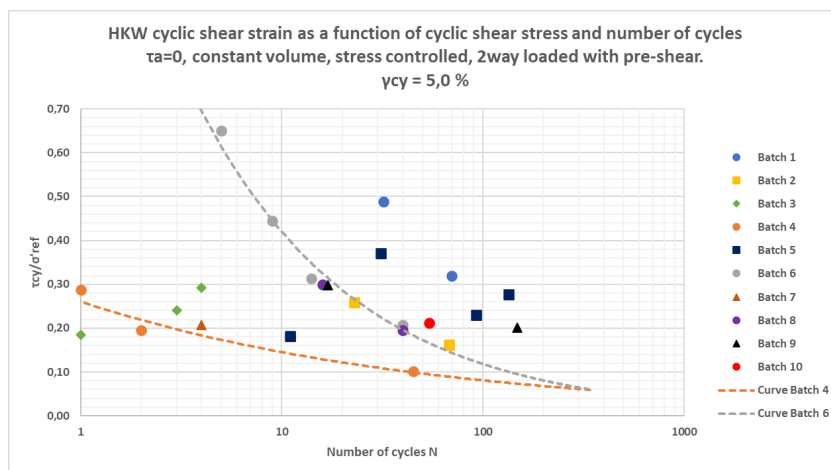
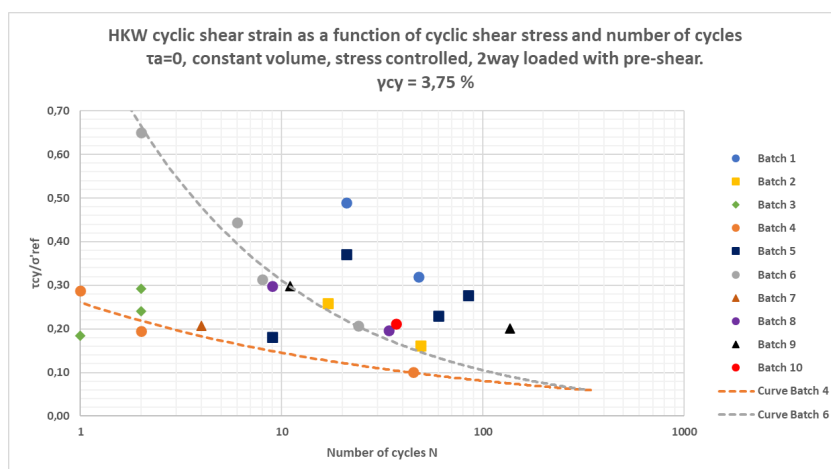


Figure A1: Cyclic resistance curve for $\gamma_{cy} = 15\%$, project HKW, pre-shear

Figure A2: Cyclic resistance curve for $\gamma_{cy} = 7.5\%$, project HKW, pre-shearFigure A3: Cyclic resistance curve for $\gamma_{cy} = 5\%$, project HKW, pre-shearFigure A4: Cyclic resistance curve for $\gamma_{cy} = 3.75\%$, project HKW, pre-shear

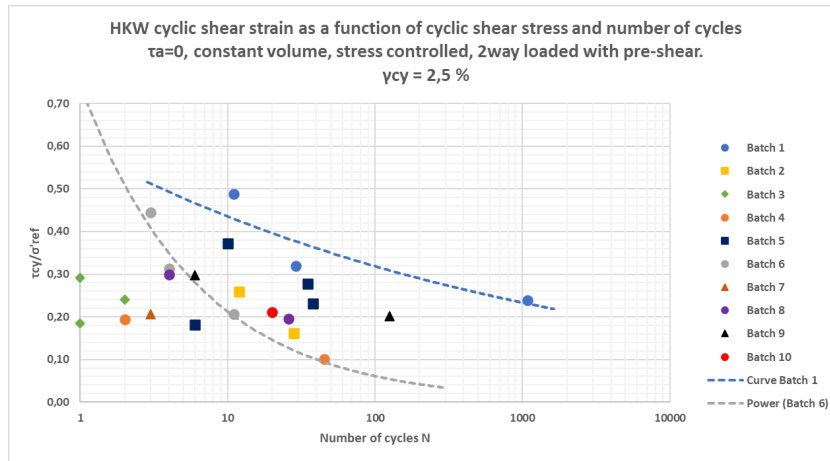


Figure A5: Cyclic resistance curve for $\gamma_{cy} = 2.5\%$, project HKW, pre-shear

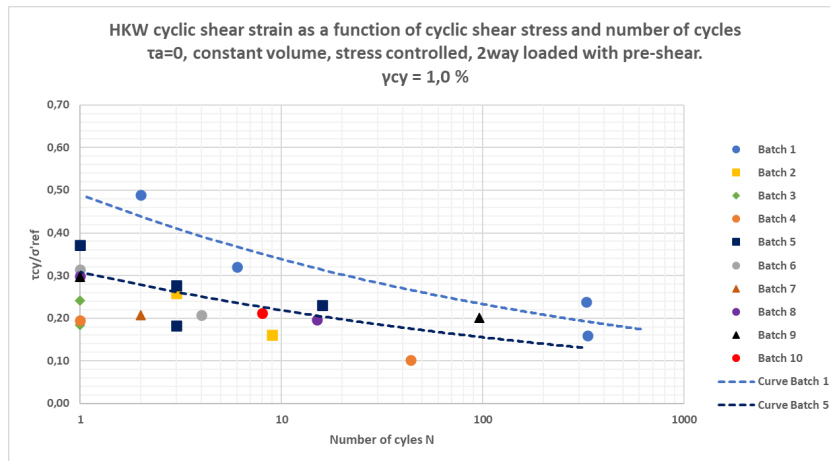


Figure A6: Cyclic resistance curve for $\gamma_{cy} = 1\%$, project HKW, pre-shear

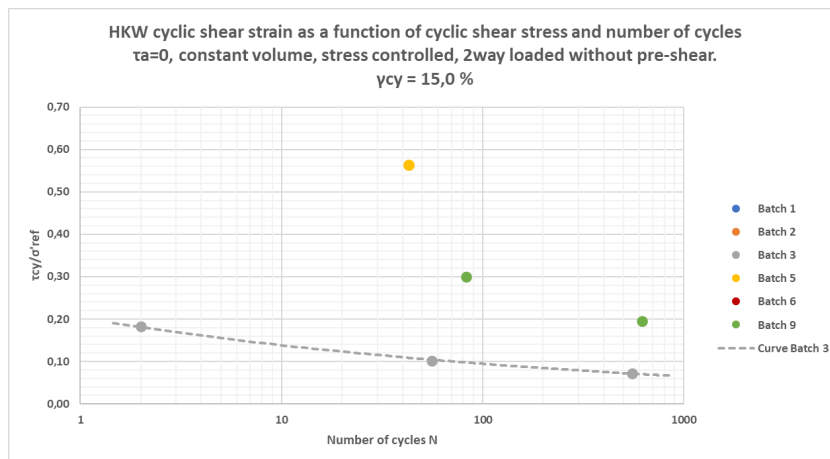
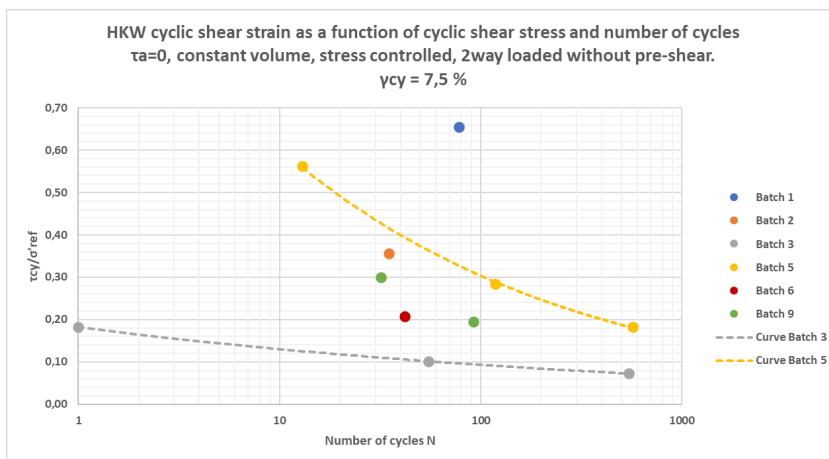
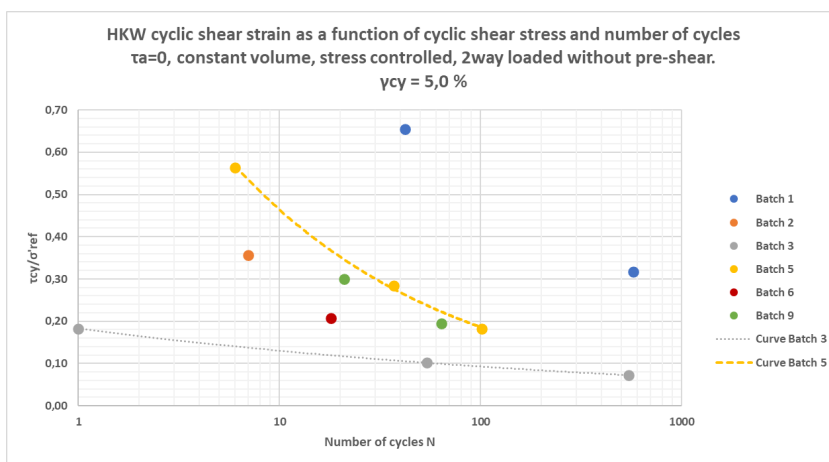
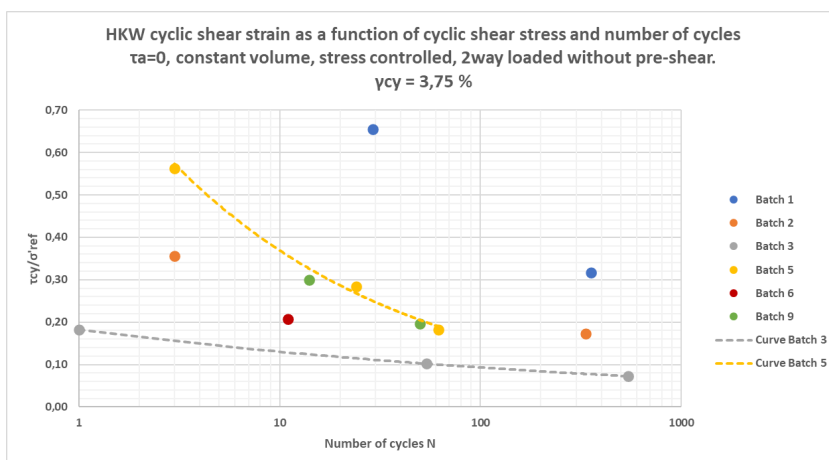


Figure A7: Cyclic resistance curve for $\gamma_{cy} = 15\%$, project HKW, without pre-shear

Figure A8: Cyclic resistance curve for $\gamma_{cy} = 7.5\%$, project HKW, without pre-shearFigure A9: Cyclic resistance curve for $\gamma_{cy} = 5\%$, project HKW, without pre-shearFigure A10: Cyclic resistance curve for $\gamma_{cy} = 3.75\%$, project HKW, without pre-shear

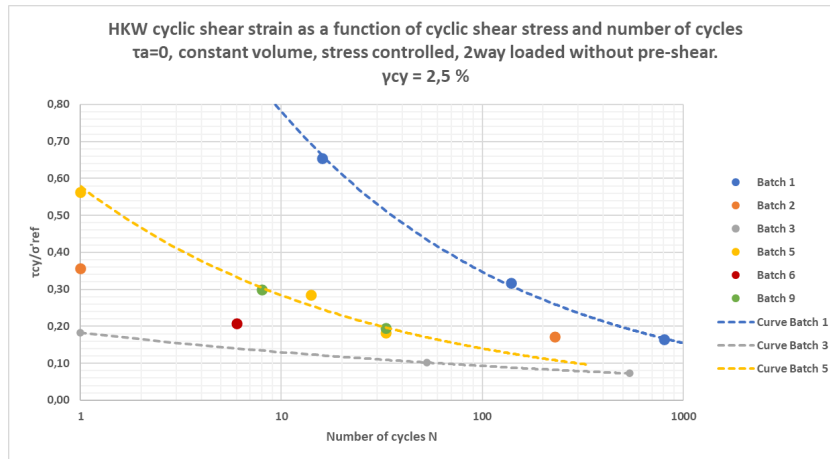


Figure A11: Cyclic resistance curve for $\gamma_{cy} = 2.5\%$, project HKW, without pre-shear

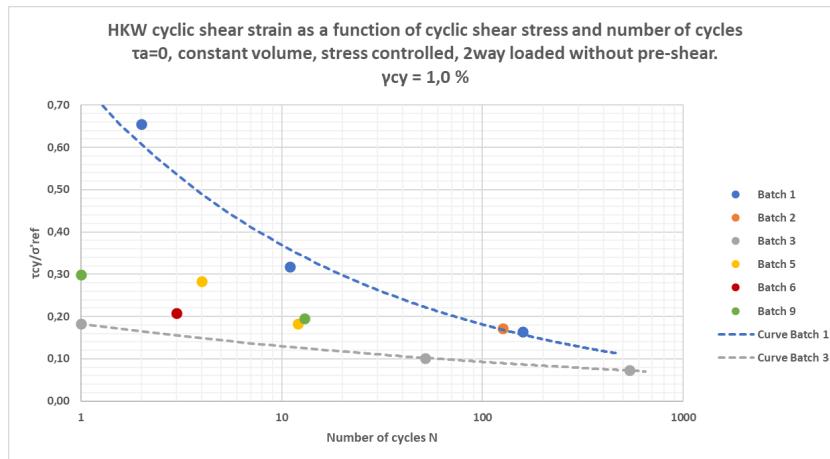


Figure A12: Cyclic resistance curve for $\gamma_{cy} = 1\%$, project HKW, without pre-shear

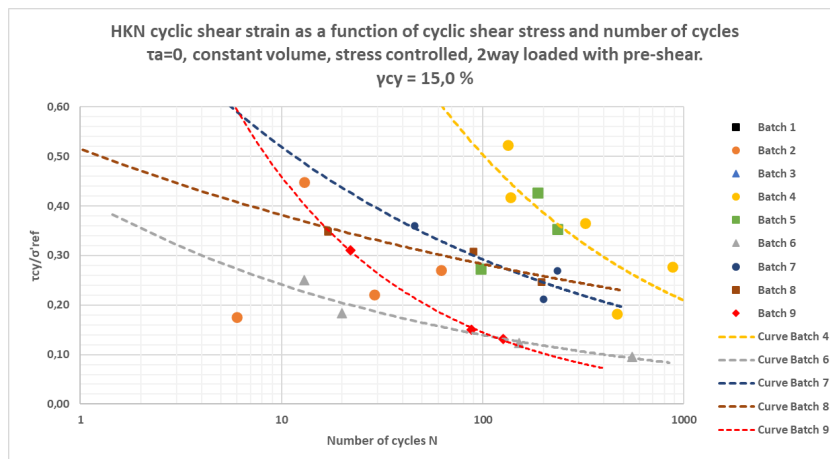


Figure A13: Cyclic resistance curve for $\gamma_{cy} = 15\%$, project HKN, pre-shear

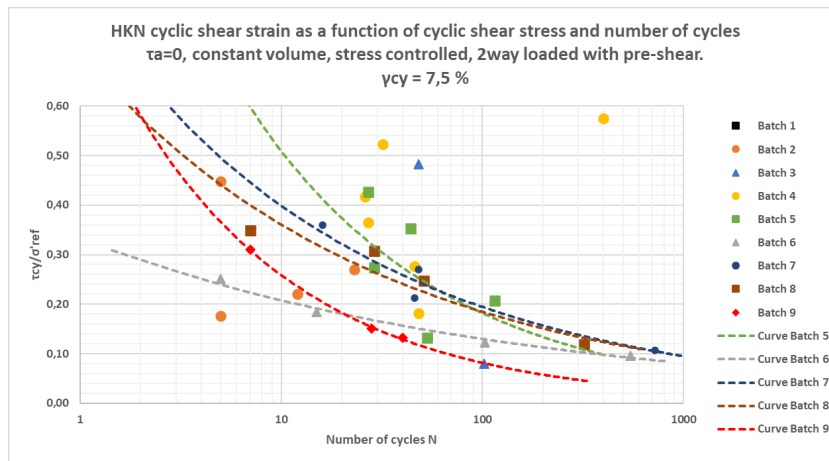


Figure A14: Cyclic resistance curve for $\gamma_{cy} = 7.5\%$, project HKN, pre-shear

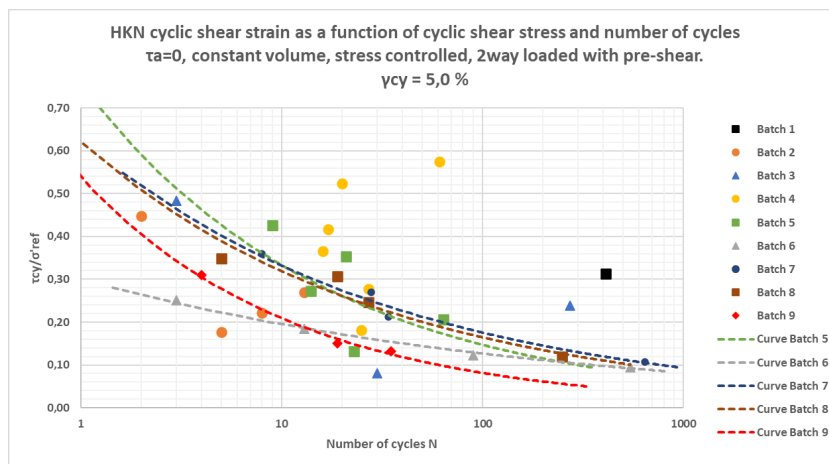


Figure A15: Cyclic resistance curve for $\gamma_{cy} = 5.0\%$, project HKN, pre-shear

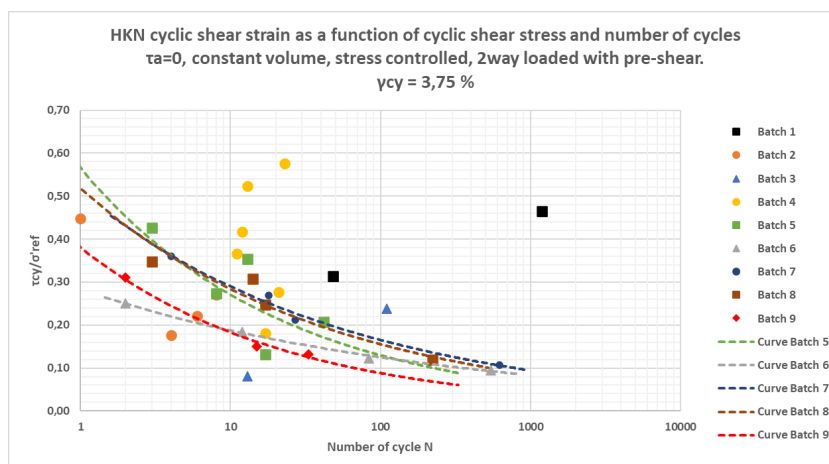


Figure A16: Cyclic resistance curve for $\gamma_{cy} = 3.75\%$, project HKN, pre-shear

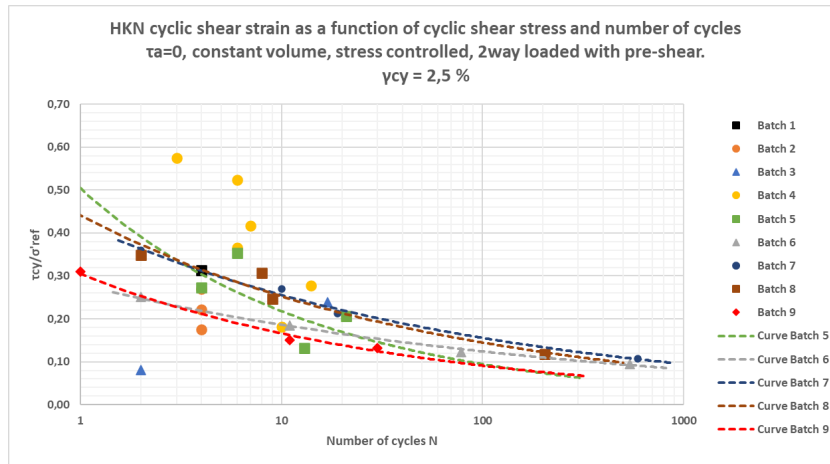


Figure A17: Cyclic resistance curve for $\gamma_{cy} = 2.5\%$, project HKN, pre-shear

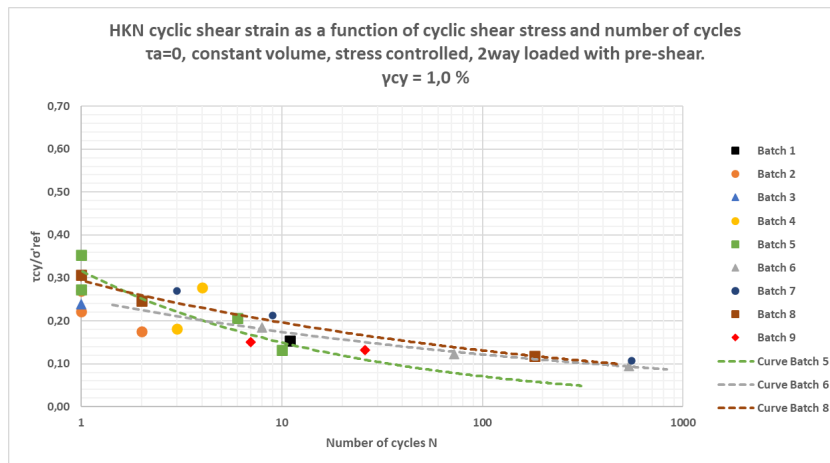


Figure A18: Cyclic resistance curve for $\gamma_{cy} = 1\%$, project HKN, pre-shear

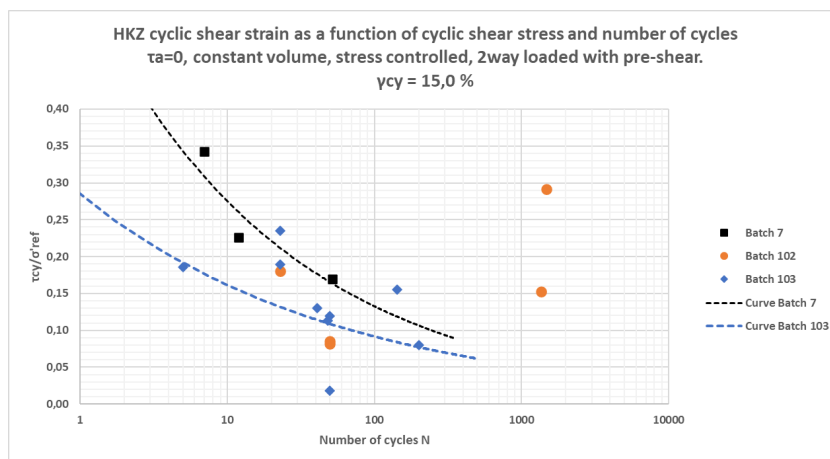


Figure A19: Cyclic resistance curve for $\gamma_{cy} = 15\%$, project HKZ, pre-shear

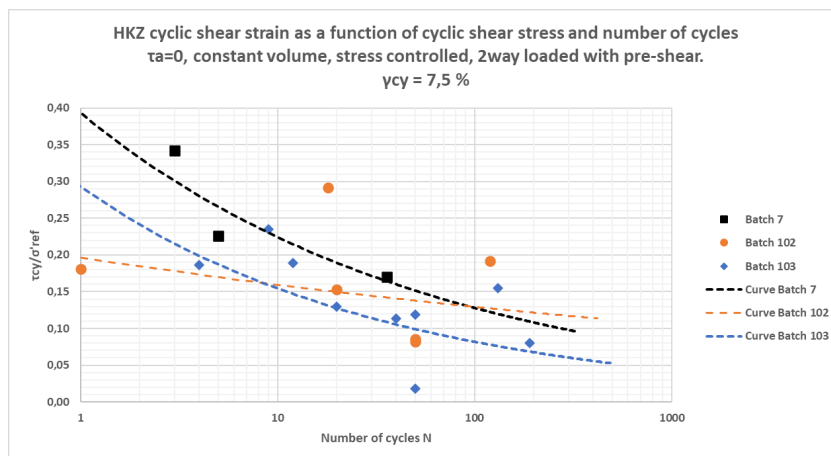


Figure A20: Cyclic resistance curve for $\gamma_{cy} = 7.5\%$, project HKZ, pre-shear

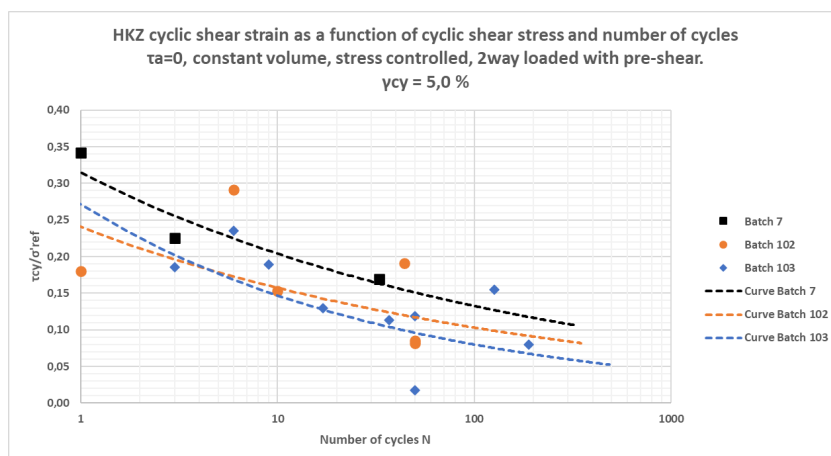


Figure A21: Cyclic resistance curve for $\gamma_{cy} = 5\%$, project HKZ, pre-shear

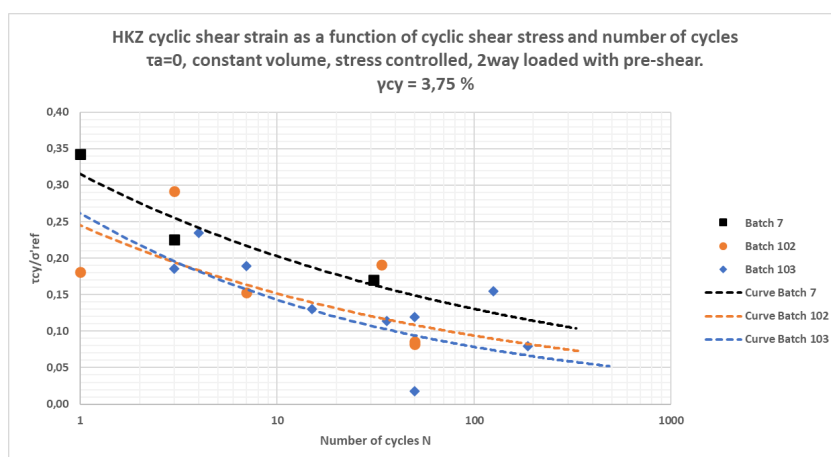
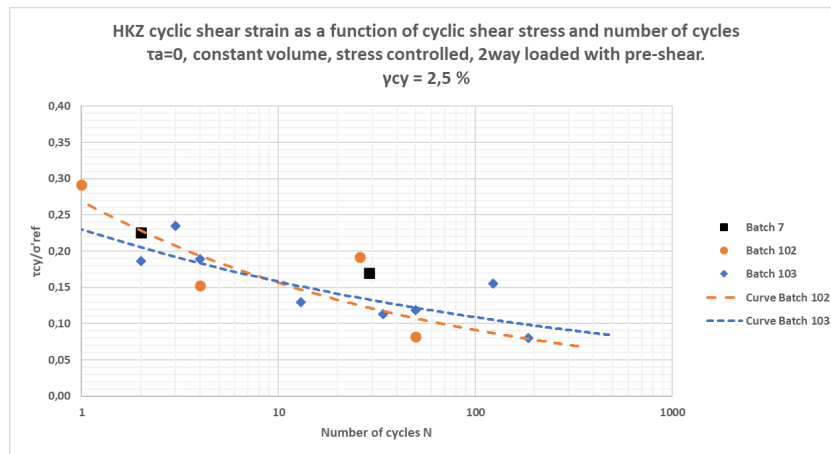
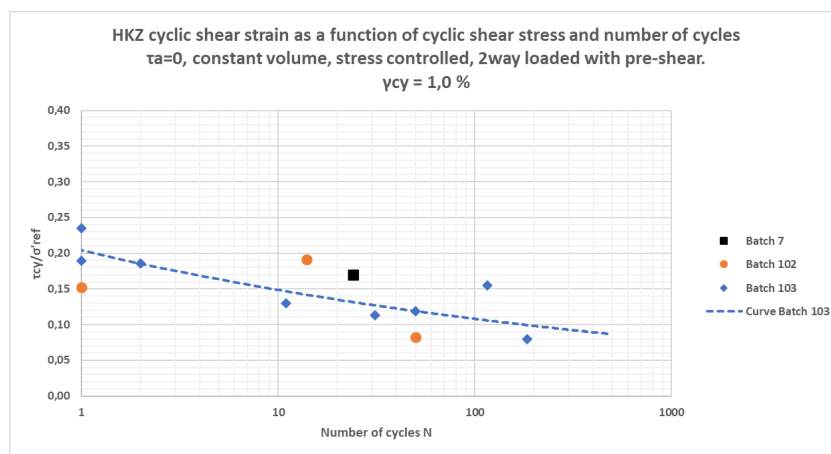


Figure A22: Cyclic resistance curve for $\gamma_{cy} = 3.75\%$, project HKZ, pre-shear

Figure A23: Cyclic resistance curve for $\gamma_{cy} = 2.5\%$, project HKZ, pre-shearFigure A24: Cyclic resistance curve for $\gamma_{cy} = 1\%$, project HKZ, pre-shear

B

Appendix B

Hollandse kust West

Table B1: Details about data to construct the cyclic resistance curve, project: HKW, pre-shear

Batch #	Batch ID	Cyclic shear stress (τ_{cyc})	σ'_{ref}	Cyclic stress ratio τ_{cyc}/σ'_{ref}	# cycles at $\gamma_{cy}(\%) = 3.75\%$
Batch 1	CSS12	3,70	23,23	0,16	1500
Batch 1	CSS13	5,62	23,51	0,24	1500
Batch 1	CSS93	7,44	23,26	0,32	48
Batch 1	CSS106	11,31	23,13	0,49	21
Batch 2	CSS21	7,85	48,65	0,16	49
Batch 2	CSS22R	12,62	48,72	0,26	17
Batch 3	CSS01	25,93	140,74	0,18	1
Batch 3	CSS02	40,91	140,33	0,29	2
Batch 3	CSS94	33,92	140,95	0,24	2
Batch 3	CSS108	8,06	140,47	0,06	1500
Batch 4	CSS30	27,09	139,20	0,19	2
Batch 4	CSS31	40,05	139,47	0,29	1
Batch 4	CSS95	14,16	139,72	0,10	45
Batch 4	CSS109	7,54	139,45	0,05	1500
Batch 5	CSS32	14,89	81,83	0,18	9
Batch 5	CSS33	22,67	81,70	0,28	85
Batch 5	CSS96	18,85	81,77	0,23	60
Batch 5	CSS110	30,41	81,89	0,37	21
Batch 6	CSS41	36,78	177,92	0,21	24
Batch 6	CSS42	55,86	178,26	0,31	8
Batch 6	CSS97	79,06	177,94	0,44	6
Batch 6	CSS111	115,98	178,45	0,65	2
Batch 7	CSS113	47,14	227,99	0,21	4
Batch 8	CSS48R	28,23	144,10	0,20	34
Batch 8	CSS49	43,05	144,07	0,30	9
Batch 8	CSS98	49,48	143,61	0,34	-
Batch 8	CSS114	14,96	144,06	0,10	1500
Batch 9	CSS57	28,96	143,91	0,20	137
Batch 9	CSS58	42,98	144,32	0,30	11
Batch 9	CSS99R	15,03	144,40	0,10	1500
Batch 10	CSS112	48,20	228,18	0,21	37

Table B2: Details about data to construct the cyclic resistance curve, project: HKW, no pre-shear

Batch #	Batch ID	Cyclic shear stress (τ_{cy})	σ'_{ref}	Cyclic stress ratio τ_{cy}/σ'_{ref}	# cycles at $\gamma_{cy}(\%) = 3.75\%$
Batch 1	CSS20	3,81	23,08	0,16	1500
Batch 1	CSS87	7,47	23,54	0,32	354
Batch 1	CSS101	15,06	23,01	0,65	29
Batch 2	CSS29R	8,33	48,38	0,17	334
Batch 2	CSS103	17,32	48,63	0,36	3
Batch 3	CSS03	25,69	140,55	0,18	1
Batch 3	CSS88	14,31	140,64	0,10	54
Batch 3	CSS104	10,17	140,02	0,07	542
Batch 5	CSSS40	14,90	81,75	0,18	62
Batch 5	CSS92	22,65	79,72	0,28	24
Batch 5	CSS130	46,01	81,72	0,56	3
Batch 6	CSS47	36,87	177,80	0,21	11
Batch 9	CSS65	28,17	144,03	0,20	50
Batch 9	CSS90	43,18	144,07	0,30	14

Hollandse kust Noord

Table B3: Details about data to construct the cyclic resistance curve, project: HKN, pre-shear

Batch #	Batch ID	Cyclic shear stress (τ_{cy})	σ'_{ref}	Cyclic stress ratio τ_{cy}/σ'_{ref}	# cycles at $\gamma_{cy}(\%) = 3.75\%$
Batch 1	CSS01	6,33	20,19	0,31	48
Batch 1	CSS02	3,12	20,20	0,15	1500
Batch 1	CSS26	9,44	20,28	0,47	1190
Batch 1	CSS38	1,73	20,06	0,09	1500
Batch 2	CSS03	32,47	72,45	0,45	1
Batch 2	CSS04	19,59	72,51	0,27	8
Batch 2	CSS30	16,08	72,78	0,22	6
Batch 2	CSS39R	12,75	72,45	0,18	4
Batch 3	CSS05	13,86	28,71	0,48	-
Batch 3	CSS06R2	6,80	28,55	0,24	110
Batch 3	CSS37	2,30	28,63	0,08	13
Batch 3	CSS40	9,13	28,50	0,32	1500
Batch 4	CSS07	31,53	86,29	0,37	11
Batch 4	CSS08	15,69	86,32	0,18	17
Batch 4	CSS31	36,09	86,57	0,42	12
Batch 4	CSS41	45,20	86,41	0,52	13
Batch 4	CSS63	49,83	86,63	0,58	23
Batch 4	CSS73	23,87	86,23	0,28	21
Batch 5	CSS09R	24,87	91,01	0,27	8
Batch 5	CSS10	12,03	91,10	0,13	17
Batch 5	CSS33	18,73	90,69	0,21	42
Batch 5	CSS42	32,11	90,95	0,35	13
Batch 5	CSS74	38,83	91,04	0,43	3
Batch 6	CSS11	43,67	174,04	0,25	2
Batch 6	CSS12	21,38	173,88	0,12	84
Batch 6	CSS32	16,60	174,06	0,10	543
Batch 6	CSS43	32,07	174,14	0,18	12
Batch 7	CSS13	51,84	244,57	0,21	27
Batch 7	CSS14R	26,02	244,39	0,11	620
Batch 7	CSS34	65,86	244,40	0,27	18
Batch 7	CSS44	87,89	244,27	0,36	4
Batch 8	CSS15	40,92	165,74	0,25	17
Batch 8	CSS16	19,63	165,45	0,12	223
Batch 8	CSS35	50,80	165,40	0,31	14
Batch 8	CSS45	57,57	165,30	0,35	3
Batch 9	CSS17	55,37	178,24	0,31	2
Batch 9	CSS18	26,77	178,01	0,15	15
Batch 9	CSS36	18,96	178,02	0,11	1500
Batch 9	CSS60	23,43	178,26	0,13	33

Hollandse kust Zuid

Table B4: Details about data to construct the cyclic resistance curve, project: HKZ, pre-shear

Batch #	Batch ID	Cyclic shear stress (τ_{cy})	σ'_{ref}	Cyclic stress ratio τ_{cy}/σ'_{ref}	# cycles at $\gamma_{cy}(\%) = 3.75\%$
Batch 7	CSS20	61,78	363,93	0,17	31
Batch 7	CSS21	82,13	363,85	0,23	3
Batch 7	CSS22	124,53	363,85	0,34	1
Batch 102	CSS05	14,80	81,95	0,18	1
Batch 102	CSS07	11,92	78,11	0,15	7
Batch 102	CSS27	6,70	81,71	0,08	50
Batch 102	CSS29	6,98	81,83	0,09	50
Batch 102	CSS46	10,26	53,62	0,19	34
Batch 102	CSS49	13,90	47,67	0,29	3
Batch 103	CSS21	25,40	223,73	0,11	36
Batch 103	CSS22	44,40	238,75	0,19	3
Batch 103	CSS23	17,98	225,14	0,08	188
Batch 103	CSS35	28,15	236,48	0,12	50
Batch 103	CSS37	4,22	236,24	0,02	50
Batch 103	CSS42	38,22	246,68	0,15	125
Batch 103	CSS43	55,49	236,25	0,23	4
Batch 103	CSS44	44,81	236,43	0,19	7
Batch 103	CSS45	27,18	209,27	0,13	15

C

Appendix C

This Appendix provides a further elaboration of the obtained cyclic resistance curves.

The obtained values for the CSR at N = 10 cycles and the soil parameters do not show a clear correlation as expected. Because the cyclic resistance curves are relatively based on a small amount of datapoints and therefore make the actual value at N = 10 more uncertain, the shape of the curves is analysed and if possible a better interpretation of the line is given based on the observed soil parameters or other factors that could be explained based on the available information about the performed tests.

C.1 Collection details about test results

The following tables include the test results as obtained in Chapter 3 and used in the assessment of the observed cyclic resistance curves.

Table C1: Collected test results

Batch #	Project + Batch ID	$(\tau_{cy}/\sigma'_{ref})_{N=10}$	Dr [%]	Dr, th [%]	e_0 [-]	FC [%]	D50 [mm]	Cu [mm]	Qtn [-]
1.	HKW 3	0.13	56	42	0.70	20.5	0.15	-	105
2.	HKW 4	0.15	61	70	0.62	56.5	-	-	102
3.	HKW 5	0.37	94	74	0.61	2.5	0.18	2.05	293
4.	HKW 6	0.31	99	88	0.57	2.6	0.26	1.86	350
5.	HKN 5	0.27	100	81	0.59	3.0	0.23	2.54	418
6.	HKN 6	0.18	36	46	0.69	4.0	0.18	2.47	36
7.	HKN 7	0.29	84	91	0.56	4.0	0.19	2.42	229
8.	HKN 8	0.29	55	60	0.65	5.0	0.17	2.37	91
9.	HKN 9	0.18	100	98	0.54	3.0	0.25	3.79	436
10.	HKZ 7	0.21	-	63	0.64	3.0	0.15	2.35	139
11.	HKZ 102	0.15	-	88	0.57	5.0	0.24	2.70	271
12.	HKZ 103	0.14	-	70	0.62	4.0	0.17	2.65	172

Table C2: Collected test results

Batch #	Project + Batch ID	$(\tau_{cy}/\sigma'_{ref})_{N=10}$	$(\tau_{cy}/\sigma'_{ref})_{N=100}$	Equation
1.	HKW 3	0.13	0.09	$0.18x^{-0.15}$
2.	HKW 4	0.15	0.08	$0.26x^{-0.25}$
3.	HKW 5	0.37	0.16	$0.86x^{-0.37}$
4.	HKW 6	0.31	0.11	$0.92x^{-0.47}$
5.	HKN 5	0.27	0.13	$0.56x^{-0.32}$
6.	HKN 6	0.18	0.12	$0.28x^{-0.18}$
7.	HKN 7	0.29	0.17	$0.51x^{-0.24}$
8.	HKN 8	0.29	0.16	$0.52x^{-0.26}$
9.	HKN 9	0.18	0.09	$0.38x^{-0.32}$
10.	HKZ 7	0.21	0.13	$0.32x^{-0.19}$
11.	HKZ 102	0.15	0.09	$0.24x^{-0.20}$
12.	HKZ 103	0.14	0.08	$0.26x^{-0.26}$

C.2 Collection of details about test results after assessment of the observed cyclic resistance curves

Table C3: Collected test results for each batch for N = 10 and N = 100 cycles, after assessment of the observed cyclic resistance curves

Batch #	Project + Batch ID	$(\tau_{cy}/\sigma'_{ref})_{N=10}$	$(\tau_{cy}/\sigma'_{ref})_{N=100}$	Equation
1.	HKW 3	0.13	0.09	$0.18x^{-0.15}$
2.	HKW 4	0.15	0.08	$0.26x^{-0.25}$
3.	HKW 5	0.37	0.16	$0.86x^{-0.37}$
4.	HKW 6	0.31	0.11	$0.92x^{-0.47}$
5.	HKN 5	0.27	0.13	$0.56x^{-0.32}$
6.	HKN 6	0.18	0.12	$0.28x^{-0.18}$
7.	HKN 7	0.29	0.17	$0.51x^{-0.24}$
8.	HKN 8	0.29	0.14	$0.44x^{-0.25}$
9.	HKN 9	0.18	0.09	$0.38x^{-0.32}$
10.	HKZ 7	0.21	0.13	$0.32x^{-0.19}$
11.	HKZ 102	0.15	0.07	$0.28x^{-0.30}$
12.	HKZ 103	0.14	0.08	$0.26x^{-0.26}$

C.3 Assessment of obtained resistance curves

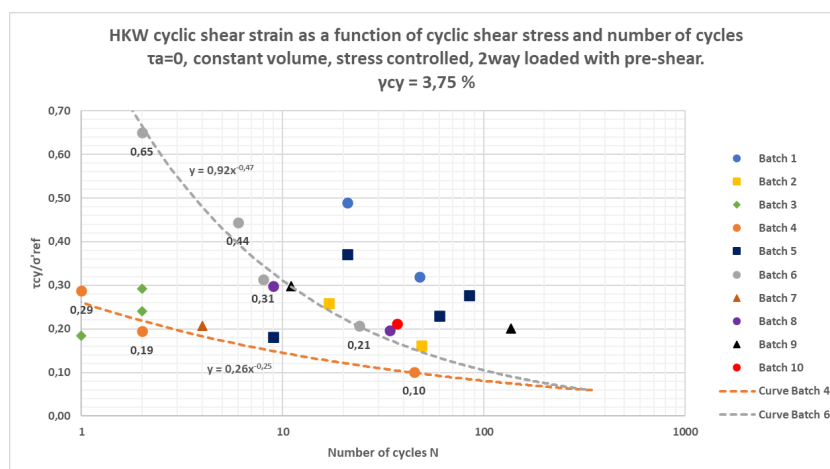


Figure C1: Cyclic resistance curve for HKW

From the first project, HKW, two resistance curves are obtained from tests that are both tested with pre-shear. These two lines show very different behaviour although these results are from the same projects. These batches show differences in values for the D_r and the FC. The results from batch 4 show a lower cyclic shear strength than the other failure line. From this could be observed that an increment of FC would have an influence and would give lower values for the CSR. By taking the D_r into account, it could be observed that higher values of D_r show a steeper line. This means that the power of the actual power function is dependent of the D_r and determines the slope of the curve. This was also found by (Boulanger & Idriss, 2014) who state that the power of the function depends on the relative density of sand. To check this observation the cyclic resistance curves from the other projects are also analysed.

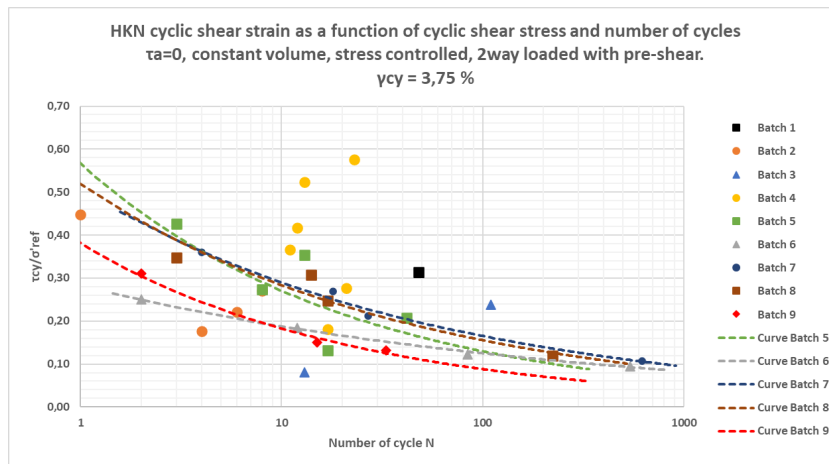


Figure C2: Cyclic resistance curve for HKN

Based on the results from project location HKW, the FC is influencing the position of the line in a strong way in comparison with the other resistance curves. In this project the results from Batch 9 (red curve) show a lower CSR just as Batch 6 (grey curve). But the difference in FC cannot be observed here. Also, these lines show both the lowest and highest value for the D_r (respectively 46% and 98%). What can be observed is that higher values of D_r gives a steeper line. The red curve (Batch 9) and the green curve (Batch 5) shows a comparable slope but at different values for CSR. Both show a steeper line probably because of the higher D_r . The difference in characteristics here is the uniformity. From this can be observed that an increase in uniformity show lower CSR values even for comparable values of D_r and FC. The resistance curve for Batch 8 (brown curve) shows a similar shape as batches with a higher D_r value although it does not have a high D_r . Therefore, this line is adjusted to a less steep line with a gradient comparable to the curve belonging to Batch 6.

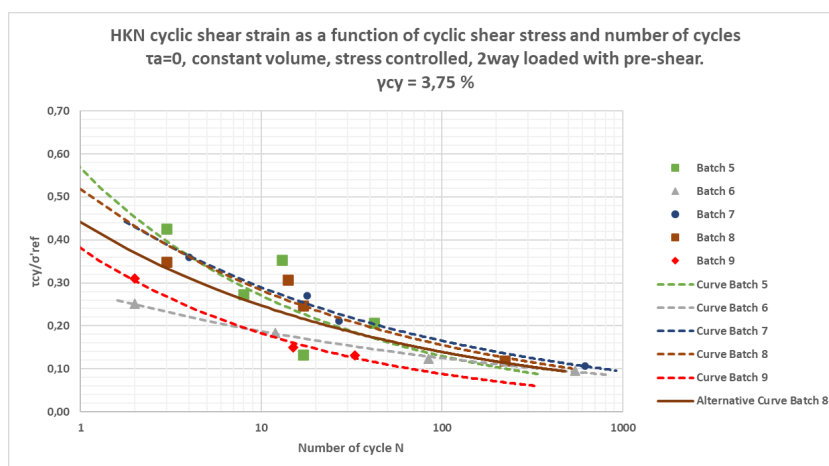


Figure C3: Alternative resistance curve for HKN

Figure C.4 shows the obtained resistance curve for the batches tested from project location HKZ.

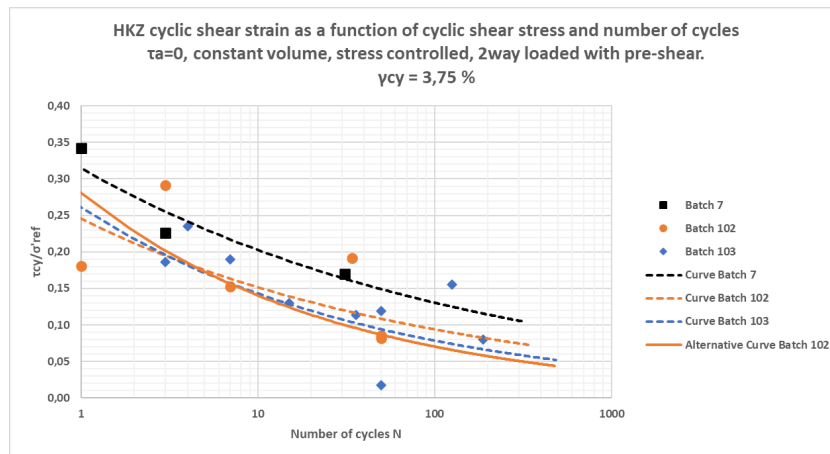


Figure C4: Alternative resistance curve for HKZ

Here three different lines from the same project are shown. Curve Batch 7 (black curve) and curve Batch 103 (bleu curve) show a similar shape and curve Batch 102 (orange curve) differs from these lines. D_r is slightly higher for Batch 102 than for the other two batches. Also, the FC is different. If the FC would be of influence, then the curve for Batch 102 would be under the curve from Batch 103. This means that the two tests results, that show higher values for CSR in the results for Batch 102 are apparently affected by another factor. The curve for Batch 102 is corrected to a curve with a higher slope, this is in line with the previous observation that the D_r influence the slope of the curves.

Figure C.5 shows the resistance curve for the two tests that were performed without pre-shear.

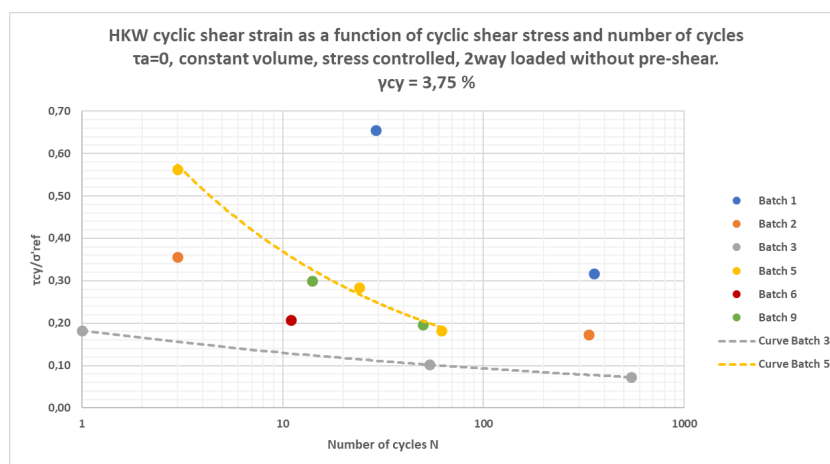


Figure C5: Cyclic resistance curve HKW, no pre-shear

These batches are from the same project but show quite some difference in the value for CSR. The difference between these batches are also the D_r and the FC. The results from batch 3 (with a $D_r = 42\%$ and a FC = 20.5%) show a lower cyclic shear strength. The test result with the higher value of D_r ($D_r = 74\%$) shows a steeper line and the higher FC show a lower value for the CSR. This is in line with the previous observations. Figure C.6 illustrates the relationship between the power of the cyclic resistance curves and the relative density. The resistance curves are of the form:

$$Y = a * X^{-b}. \quad (C.1)$$

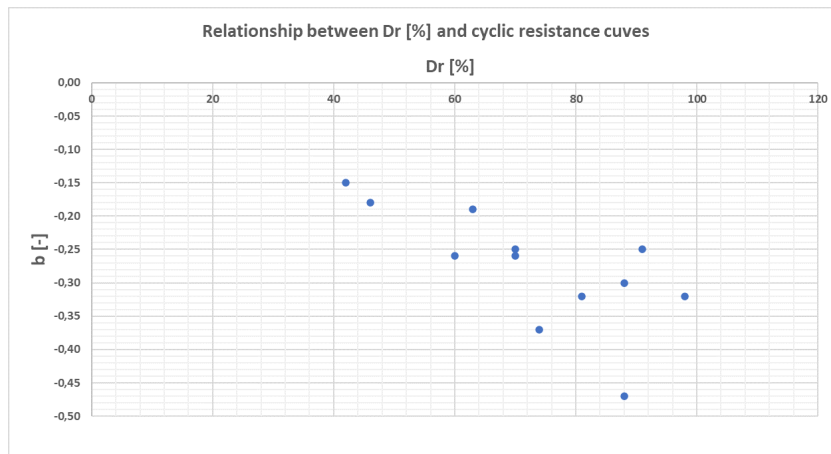


Figure C6: Relationship between Dr [%] and the slope of the cyclic resistance curves